DOKUZ EYLÜL UNIVERSITY
GRADUATE SCHOOL OF NATURAL AND APPLIED SCIENCES

PREPARATION AND CHARACTERIZATION OF Al-, Fe- AND Zr- PILLARED CLAYS AND THEIR APPLICATIONS

by
Zehra MOLU

July, 2009
İZMİR

PREPARATION AND CHARACTERIZATION OF Al-, Fe- AND Zr- PILLARED CLAYS AND THEIR APPLICATIONS

A Thesis Submitted to the
Graduate School of Natural and Applied Sciences of Dokuz Eylül University
In Partial Fulfillment of the Requirements for the Degree of Doctor of Chemistry,
Chemistry Program

by
Zehra MOLU

July, 2009
İZMİR

Ph.D. THESIS EXAMINATION RESULT FORM

We have read the thesis entitled **"PREPARATION AND CHARACTERIZATION OF Al-, Fe- AND Zr- PILLARED CLAYS AND THEIR APPLICATIONS"** completed by **ZEHRA MOLU** under supervision of **PROF. DR. KADİR YURDAKOÇ** and we certify that in our opinion it is fully adequate, in scope and in quality, as a thesis for the degree of Doctor of Philosophy.

.....

Prof. Dr. Kadir YURDAKOÇ

Supervisor

.....	.....
Prof. Dr. Melek MERDİVAN	Prof. Dr. İ. Akın ALTUN
Thesis Committee Member	Thesis Committee Member
.....	.....
Examining Committee Member	Examining Committee Member

Prof. Dr. Cahit HELVACI

Director

Graduate School of Natural and Applied Sciences

ACKNOWLEDGMENTS

I would like to thank my supervisor, Prof. Dr. Kadir YURDAKOÇ for his guidance, his support and his critical suggestions throughout my doctoral studies. It was a privilege to study under his supervision.

I gratefully want to thank the committee of this dissertation, Prof. Dr. Melek MERDİVAN and Prof. Dr. İ. Akın ALTUN, for their comments and suggestions. They both brought unique perspectives to my research, enriching it greatly. I would also like to thank Prof. Dr. Mürüvvet YURDAKOÇ for her comments and valuable guidance.

I gratefully acknowledge the monetary and moral support of Scientific and Technical Research Council of Turkey (TUBİTAK) -Münir Birsel Foundation for the Doctorate award.

I'm also grateful to Research Foundation of Dokuz Eylül University (Project No: 2007.KB.FEN.028) for financial support.

Very special thanks would be given to my parents, Fatma and Hüseyin Bekçi, and my brother, Ethem, for their forever love, confidence in me and understanding.

Finally, I would like to express my special gratitude to my dear husband, Cafer Molu, for his love, endless support, understanding and sacrifices. He always gives me strength to carry on…

Zehra BEKÇİ MOLU

PREPARATION AND CHARACTERIZATION OF Al-, Fe- AND Zr- PILLARED CLAYS AND THEIR APPLICATIONS

ABSTRACT

Aluminum, iron, zirconium - pillared clays were prepared by using Montmorillonite KSF and K10 and used as inorganic fillers for synthesis poly(acrylic acid/ Aluminum and zirconium pillared clays) superabsorbent composites. Pillared clays and Al- KSF, Al-K10 and Zr-KSF based superabsorbents were characterized by XRD, FTIR, gas adsorption analysis, SEM and TGA. Pillaring process resulted in a strong increase in the d_{001} basal spacing. BET surface area analyses indicated that the surfaces areas of pillared clays were increased. The superabsorbents showed pH dependent and reversible swelling behaviors. Decreasing of swelling ratio was observed by increasing the content of Zr-KSF on the superabsorbent. The more crosslinking ratio of Al-K10 based superabsorbents was understood from less swelling character than Al-KSF based superabsorbents. XRD revealed that the layers of clay dispersed on the composite. FTIR analyses indicated that the shifts of stretching vibrations of O-Si-O tetrahedra and OH bands supported ester formation between acrylic network and pillared clay. Additionally, the efficiency of aluminum-pillared-layered K10 and KSF montmorillonites (Al-PILCs) for the removal of Trimethoprim (TMP) was investigated. The removal percentage was highly depended on pH. TMP and the adsorbent surface, both carrying positive charges at acidic pH values may explain the poor adsorption. Al-K10 exhibits higher removal capacity of TMP at lower adsorbent dosages in comparison with Al-KSF. Adsorption is increased by increasing temperature onto Al-KSF and increased by decreasing temperature onto Al-K10. From Dubinin–Radushkevich isotherm equation, the adsorption onto Al-KSF and Al-K10 can be explained by ion-exchange mechanism and physical adsorption type, respectively. Standard enthalpy value of the sorption indicates that adsorption is endothermic while the standard entropy suggests that randomness increases during adsorption.

The results showed that Al-PILCs are potential useful adsorbents for the removal of TMP from wastewater treatment plants and fine inorganic fillers for synthesis of superabsorbent composites.

Keywords: Pillared clays, hydrogel, superabsorbent composite, adsorption

Al-, Fe- VE Zr- SÜTUNLU KİLLERİN HAZIRLANMASI VE KARAKTERİZASYONU VE UYGULAMALARI

ÖZ

Alüminyum, demir, zirkonyum–sütunlu killeri Montmorillonit KSF ve K10 kullanılarak hazırlandı ve poli(akrilik asit/ Alüminyum ve Zirkonyum sütunlu killeri) süperabsorplayıcı kompozitlerde inorganik dolgu maddesi olarak kullanıldı. Sütunlu killer ve süperabsorplayıcılar XRD, FTIR, gaz adsorpsiyon analizi, SEM ve TGA ile karakterize edildi. Sütunlama işlemi d_{001} bazal aralıkta büyük bir artışla sonuçlandı. BET yüzey alanı analizleri sütunlu killerin yüzey alanlarının arttığını gösterdi. Süperabsorplayıcıların pH'a bağımlı ve tersinir şişme özelliğine sahip oldukları yapılan şişme deneyleri ile anlaşıldı. Süperabsorplayıcıdaki Zr-KSF'nin miktarı artmasıyla şişme oranında düşme gözlenmektedir. Al-K10 tabanlı süperabsorplayıcının Al-KSF tabanlı süperabsorplayıcıya göre daha çok çapraz bağlanma yaptığı daha az şişme özelliği göstermesinden anlaşılmaktadır. XRD sonuçları kilin tabakalarının kompozit içinde dağıldığını ortaya çıkarmıştır. FTIR analizleri, O-Si-O tetrahedral gerilmedeki ve OH bandlarındaki kaymaların akrilik yapı ile sütunlu kil arasında ester oluşumunu desteklediğini göstermektedir. Bunlara ek olarak, bu çalışma alüminyum- sütunlanmış-tabakalı K10 ve KSF montmorillonitlerin (Al-PILC'ler), Trimetoprimin (TMP) sulu çözeltiden uzaklaştırılmasında etkinliğini araştırmıştır. TMP'nin uzaklaştırılma yüzdesi büyük oranda pH'a bağlıdır. TMP ve adsorplayıcı yüzeyinin her ikisinin de asidik pH değerlerinde pozitif yük taşıması, Al-PILC'lerin yüzeylerine TMP'nin daha zayıf tutunmasını açıklayabilmektedir. Al-K10, Al-KSF ile kıyaslandığında daha düşük adsorplayıcı miktarında daha yüksek TMP'i uzaklaştırma kapasitesi göstermektedir. TMP'nin Al-KSF üzerine olan adsorpsiyonu sıcaklık artarken, Al-K10 üzerine olan ise sıcaklık düşerken artmaktadır. Dubinin–Radushkevich izoterm denkleminden, Al-KSF ve Al-K10 üzerine olan adsorpsiyon sırasıyla iyon-değişimi ve fiziksel adsorpsiyonla açıklanabilir. Standart entalpi değeri adsorpsiyonun endotermik olduğunu gösterirken standart entropi değeri de düzensizliğin adsorpsiyon sırasında arttığını belirtmektedir.

Al-PILC’ler atık su arıtma tesislerinden TMP’nin uzaklaştırılmasında potansiyel yararlı bir adsorplayıcı ve süperabsorlayıcı kompozitlerin sentezinde ise iyi bir inorganik dolgu maddesi olduğunu sonuçlar göstermektedir.

Anahtar sözcükler: Sütunlu kil killer, hidrojel, süperabsorplayıcı kompozit, adsorpsiyon

CONTENTS

Page

CHAPTER ONE

INTRODUCTION

1.1 Clays and Catalysts

The main properties of cationic and anionic clays as well as their role in catalysis are discussed in light of the versatility and potential usage of these materials. Clays exhibit specific features such as high versatility, wide range of preparation variables, use in catalytic amounts, ease of set-up and work-up, mild experimental conditions, gain in yield and or selectivity, low cost, etc., which may be very useful tools in the move towards establishing environmentally friendly technologies. Furthermore, the possibility of upgrading these materials by the pillaring process opens new and interesting perspectives, also considering possible shape selective advantages. Recent catalytic applications of cationic and anionic clays in organic or fine chemistry (acid- or base-catalyzed reactions, Diels–Alder reactions, reactions using metallic nitrates, etc.) ,environmental catalysis (DeSOx, DeNOx or contaminant oxidation) and energy exploitation (partial oxidation of methane) are discussed as very promising research subjects with a wide range of possible future developments with the transition from 2- 3-dimensional structures via the preparation of pillared clays (Vaccari, 1998, s.161).

1.2 Clays

Clays are very versatile materials and hundred of millions of tons currently find applications not only in ceramics and building materials, paper coatings and fillings, drilling muds, foundry moulds, pharmaceuticals, etc, but also as adsorbents, catalysts or catalyst supports, ion exchangers, etc, depending on their specific properties (Grim, 1968; Van Olphen, & Fripiat, 1979; Nemecz, 1981; Fodwen et al., 1984; Reichle, 1986; Newman, 1987; Schoonheydt, 1991; Cavanie et al., 1991).

"Clay minerals" refers collectively to the group of fine- grained hydrous silicates of aluminum (and also to some extent of magnesium or iron). When examined under the scanning electron microscope, these minerals are seen to consist of readily identifiable particles, which can have a variety of geometric shapes. Despite this variety of morphology, clays are closely interrelated in terms of their basic crystal structures, and also in the characteristic physical and chemical properties resulting from their crystal chemistry (Wilson, 1987).

1.2.1 Structure of The Clay Minerals

Most clay minerals involve two basic types of units in their atomic structure. The manner in which these units are combined and the type of exchangeable atoms that are present will play a very significant role in the type of clay mineral that forms.

The first unit is built of silica tetrahorns. The tetrahedral sheet is composed of silicon bounded to four oxygen atoms. Each unit consists of a central four-coordinated atom (e.g. Si) surrounded by four oxygen atoms that, in turn, are linked with other nearby atoms (e.g. Si), thereby serving as inter-unit linkages to hold the sheet together (Juma, 1998).

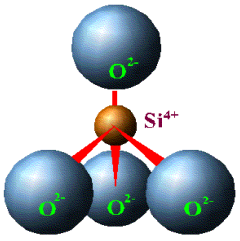

Figure 1.1 Silica tetrahedral units

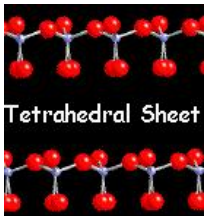

Figure 1.2 Tetrahedral Sheet

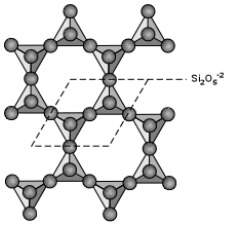

Figure 1.3 A Basic structural unit of $Si_2O_5^{2-}$

The second unit consists of octahedrals. An octahedral sheet, consisting of two layers of oxygen atoms or hydroxyl groups, between which aluminium, magnesium, iron are bonded in six – fold coordination. If the layer contains mainly trivalent aluminium ions which occupy two thirds of the available octahedral interstices, this is known as a gibbsite type or dioctahedral layer. Conversely, if the layer contains mainly divalent magnesium ions, this will occupy all of the octahedral sites, and the layer is called a brucite – like or trioctahedral layer (Wilson, 1987).

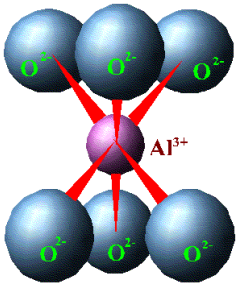

Figure 1.4 Octahedral unit

Figure 1.5 Octahedral sheet

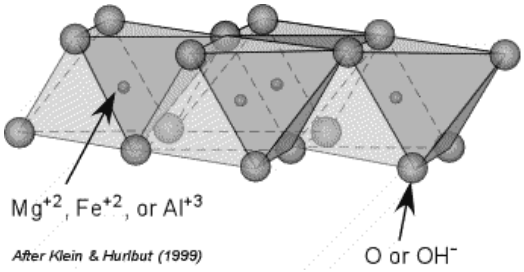

Figure 1.6 Octahedral sheet

The structural units of clays therefore consist of either alternating tetrahedral (T) and octahedral sheets (O) (OT or 1:1 structure), as in the kaolinite group of clay minerals; tetrahedral sheets (TOT or 2:1 structure), as in illite and the smectite clay minerals, of which the most common member is montmorillonite; or an arrangement in which the layer TOT units alternate with a brucite layer (2:1:1 structure) as in chlorite. The basic structural arrangements of the more common clay minerals are illustrated schematically in Figure 1.7 (Wilson, 1987).

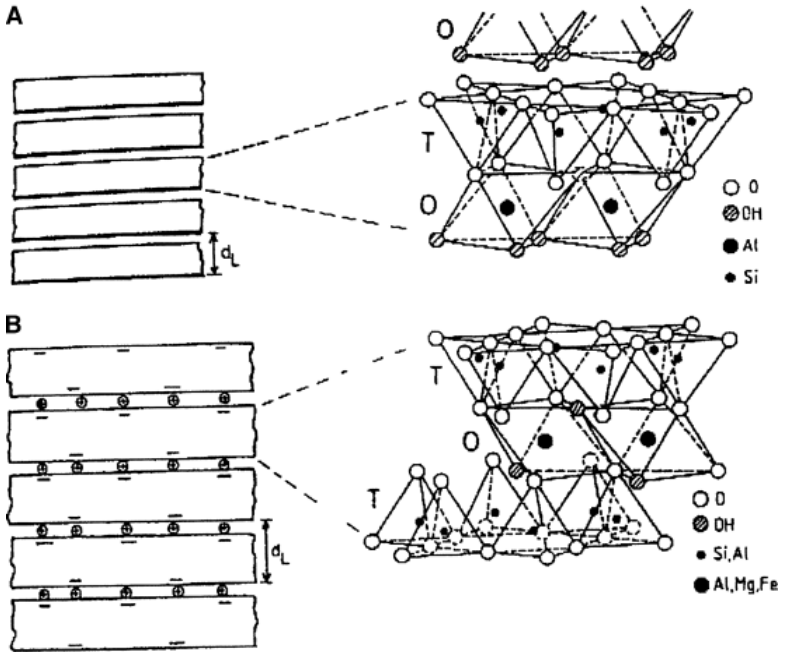

Figure 1.7 Layer structures of two-layer minerals (1:1 clay minerals)
(A) and of three-layer minerals (2:1 clay minerals)
(B); T, O=tetraeder and octaeder layers, respectively; d_L=layer distance.

Table 1.1 Clay minerals and their net charge

Group	Layer Type	Net Negative Charge (Coulombmolkg^{-1})	Surface Area (m^2/g)	Basal Spacing (nm)
Kaolinite	1:1	2-5	10-30	0.7
Fine-grained mica	2:1	15-40	70-100	1.0
Smectite	2:1	80-120	600-800	1.0-2.0
Vermiculite	2:1	100-180	550-700	1.0-1.5
Chlorite	2:1:1	15-40	70-100	1.4

1.2.1.1 Smectite [2:1 or TOT structure]

Smectite minerals have three layers with the aluminum atoms lying between two layers of silicon atoms in a 2:1 structure, sharing the valencies of their oxygen atoms (Juma, 1998).

This group is composed of several minerals including pyrophyllite, talc, vermiculite, sauconite, saponite, nontronite and montmorillonite. They differ mostly in chemical content. Montmorillonite, a type of smectite is expanding clay mineral and different layers are held together by bonding between divalent cations and water with basal oxygen atoms of the tetrahedral sheets. The formula for montmorillonite is $(Si_{7.8}Al_{0.2})(Al_{3.4}Mg_{0.6})O_{20}(OH)_4$. The formula indicates that there is substitution for Si^{4+} by Al^{3+} in the tetrahedral layer and for Al^{3+} by Mg^{2+} in octahedral layer (Juma, 1998).

These substitutions lead to net negative charges on the clay structure which must be satisfied by the presence of charge-balancing cations somewhere else in the structure. The interlayer is hydrated, which allows cations to move freely in and out of the structure. Because the interlayer is open and hydrated, cations may be present within the interlayer to balance negative charges on the sheets themselves. These cations between the layers are part of the cation exchange capacity of the soil. Smectites will have a CEC of around 80 to 150 meq/100 g. (Juma, 1998). Also, the amount of water present in the interlayer of montmorillonite results in swelling under wet conditions and shrinking in dry conditions (Juma, 1998).

Smectites are swelling clays, thus water is able to enter into the interlayer region, thereby expanding the clay layers, and the hydrated cations can be exchanged with other type of larger hydrolysed metal cations or organic/ inorganic complexes. These two properties of smectites, swelling and ion-exchangeability are critical for the successful synthesis of PILCs (Pillared Clays).

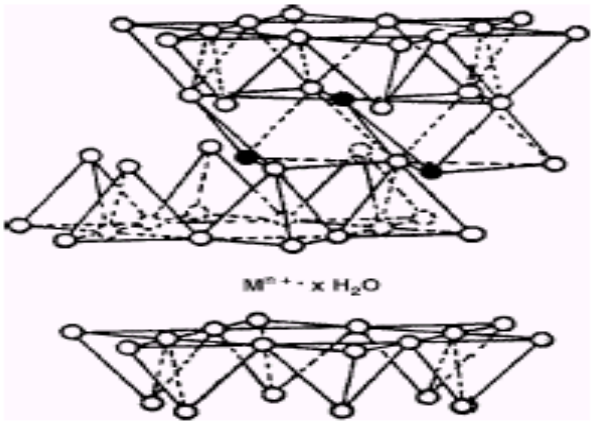

Figure 1.8 Idealised structure of a smectite clay mineral showing the (O) Oxygen atoms and (•) hydroxyl groups

Therefore, the common procedure for the preparation of PILC materials is considered to be: (i) swelling of smectite in water; (ii) exchanging the interlayer cations by partially hydrated polymeric or oligomeric metal cation complexes in the interlamellar region of the clay; (iii) drying and calcining of the wet cake of expanded clay to transform the metal polyoxocations into metal oxide pillars, which would 1) open up the silicate platelets permanently and 2) form covalent bonds with the tetrahedral sheets of the clay. So, in step (ii) it is still possible to exchange the pillars, while in step (iii), the pillars are permanently bonded to the clay layers (Ding, Kloprogge, & Frost, 2001).

The main properties relevant for catalytic applications are affected considerably by the composition and particle size (Grim, 1968). As a function of their small particle size, clays may exhibit both Bronsted and Lewis acid sites: the former are the external OH^- groups, while the Lewis sites are the exposed or three-fold coordinated Al^{3+} ions, substituting for the Si^{4+} ions in the tetrahedral sheets. The strength of the Bronsted sites may be determined by Hammet indicators, butylammine titration or IR spectroscopy using probe molecules (Newman, 1987; Schoonheydt, 1991; Knozinger, 1993), with a direct correlation between acid strength and composition. The surface acidity decreases as the amount of residual water in the clay increases, with an extension related to the nature of the exchangeable cations (Schoonheydt, 1991).

Not only acid sites, but also electron-accepting or oxidizing sites may be located at the edges or in the structure. The former may be identified as trigonal Al^{3+} ions, acting as Lewis sites, while Fe^{3+} ions in the lattice are the structural oxidizing sites (Theng, 1974). Moreover, redox properties may be induced by the exchangeable cations, such as Cu^{2+} , Ag^{+} , Fe^{3+} or Ru^{3+} (Y. Soma, M. Soma and I. Harada, 1986).

1.3 Pillared Clays

1.3.1 A Historical Perspective

Barrer and McLeod (1995) demonstrated the concept of intercalation of clays by organic compounds. However, organic and organometallic intercalating or pillaring agents decompose at relatively modest temperatures causing the pillared clay structure to collapse.

Nowadays, these types of pillared clays are industrially used as gelling agents, thickeners, and fillers (Schoonheydt, 1991).

The escalation of the oil prices in 1973 confronted the oil industry with the problem of how to maximize the processing of crude oil, especially the heavy fractions to gasoline components (Ding, Kloprogge & Frost, 2001). The problems then cascaded to fluid catalytic cracking (FCC) catalyst design and process development. The inherent problem with zeolite catalysts in processing such material is the relatively small pore size of zeolites, and the large amount non-selective pre-cracking that would have to take place before the large reside molecules were reduced to a size capable of diffusing into the very active and selective zeolite component of the catalysts (Smith & Dytrych, 1984; Meier, 1986). A strong impetus was thus given to the development of catalysts with relatively large pore sizes, able to deal with larger molecules than the existing molecular sieves, and good thermal and hydrothermal stability. The oil crisis thus resulted in a renewed interest in the concept of pillared clays. The use of inorganic hydrated

polyoxocations as pillaring agents provided thermally stable pillared clays with high specific surface areas (200 to 500 m^2/g). Upon calcination the hydrated polyoxocations dehydrate and dehydroxylate, and react to form fixed metal oxide pillars.

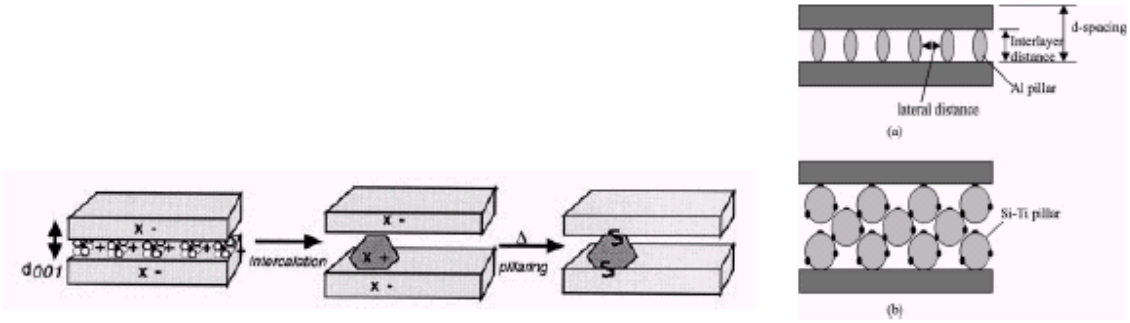

Figure 1.9 Schematic structures of the single and mixed metal oxide PILCs with various d-spacings. (a) Al-PILC; (b) Si/Ti-PILC.

1.3.2 Pillaring

Pillared layered clays PILC's, nanocomposite materials with open and rigid structures are obtained by linking robust, three-dimensional species to a layered host. The final properties of PILC's can be modulated by carefully choosing the different parameters, such as nature of the pillaring agent, type of clay and particle size, pillaring procedure, thermal treatments, etc., thus offering a very powerful and flexible way to design tailored catalysts. Therefore, control of the pillaring process is a very promising means to obtain solids with i) very high surface areas (up to 600 m^2g^{-1}), ii) a broad spectrum of properties structural, chemical, catalytic, etc., and iii) controlled internal structures, with reactive sites and/or species chosen to match particular applications or provide host structures for chemical or physical processes (Vaccari, 1999).

Many different pillaring agents have been reported in the literature organic compounds, metal trischelates, organometallic complexes, metal cluster cations, metal oxide sols, polyoxocations, etc. Many of these species however have some drawbacks, such as low reactivity or lack of thermal stability. Polyoxocations are by far the most

widely employed pillaring agent. Different polyoxocations (Al, Ni, Zr, Fe, Cr, Mg, Si, Bi, Be, B, Nb, Ta, Mo, Ti and more recently Cu and Ga) have been reported in the open and patent literature and clays with multielement pillars also have been prepared (Schoonheydt, 1991; Vaughan, D.E.W. 1987).

Preparation of PILC's consists in a controled hydrolysis reaction which can be carried out in solution or in the interlamellar space of the clay. The calcination process also plays a key role. Three general cases may occur: i) the polyoxocations exit from the clay (no pillaring) , ii) they degrade in situ giving rise to layers of aluminum hydroxide (1.4 nm thick, corresponding to a pseudo-chlorite), and iii) in the case of true pillaring, the polyoxocations dehydrate up to 573 K and dehydroxylate between 573 and 673 K. At higher temperatures, the pillars transform progressively, but the clays maintain the initial spacing of about 1.9 nm, while at T >1073–1173 K the clays degrade (Vaccari, 1999). The stability of pillared clays as a function of the calcination temperature depends on the nature of the clays and the composition of the pillars. For example, an increase in stability may be achieved using mixed polyoxocations or by doping with small amounts of another element (Vaughan, 1987; Carrado, Kostapapas, Suib,& Coughlin, 1986 & Occelli, 1986).

From the viewpoint of making catalysts at a competitive price, three important criteria need to be met: i) use the whole clay material, after minimal refining (i.e., low cost) , ii) pillar the Ca or (Ca, Na) forms, not only the Na forms (i.e., no pre-exchange), and iii) be able to use clay-polyoxocation concentrations (>15% solids) that can be economically and effectively spray-dried to give a usable particle size distribution (40–200 μm) (Burch & Warburton, 1987).

1.3.3 Catalytic Applications of PILCs

1.3.3.1 Suface Acidity–Dependent Application

PILCs are used in catalytic cracking process, and also PILCs find application as acid catalysts in the synthesis of chemicals. Different types of reactions have been studied, such as hydroisomerisation (Moreno, Kou, & Poncelet, 1996, 1997; Moreno, Gutierrez, Alvarez, Papayannakos, & Poncelet, 1997; Moreno, Kou, Molina, & Poncelet, 1999), dehydration (Jones & Purnell, 1994), dehydrogenation (Lourvanij & Rorrer, 1997), hydrogenation (Louloudi & Papayannakos, 1998), aromatisation (Liu, Zhao, Sun & Min, 1999), disproportionation (Chevalier, Franck, Suquet, Lambert & Barthomeuf, 1994), esterification (Wang & Li, 2000), alkylation (Geatti, Lenarda, Storaro, Ganzerla & Perissinotto, 1997), etc. Yang and co-workers have published a series of reports on SCR of NO to nitrogen with either ammonia or hydrocarbon as reductants (Yang, Chen, Kikkinides, Cheng & Cichanowicz, 1992).

1.3.3.2 Catalytic Active Substrates- Dependent Applications

Modification of PILCs by metal deposition can be easily achieved through impregnation methods (Wang & Li, 2000). These metals, such as Pt, Ni, Cu, etc., are generally active for a variety of catalytic reactions. In addition, some types of metal oxides in PILCs are also catalytically active. Therefore, apart from exploiting the surface acidity and porous structure of the PILC in catalytic applications, it is of great interest to take advantages of these catalytically active substrates. In fact, all these three characteristics, surface acidity, porous structure and catalytic active substrates, would have correlative effects on the catalytic performance of PILCs and one of them will generally be dominant.

Loading a PILC with transition metal ions, because of the oxidation state of these metal ions, will lead to new materials that have the potential to be applied as a catalyst in

redox reactions. In recent years, complete mineralization of organic pollutants in water, termed advanced wastewater treatment, had drawn more and more attention (Liu, Liptak, & Bouis, 1997; Baird, 1998). In this process, the organic compounds are oxidized to carbon dioxide and water, thereby preventing secondary pollution. The most popular methods for this process include homogeneous photocatalytic oxidation (Legrini, Oliveros & Braun, 1993), wet air/peroxide oxidation (Lei, Hu, & Yue, 1998), heterogeneous photocatalytic oxidation (Ollis, Pelizzetti & Serpone, 1991) and catalytic wet air/peroxide oxidation (Schiavello, 1997). The first two methods employ only ozone or hydrogen peroxide as oxidant, while the latter two methods involve heterogeneous catalysts. The most popular catalyst for heterogeneous photocatalysis is TiO_2 (Serpone, 1995), while for catalytic wet oxidation, Cu or Fe loaded on particle supports is widely investigated (Barrault, et al., 1998). Therefore, it is interesting to utilize PILC as a support for these active substrates. However, only limited research has been conducted in this area.

1.3.4 The Importance of the Surface Acidity

PILCs possess both Bronsted acid (proton donor) sites and Lewis acid (electron pair acceptor) sites (Chevalier & et al., 1994). To investigate the surface acidity on PILC samples, the most commonly used methods are the study of adsorbed ammonia or pyridine by infrared (IR) spectroscopy and temperature programmed desorption (TPD) of adsorbed ammonia and amine titration using Hammett indicators. By choosing adsorbed substrates with different basicity, both the number and strength of the acid sites can be determined. It is reported that 2,6-dimethylpyridine (DMPY) is selectively adsorbed on Brønsted acid sites, thus it can be used as a good probe molecule for the determination of Brønsted acidity in clays and PILCs. Generally, it is believed that Brønsted acidity is mainly coming from the clay layer structural hydroxyl groups, while Lewis acidity is attributed to the metal oxide pillars. In addition, the amount and strength of Brønsted and Lewis acid sites are closely related to the types of clays and metal oxide pillars.

Apart from the types of starting clay materials and metal oxide pillars, acid-activation of clays before pillaring is widely accepted as another feasible way to improve the acidity, particularly Brønsted acidity. In addition, such acidity enhancement always coupled with the increase of the pore volume and average pore diameter (Mokaya, Jones, Davies, & Whittle, 1993).

1.3.5 The importance of Porous Structure

The pore size of PILCs can be varied from 5 Å to over 20 Å, depending on the synthesis conditions, such as type of the starting clay materials, cation exchange capacity (CEC) of clays, type of the metal oxide pillars, and thermal treatment temperature. Recent reports show d-spacing as high as 60 Å can be obtained on some composite PILCs, such as Si/Ti-PILC (60 Å), Si/Cr-PILC (47 Å), Si/Fe-PILC (63 Å) (Han, Matsumoto & Yamanaka, 1997) etc. In general, the porous structure of PILCs can be stable up to 673–773 K. Further increase the heating temperature will lead to the collapse of the clay layers because of the sintering of the pillars and the dehydroxylation of the clay sheets. Both the nature of the clay materials and type of metal oxide pillars will affect the thermal stability of the resulting PILCs. It has been reported that a homogeneous distribution of pillars is beneficial for improving the thermal stability. Katdare and co-workers showed that an Al-PILC prepared by a simplified method with ultrasonic modification had superior thermal and hydrothermal stability (Schiavello, 1997).

1.3.6 Aluminum Pillared Clays (Al-PILC)

Pillared clays have reached considerable interest as catalysts and catalysts supports over the past years. Their porosity, reactivity and thermal stability are being widely applied in adsorption and catalysis (Kikuchi, & Matsuda, 1988; Mrada, Ghorbela, Tichit, & Lambertc, 1997). Metals commonly used as ionic precursors are Al, etc. Aluminium

has been profusely used as pillaring agent due to its hydrolisis capability to form large inorganic polymeric oxy-hydroxy cations of several nuclearities. The major aluminium species used is the $[Al_{13}]^{7+}$ polymer but other mono and polynuclear species may be present in solution depending on its pH (Lambert, & Poncelet, 1997). The actual exchange is dependent, as in every diffusion process, on the pillaring agent solution concentration and the ageing conditions of the formed cation whose size and charge (n/q ratio) deeply depends on the synthesis conditions. Also, the effect of the drying method is claimed to be more important than the pillaring reagent itself or even the clay layer charge on PILCs pore opening, giving rise to products with uniform pore size when air-dried or with a continuous distribution of larger pores when freeze-dried. With all that in mind, the possibility of tuning the properties of PILCs by varying the synthesis conditions seems plausible (Hutson, Hoekstra, & Yang, 1999; Flegoa, Galassoa, Millinia, & Kirics, 1998).

In general, the pillaring processes are carried out in diluted systems, less than 2 wt.% of clay suspension and less than 0.5 M of pillaring solution (Figueras, 1988; Lambert, & Poncelet, 1997). When a large amount of materials has to be prepared, a quite large volume of solutions has to be handled which turns the PILCs synthesis in a non-viable industrial method. Vaugan (Vaugan, 1988) proposed the first approaches to prepare PILCs in large quantities. More recently, a method of synthesis based on the use of highly concentrated clay suspensions without any previous purification or homoionisation of clay prior to pillaring has been developed (Storaroa, Lenardaa, Gazerlaa, & Rinaldi, 1998). The method enables the preparation of industrial quantities of pillared materials with uniform properties, and its scale-up seems promising. However, only scarce information has been, up to the moment, reported on the physico-chemical characteristics of the resulting materials and on their comparison with those obtained by the more conventional method of diluted suspensions (Salerno, Asenjo, & Mendioroz, 2001).

The first step in the pillaring process is to prepare a pillaring agent. In the case of the Al_{13} polyoxocation, two methods are commonly used: (1) mixing of aqueous $AlCl_3$ with Al to form a chlorohydrate which is also commercially available, and (2) addition of a base to $AlCl_3$ or $Al(NO_3)_3$ solutions with OH/Al^{3+} ratios up to 2.5. The polyoxocation complex produced has been analyzed and is thought to be the tridecamer $[AlO_4Al_{12}(OH)_{24}(H_2O)_{12}]^{7+}$, also referred to as the Keggin ion (Kloprogge, 1998; Kloprogge, Seykens, Geus, Jansen, 1992; Kloprogge, & Frost, 1999).

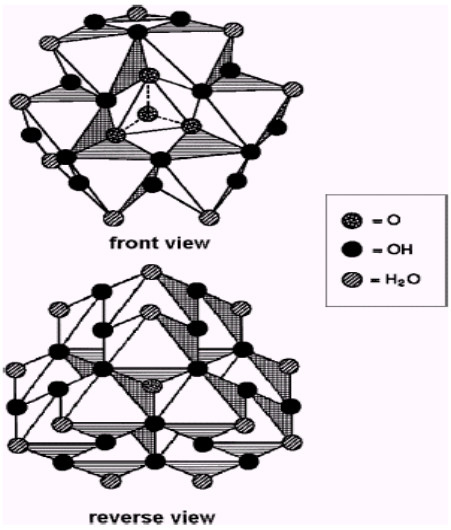

Figure 1.10 Structure of the Al_{13} complex.

The next step is the mixing of a clay suspension with this polyoxocation solution. This allows the interlayer cations in the clay to exchange with the polyoxocation in solution through cation exchange reaction or intercalation (Gil, Gandia, 2000). After the intercalation process is complete, the clay is separated, washed and then calcined. The property of the stable pillared structure obtained is greatly affected by factors such as clay used, mixing and drying conditions and polycation/s used.

1.3.7 Zirconium Pillared Clays (Zr-PILC)

Several experimental parameters (ageing temperature, ageing time, pH, and concentration) can affect the degree of polymerization of hydroxyl zirconium species in

aqueous solution. The solution chemistry of Zr is complex, but it is known that zirconyl ion is present in solid zirconium chloride as the tetramer, $[(Zr\ (OH)_2.4H_2O)_4)\ ]^{8+}$ (Clearfield & Vaughan, 1956). The four Zr ions are located at the corners of a slightly distorted square and are linked together by OH bridges above and below the plane of the square. When dissolved in water the solution becomes quite acidic due to hydrolysis of the tetramers. Further hydrolysis eventually leads to a tetramer with the formula $[Zr_4(OH)_{14}.(H_2O)_{10}]^{2+}$. Here, two of the zirconium ions have a single positive charge and the other two are neutral. On ageing the solution larger species are observed (Muha, & Vaughan, 1960) which are believed to be due to a polymerization reaction in which a neutral site on one tetramer reacts with a singly charged site on another tetramer, the result being that the zirconium ions are connected by two OH bridges. Continuation of this process leads to the formation of large "rafts" or two-dimensional hydroxy polymers. Further polymerization eventually results in the precipitation of hydrous $Zr(OH)_4$ (Ross, 1988).

1.3.7.1 Influence of pH on Preparation of Zr-PILC

Increasing of the pH of the solution, by addition of NaOH for instance, favours the hydrolysis reaction and this in turn leads to an increase in the degree of polymerization as the number of neutral zirconium ions increases. Precipitation of hydrous $Zr(OH)_4$ begins at a pH of about 3 (Vaughan, Lussier, & Magee, 1979) give an example of a preparation of a Zr-PILC in which the zirconyl chloride solution is treated with Na_2CO_3. This will increase the degree of polymerization and lead to polymeric hydroxyl zirconium pillars (Ross, 1988).

1.3.7.2 Influence of concentration on Preparation of Zr-PILC

A solution of lower concentration will have a higher pH and so the degree of polymerization will be higher. Concentrations typically used in the preparations described in the earlier literature are in the range 0.1 – 0.33 (Ross, 1988).

1.3.7.3 Influence of temperature and time on Preparation of Zr-PILC

Heating of the zirconyl chloride solution also leads to an increase in the degree of polymerization, as demonstrated by Clearfield, & Vaughan, 1956. This is simply due to an increase in the rate of hydrolysis with temperature. Similarly, increasing the ageing time at any specific temperature will increase the degree of polymerization.

Surface areas obtained are critically dependent on the method of preparation. Samples synthesized from refluxed Zr solutions had markedly higher surface areas than those prepared using fresh, unrefluxed Zr solutions. As already mentioned, the effect of refluxing is to increase the degree of polymerization. Hence, as might be expected, it appears that an increase in the degree of polymerization produces an increase in the surface area of pillared clay (Ross, 1988).

The highest stability was obtained by refluxing the Zr solution prior to mixing with the dispersed clay, combined with a subsequent refluxing of the mixture (Burch, & Warburton, 1986; Bartley, & Burch, 1985). Intercalation of the clay by Zr polymers is very slow at room temperature. When the clay is intercalated with an unheated zirconyl chloride solution (i.e., containing only Zr tetramers) the PILC formed has the lowest surface area of all.

1.3.7.4 Effect of Drying Conditions on the Structure of Zr-PILC

Bartley, & Burch, 1985 have investigated the effect of the drying temperature on the surface area and interlayer spacing of Zr –PILC and found that a PILC with a basal spacing up to 2.5 nm, and a markedly higher surface area, was produced by replacing the water with methanol and drying at < 60°C. These polymers are believed to be mobile within the interlayer cavity of the clay prior to drying. Removing water at 110°C may cause the polymers to rearrange their positions to reduce stacking. The dried PILC

contains stacked polymer units and this results in much larger surface are being obtained.

1.3.7.5 Structure and Stability of Zr-PILC

Bartley, & Burch, 1985 found that the highest thermal stability was obtained by first refluxing the Zr solution prior to mixing with the clay and then refluxing the slurry. Table 1.2 shows the influence of the method of preparation on the thermal stability of these Zr-PILCs.

Table 1.2 Thermal stability of pillared hectorites (Occelli, & Finseth, 1986)

Heating temperature/°C	Percentage retention of surface area		
	Al-PILC	Al Zr-PILC	Zr-PILC
300	100.0	100.0	100.0
400	99.0	91.0	95.4
500	95.0	91.0	96.4
600	81.0	89.5	95.3
700	44.7	44.2	77.0

Zr-PILC with good thermal stability can be prepared and the interlayer spacing, the interpillar distance, the surface area, and the Zr content can be manipulated over wide ranges by varying the method of preparation. Zr-PILCs have some interesting catalytic properties. They are active for cracking reactions, for the dehydration of methanol, and when used as a support for Cu they can be used to synthesize olefins directly from CO/H_2 gas mixtures (Ross, 1988).

1.3.8 Iron Pillared Clays (Fe-PILC)

Of these publications the great majority have been concerned with Al or Zr-PILC, as these seem to offer the greatest thermal stability. In contrast, very few papers have been concerned with Fe-PILC. This is perhaps surprising given that Fe-PILC are cheaper to prepare and would not only have acidic properties, but would also contain pillars which in themselves may be catalytically active.

In order to prepare Fe-PILC it is important to understand the hydrolysis chemistry of Fe(III) solutions so that some control over the size of pillaring cations may be exercised. Although the dissolution of Fe(III) salts in water is known to result initially in simple hydrolysis products such as $Fe(OH)^{2+}$, $Fe(OH)_2^{+}$, $Fe_2(OH)_2^{4+}$ and $Fe_3(OH)_4^{5+}$ (Bjerrum, Schwarzcnbach, & Sillen, 1964; Sylva, 1972), the above studies suggest that further hydrolysis leads to the formation of discrete spherical polycations. These gradually link up to give rods comprising 2 to 6 spheres. On further hydrolysis these rods appear to combine to give raft- like polycations 20x3 nm in size, which continue to grow, whole process may be brought about by either prolonged aging at room temperature, addition of base, or aging at high temperature, it is recommended that the addition of base is used, since this appears to offer the greatest degree of control over the size of the pillaring species (Warburton, 1988).

Tzou found that $FeCl_3$, $Fe(NO_3)_3$ and $Fe_2(SO_4)_3$ solutions previously aged at 25°C for 24 h gave Fe-PILC with interlayer spacing of about 0.3 nm. It was concluded that only simple hydrolysis products were responsible for pillaring in such materials (Tzou, 1983). On increasing the OH/Fe ratio from 0.0 to 1.0 interlayer spacings were found to increase (from 0.3 to1.4 nm), particularly for the chloride and nitrate systems, and thereafter increased slowly as the OH/Fe ratio was raised to 2.5. The sulphate system, in contrast, was found to give interlayer spacings of only 0.3 nm regardless of the OH/Fe ratio employed. Precipitation in this system was observed to occur at a lower OH/Fe ratio (1.5) than in the other systems (2.5). Since all precipitates were removed from the

pillaring solutions before use, the small spacings observed were attributed to pillaring by the small polycations remaining in solution (Tzou, 1983).

Tzou also showed that large interlayer spacings of 1.7 nm could be obtained using longer aging periods or higher aging temperatures, providing precipitation was avoided (Tzou, 1983).

Fe-PILC prepared from partially hydrolyzed Fe(III) solution lacked thermal stability above 300°C. This lack of thermal stability was attributed to the fact that hydroxy Fe(III) cations were unstable in water and were partially washed out during the final washing step. To overcome this problem Yamanaka et al. introduced iron pillars by exchanging Na-montmorillonite with partially hydrolyzed trinuclear aceto Fe(III) ions, which when thermally decomposed gave oxide pillars between the silicate sheets (Yamanaka, Doi, Sako, & Hattori, 1984). Using this procedure a thermally stable Fe-PILC was prepared which possessed a surface area and interlayer spacing of 280 m^2 g^{-1} and 0.7 nm, respectively, after calcination at 500°C (Warburton, 1988).

Using a small excess of Fe^{3+} for the pillaring reaction (i.e. 7 mmolFe^{3+} /meq) surface areas of the dried materials were found to increase with OH/Fe ratio. The larger exess of Fe^{3+} lengthening the final washing procedure considerably, leads to a more complete pillaring, resulting in a higher surface area. As the polymeric cations produced at 75°C would be expected to lead to a larger separation of the clay layers and therefore a larger surface area (Warburton, 1988).

The surface areas of the materials calcined at 500°C generally indicate that the Fe-PILC possess good thermal stability, suffering only small reductions due to a decrease in microporosity and an increase in mesoporosity (Warburton, 1988).

1.4 Adsorption Phenomena

The use of solids for removing substances from either gaseous or liquid solutions has been widely used since biblical times. This process, known as *adsorption,* involves nothing more than the preferential partitioning of substances from the gaseous or liquid phase onto the surface of a solid substrate (Marczewski, 2002).

The interface of two different phases is always anisotropic. That is, in the interface the molecular interactions in one side differ from interactions in the other side. If the molecules in a phase are mobile (e.g., gas – solid or liquid – solid interfaces), then these different molecular interactions cause a concentration difference between the interface and bulk phase of mobile molecules. This type of change in concentration taking place in the interface is called *adsorption*. This is the reason why the interface is often referred to as the adsorption space or adsorbed phase. If the mobile molecules can penetrate into the bulk of the other phase, then this process is called *absorption*. It is sometimes difficult or impossible to distinguish between adsorption and absorption; it is then convenient to use the wider term *sorption*. The name of the phase with localized (non-mobile) molecules is the *adsorbent*, and the mobile molecules bound on the adsorbent surface called *adsorbate*. The phase with mobile molecules before the adsorption, i.e., the phase that is capable of being adsorbed is named adsorptive. So the whole process of adsorption can be expressed with the following simple and symbolic relationship (Adamczyk, 2002).

$$\text{Adsorbent} + \text{Adsorptive} \longrightarrow \text{Adsorbate}$$

(Toth, 2002).

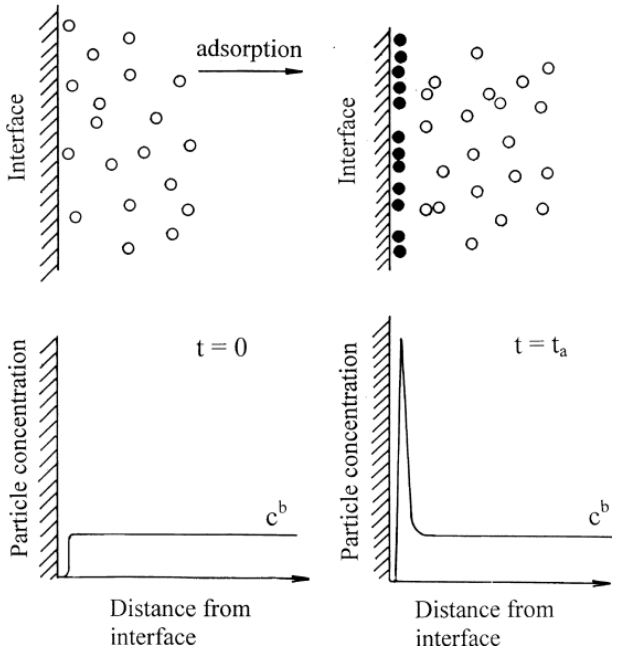

Figure 1.11 Schematic representation of particle adsorption at solid / liquid interfaces

The solid adsorbents are often characterized by their specific surface area (a_s) and pore size distribution. The value of as refers to unit mass (m) of adsorbent:

$$a_S = \frac{A_s}{m}$$

the pore size distribution provides information on the size and amount of pores present in the solid adsorbent: Macropores are pores with widths exceeding about 50 nm. Mesopores are pores widths between 2 nm and 50 nm. Micropores are pores with widths not exceeding about 2 nm (Toth, 2002).

A large specific surface area is preferable for providing large adsorption capacity, but the creation of a large internal surface area in a limited volume inevitably gives rise to large numbers of small sized pores between adsorption surfaces. The size of the micropores determines the accessibility of adsorbate molecules to the internal adsorption

surface, so the pore size of the micropores is another important property for characterizing adsorptivity of adsorbents. Especially materials such as zeolite and carbon molecular sieves can be specifically engineered with precise pore size distributions and hence turned for a particular separation (Marczewski, 2002).

Surface polarity corresponds to affinity with polar substances such as water or alcohols. Polar adsorbents are thus called “hydrophilic” and aluminosilicates such as zeolites, porous alumina, silica gel or silica-alumina are examples of adsorbents of this type. On the other hand, nonpolar adsorbents are generally “hydrophobic”. Carbonaceous adsorbents, polymer adsorbents and silicate are typical nonpolar adsorbents. These adsorbents have more affinity with oil or hydrocarbons than water (Marczewski, 2002). The average thickness of the adsorbate is often expressed with names mono- and multilayer adsorption. In monolayer adsorption, all the adsorbed molecules are in contact with the surface of the adsorbent. In the multilayer adsorption, the adsorption space accommodates more than one layer or molecules so that not all adsorbed molecules are in direct contact with the molecules of the adsorbent (Toth, 2002). Coverage is a measure of the extent of adsorption of a species onto a surface. Usually denoted by the lower case Greek “theta”, Q. Exposure is a measure of the amount of gas which as surface has seen; more specifically, it is the product of the pressure and time of exposure (normal unit is the Langmuir, where 1 L = 10-6 Torrs).

1.4.1 Adsorption Processes

There is two type of adsorption, the first type is known as physisorption (physical adsorption) and the second one is called as chemisorption (chemical adsorption). Adsorption in which the forces involved are intermolecular forces (van der Waals forces) of the same kind as those responsible for the imperfection of real gases and the condensation vapors, and which do not involve a significant change in the electronic orbital patterns of the species involved. The term van der Waals adsorption is synonymous with physical adsorption (IUPAC Compendium of Chemical Terminology

2nd Edition, 1997). The only bonding is by weak van der Waals – type forces. There is no significant redistribution of electron density in either the molecule or at the substrate surface. A chemical bond, involving substantial rearrangement of electron density, is formed between the adsorbate and substrate. The nature of this bond may lie anywhere between the extremes of virtually complete ionic at complete covalent character. This is called as chemical adsorption (Blatt, 1980, Hillier, 1995, & Velde, 1995).

Table 1.3 Typical characteristics of adsorption process

Properties	**Chemisorption**	**Physisorption**
Binding force	Due to chemical forces or bonding, thus this process is also called as activated adsorption.	Due to physical force of attraction, thus this process is also called as Van der Waals adsorption.
Saturation uptake	Single layer phenomena	Multilayer phenomena
Activation energy	May be involved.	No activation energy involved.
Temperature range (over which adsorption occurs)	Adsorption can take place even at higher temperatures. When temperature increases adsorption increases.	Adsorption is appreciable at lower temperature below boiling of adsorbate. When temperature increases adsorption decreases
Nature of adsorption	Often dissociative may be irreversible	Non- dissociative. Reversible
Crystallographic specificity	Marked variation between crystal planes	Virtually independent of surface atomic geometry
Heat of adsorption	50-100 kCal/mole	1 kCal/mole
Kinetics of adsorption	Very variable-often an activated process.	Fast- since it is a non–activated process

The problem of distinguishing between chemisorption and physisorption is basically the same as that of distinguishing between chemical and physical interaction in general.

Changes in the electronic state may be detectable by suitable means (e.g. UV, infrared or microwave spectroscopy, electrical conductivity, magnetic susceptibility).

1.4.2 Adsorption Isotherms

An adsorption isotherm for a single gaseous adsorptive on a solid is the function which relates at constant temperature the amount of substance adsorbed at equilibrium to the pressure (concentration) of the adsorptive in the gas phase (IUPAC Compendium of Chemical Terminology 2nd Edition, 1997).

The successful representation of the dynamic adsorptive separation of the solute from solution onto an adsorbent depends upon a good description of the equilibrium separation between the two phases. Adsorption equilibrium is established when the amount of solute being adsorbed onto adsorbent is equal to the amount being desorbed. At this point, the equilibrium solution concentrations remain constant. By plotting solid phase concentration against liquid phase concentration graphically, it is possible to depict the equilibrium adsorption isotherm. There are many theories relating to adsorption equilibrium.

1.4.2.1 Langmuir Isotherm

The Langmuir isotherm theory assumes monolayer coverage of adsorbate over a homogenous adsorbent surface (Langmuir, 1918). Langmuir isotherm was originally derived from adsorption kinetics by equating the rates of adsorption and desorption onto a flat surface.

The Langmuir equation is based on the following assumptions:

1- Adsorption of adsorbate molecules takes place at well-defined adsorption sites and each site can contain only one molecule.

2- The surface is homogeneous; the energy of adsorption is equal for all adsorption sites.

Whenever a gas is in contact with a solid there will be an equilibrium established between the molecules in the gas phase and the corresponding adsorbed species (molecules or atoms) which are bound to the surface of the solid.

As with all chemical equilibrium, the position of equilibrium will depend upon a number of factors:

1. The relative stability of the adsorbed and gas phase species involved
2. The temperature of the system (both the gas and surface)
3. The pressure of the gas above the surface

In general, factor (2) and (3) exert opposite effects on the concentration of adsorbed species. We can say that the surface coverage may be increased by raising the gas pressure but will be reduced if the surface temperature is raised.

We may derive the Langmuir isotherm by treating the adsorption process as we would any other equilibrium process - except in this case the equilibrium is between the gas phase molecules (M), together with vacant surface sites, and the species adsorbed on the surface. Thus, for a non-dissociative (molecular) adsorption process we consider the adsorption to be represented by the following chemical equation:

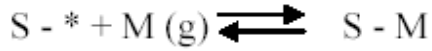

S - *, represents a vacant surface site

In writing this equation we are making an inherent assumption that there are a fixed number of localized surface sites present on the surface.

We may now define an equilibrium constant (K) in terms of the concentrations of "reactants" and "products"

$$K = \frac{[S-M]}{[S-*][M]} \tag{1}$$

We may also note that:

[S-M] is proportional to the surface coverage of adsorbed molecules, i.e. proportional to θ

[S -*] is proportional to the number of vacant sites, i.e. proportional to (1-θ)

[M] is proportional to the pressure of gas, P

Hence, it is also possible to define another equilibrium constant, b, as given below. Rearrangement then gives the following expression for the surface coverage.

$$b = \frac{\theta}{(1-\theta)P} \tag{2}$$

This is the usual form of expressing the Langmuir Isotherm.

Graphically, a plateau characterizes the Langmuir isotherm. Therefore, at equilibrium, a saturation point is reached where no further adsorption can occur. Sorption is assumed to take place at specific homogeneous sites within the adsorbent. Once a molecule occupies a site, no further adsorption can take place at that site. In Eq. (3), K_L and a_L are the Langmuir isotherm constants; C_e and C_s are the liquid phase concentration and solid phase concentration of adsorbate at equilibrium.

$$C_s = \frac{K_L}{1 + a_L C_e} C_e \quad (3)$$

The Langmuir constants, K_L and a_L are evaluated through linearization of Eq. (3):

$$\frac{C_e}{C_s} = \frac{1}{K_L} + \frac{a_L}{K_L} C_e \quad (4)$$

Hence by plotting C_e / C_s against C_e it is possible to obtain the value of K_L from the intercept which is $(1/K_L)$ and the value of a_L from the slope, which is (a_L/K_L). The theoretical monolayer capacity is C_m and is numerically equal to (K_L/a_L). So Eq. (4) is rearranged as the below.

$$\frac{C_e}{C_s} = \frac{1}{C_m a_L} + \frac{C_e}{C_m} \quad (5)$$

The Langmuir equation is applicable to homogeneous sorption where the sorption of each molecule has equal sorption activation energy. The equation is thermodynamically consistent and follows Henry's Law at low concentrations. As C_e becomes lower, $a_L C_e$ is much less than unity and $C_s = K_L C_e$, that is, analogous to Henry's Law (Allen, Gan, Matthews, & Johnson, 2003).

To determine if the adsorption process is favorable or unfavorable, for the Langmuir type adsorption process, the isotherm shape can be classified by a term 'R_L', a dimensionless constant separation factor, which is defined as below (Arslanoğlu, Kar, & Arslan, 2005).

$$R_L = 1/[\,1 + a_L A_0] \quad (6)$$

where R_L is a dimensionless separation factor. A_0 is initial absorbance and a_L Langmuir constant.

The shapes of the isotherms for $0< R_L < 1$, $R_L > 1$, $R_L = 1$ and $R_L = 0$ are favorable, unfavorable, linear and irreversible, respectively (Weber, & Chakkravorti, 1974).

1.4.2.2 Freundlich isotherm

The Empirical Freundlich expression (Eq. (7)) is an exponential equation and therefore, assumes that as the adsorbate concentration increases so too does the concentration of adsorbate on the adsorbent surface. Theoretically, using this expression, an infinite amount of adsorption can occur (Freundlich, 1906).

Freundlich equation is based on a monolayer adsorption by the adsorbent with a heterogeneous energy distribution of active sites (Aksu & Kabasakal, 2004)

$$C_s = K_f C_e^{nf} \quad (7)$$

In this equation K_f and n_f are the Freundlich constants characteristic on the system. K_f and n_f are indicators of adsorption capacity and heterogeneity factor, respectively.

The Freundlich equation aggress well with the Langmuir expression, it does not reduce to the linear isotherm (Henry's Law) at low surface coverage and provides no information on the monolayer adsorption capacity (Allen et. al, 2003).

Both these theories suffer from the disadvantage that equilibrium data over a wide concentration range cannot be fitted with a single set of constants (McKay, Bino, & Altemeni, 1980).

To determine the constants K_f and n_f , the linear form of the equation shown below may be used to produce a graph of $\ln C_s$ against $\ln C_e$ (Allen et. al, 2003).

$$\ln C_s = \ln K_f + n_f \ln C_e \quad (8)$$

1.4.2.3 Dubinin – Radushkevich (DR) Isotherm

Langmuir and Freundlich isotherms do not give any idea about adsorption mechanism. In order to understand the adsorption type, equilibrium data is applied to following linear form of DR isotherm:

$$\ln C_{sorb} = \ln X_m - \beta\varepsilon^2 \quad (9)$$

where C_{sorb} is the amount of ions sorbed onto the adsorbent ($molg^{-1}$), X_m represents DR monolayer capacity of the sorbent ($molg^{-1}$), β a constant related to sorption energy (mol^2/kJ^2) and ε Polanyi sorption potential, the amount of energy required to pull a sorbed molecule from its sorption site to infinity which is equal to:

$$\varepsilon = RT \ln (1+1/C_e) \quad (10)$$

where R is the gas constant in $kJmol^{-1}K^{-1}$; T is the temperature in Kelvin and C_e is the equilibrium concentration in solution ($mol\ dm^{-3}$). The Polanyi adsorption theory postulates fixed volume of sorption site close to sorbent surface and existence of sorption potential over these sites. The sorption potential is related to an excess of sorption energy over the condensation energy and is independent of temperature. The plot of $\ln C_{sorb}$ versus ε^2 follows linearity. The value of X_m is determined from the intercept and the value of β is derived from the slope. The sorption energy, E for ions onto adsorbent calculated using the expression:

$$E = -\frac{k^{-1/2}}{\sqrt{2}} \quad (11)$$

is the range of 8-16 $kJmol^{-1}$ designated for ion exchange mechanism (Malik, Hasany, & Subhani, 2005). If the value of E is smaller than $8kJmol^{-1}$, this shows physical adsorption due to weak van der Waals forces (Singh & Pant, 2004).

1.4.3 Adsorption Kinetics

In order to optimize the design of an adsorption system, it is important to establish the most appropriate correlations for the equilibrium data for each system. In this respect, several kinetic models including the pseudo-first-order equation, pseudo-second-order equation, and intraparticle diffusion model are applied to find out adsorption mechanism.

$1/q_t = (k_1/q_1)(1/t) + 1/q_1$ Pseudo-first-order (12)

$t/q_t = 1/k_2.q_2^2 + (1/q_2).t$ Pseudo-second-order (13)

$q_t = k_p\, t^{0.5} + C$ (14)

where

q_t is the amount of trimethoprim adsorbed (mgg^{-1}) on montmorillonite KSF at various time t ,

q_1 is the maximum adsorption capacity (mgg^{-1}) for the pseudo-first order adsorption ,

k_1 is the pseudo-first-order rate constant for the adsorption process (min^{-1}),

q_2 is the maximum adsorption capacity (mgg^{-1})for the pseudo-second-order adsorption,

k_2 is the rate constant of pseudo-second-order for the adsorption ($g\ mg^{-1}min^{-1}$),

C is the intercept for the intraparticle diffusion model (mgg^{-1}),

k_p is the intraparticle diffusion rate constant ($mg\ g^{-1}\ min^{-0,5}$).

The straight-line plots of $1/q_t$ versus $1/t$ for the pseudo-first-order reaction and t/q_t vs (versus) t for the second-order reaction for the adsorption have also been tested to obtain the rate parameters. The k_1, k_2, q_1, q_2 and correlation coefficients R_1^2 and R_2^2 of were calculated from these plots (Özcan, & Özcan, 2004).

Adsorption kinetics are usually controlled by different mechanisms, of which the most limiting are the diffusion mechanisms, including the initial curved portion, attributed to rapid external diffusion or boundary layer diffusion and surface adsorption, and the linear portion, a gradual adsorption stage due to intraparticle diffusion starts to decrease due to the low concentration in solution as well as fever available adsorption sites.

The rate-limiting step may be due to intraparticle diffusion. The rate constant for the intraparticle diffusion was obtained using the (14) equation.

C gives an idea about the boundary layer thickness. If the intraparticle diffusion is involved in the adsorption process, then a plot of the square root of time ($t^{1/2}$) versus the uptake (q_t) would result in a linear relationship and the particle diffusion would be the controlling step if this line passed through the origin.

When the plots do not pass through the origin, this is indicative of some degree of boundary layer control and the further show that the intraparticle diffusion is not the only rate-controlling step, but also other processes may control the rate of adsorption, all of which may be operating simultaneously.

The slope of the linear portion can be used to derive values for the rate parameter, k_p, for the intraparticle diffusion. The larger the intercept (C value), the greater is the boundary layer effect. (Özcan, et. al, 2004).

1.4.4 Thermodynamic Parameters of Adsorption

The thermodynamic parameters of the adsorption process are obtained from experiments at various temperatures. It is essential to clarify the change of thermodynamic parameters. Gibbs free energy change, ΔG, standard enthalpy, ΔH, and standard entropy, ΔS are estimated by applying thermodynamic equations. The Gibbs free energy change of adsorption is estimated from the following equation (Özcan, et. al, 2004).

$$\Delta G^\circ = -RT \ln K_d \quad (15)$$

where

K_d = The equilibrium constant at temperature T,

R = gas constant (8.314 J mol^{-1} K^{-1}),

T = absolute temperature (K).

K_d was estimated using the following equation;

$$K_d = C_s / C_e \quad (16)$$

where

C_e = equilibrium concentration

C_s = the amount of adsorbed

To determine the values of ΔH° and ΔS°, the van't Hoff equation is used;

$$\ln K_d = (\Delta S^\circ/R) - (\Delta H^\circ/RT) \quad (17)$$

ΔH° and ΔS° can be obtained from the slope and intercept of a van't Hoff plot of ln K_d versus 1/T (Aksu, & Kabasakal, 2004).

The negative value of the Gibbs free energy demonstrates a spontaneous and favorable adsorption process. The higher negative value reflects a more energetically favorable adsorption (Aksu, et al, 2004).

The negative value of $\Delta H°$ indicates that the adsorption process is exothermic in nature and the negative value of $\Delta S°$ showed the decrease in degree of freedom or decrease the disorder of adsorption process. The negative value of $\Delta S°$ suggests decreased randomness at solid/ solution interface and no significant changes occur in the internal structure of the adsorbent through the adsorption (Özcan, et. al, 2004).

The activation energy, Ea, was obtained from an Arrhenius plot. Arrhenius equation is shown below;

$$k = A\, e^{-Ea/RT} \quad \text{or} \tag{18}$$

$$\ln k = \ln A - E_a/RT \tag{19}$$

where

k_2 = rate constant,

A = The Arrhenius factor,

R = gas constant (8.314 $Jmol^{-1}\ K^{-1}$),

T = absolute temperature (K).

The plot of lnk versus 1/T for the adsorption was applied to obtain the activation energy, E_a from the slope.

If the activation energy value is between 5-40 $kJmol^{-1}$values, it is understood that the physical adsorption mechanism is occurred. When the activation value is higher than $40kJmol^{-1}$, it can be easily said that Ea represents the nature of chemical adsorption.

1.5 Trimethoprim

Trimethoprim (TMP) is among the most important antibacterial agents (synthetic antibiotics) used in human and veterinary medicine worldwide acting as an inhibitor in the chemotherapy treatment due to its antifolate effect by interaction with dihydroflate coenzymes (Florey, 1978; Hitchings, Burchall, 1965).

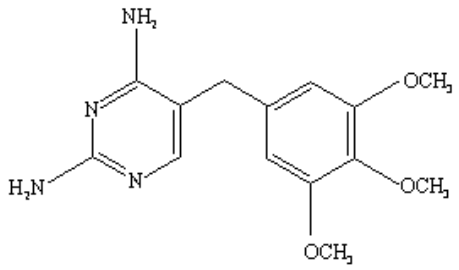

Figure 1.12 Chemical structure of trimethoprim

Trimethoprim is a weak base with a pKa of 7.3. It is lipophilic. The chemical designation of trimethoprim is 5-[(3, 4, 5-trimethoxyphenyl) methyl]-2, 4-pyrimidine diamine. It is a white to yellowish compound with bitter taste.

Table 1.3 Physical properties of Trimethoprim

Empirical Formula	$C_{14}H_{18}N_4O_3$
Molecular Weight	290.32 $gmol^{-1}$
Appearance	White to yellowish powder
Melting Point	199 - 203 °C
Solubility	Insoluble in water, freely soluble in alcohol
State/Form	Crystalline powder
Stability	Stable under ordinary conditions
Particle size	80 - 100 (mesh)
Storage	Sealed, in dark place

In respect of many articles, TMP was detected in hospital sewage water in Sweden (Lindberg, Jarnheimer, Olsen, Johansson & Tysklind, 2004), in wastewater effluents from East Aurora and Holland (Batt, & Aga, 2005), in manure and soil in a German farming area (Miao, Bishay, Chen, & Metcalfe, 2004) and in two municipal wastewater treatment plants in USA (Renew & Huang, 2004) and in U.S. Streams (Kolpin, et.al, 2002).

Release of antibiotics to the environment may lead to high, long-term concentration and promote unnoticed adverse effects on aquatic and terrestrial organisms. Prolonged exposure to low doses of antibiotics leads to the selective proliferation of resistant bacteria which could transfer the resistance genes to other bacterial species (Levy, 1997). Effect can accumulate so slowly that changes remain undetected until they become irreversible (Diaz-Cruz, de Alda, & Barcelo, 2003). Because it is impossible to stop antibiotic usage, it must be taken precautions against continual input of antibiotics to environment by using adsorbents such as natural and synthetic zeolite, clay minerals and pillared clays for the goal of removing antibiotics from wastewater treatment plants.

This study is carried out for the purpose of removing trimethoprim in wastewater treatment plants and in any where that drug effluents are present via the adsorption behavior of the pillared clay catalysts. For this reason batch adsorption experiments are made to clarify the adsorption process of trimethoprim onto PILCs.

1.6 Characterization Techniques of Pillared Clays

The surface area and pore volume of the prepared systems are clarified. As a result of pillaring, surface area and pore volume increases drastically.

1.6.1 The BET Analysis

Derivation of the Langmuir isotherm expression was based on the idea of coverage of the surface with single layers of adsorbent. Isotherm curves for adsorption rather than flatten out after initial stage of adsorption suggest a secondary adsorption stage. S. Brunauer, P. H. Emmett, and E. Teller have worked out a description of this process, and expression for the corresponding adsorption isotherm, known as the BET isotherm. The adsorption process can be described as adsorbed molecules on the surface sites and attachment of molecules to sites where occupied by adsorbed molecules. In order to represent x for P/P_0 the expression for the BET isotherm is

$$\frac{V}{V_m} = \frac{c\,x}{(1-x)\,(1-x+cx)}$$

If we take the reciprocal of each side of the equation and multiply both sites by V_m and by x/ (1-x), it will be

$$\frac{x}{1-x}\frac{1}{V} = \frac{1}{cV_m} + \frac{(c-1)x}{c\,V_m}$$

If we plot left side of the equation against x, it will give a straight line. The values of the intercept on the x =0 axis and that of the slope can be calculated to obtain the V_m and c values. By using V_m values, one can calculate the specific surface area of the adsorbents.

1.6.2 X-Ray Powder Diffraction

With the exception of surface area and pore volume measurements, the easiest way to determine whether pillar intercalation is successful is to record the X-ray diffraction pattern of and oriented film of the product. For example, Figure 1.13 depicts XRD patterns of montmorillonite and FeAl PM. The broad bands obtained in the XRD spectrum, instead of sharp peaks can be attributed to semi crystalline nature of clays.

The only data that can be obtained is the d spacing of (001) plane, which indicates the extent of propping apart of clay layers. The characteristic d_{001} spacing of montmorillonite increased from 9.8 Å to 17.8 Å for FeAl PM. Shifting of 2θ values clearly suggests expansion of clay layer during pillaring process. The increase in d spacing of (001) plane to 17.8 Å is indicative of the presence of Al_{13} like polymers.

The XRD patterns were exactly identical to that of montmorillonite. Thus, it can be concluded that insertion of the second metal after the formation of stable pillars does not destabilise the porous network. Additional peaks corresponding to the exchanged metal oxides were not noticed. This may be due to the diminutive amounts of the exchanged metal in these samples (Kurian, & Sugunan, 2006).

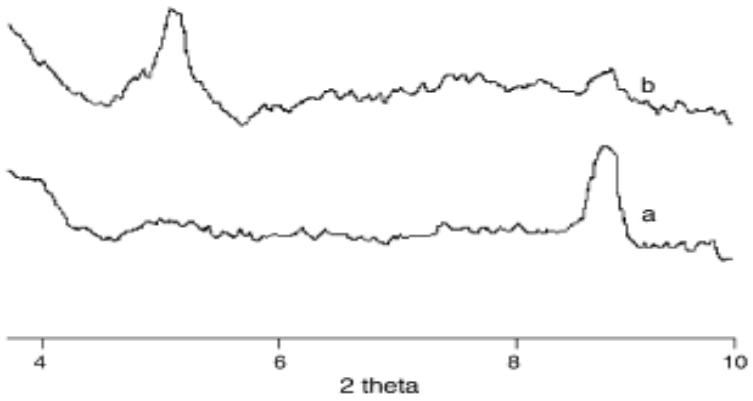

Figure 1.13 XRD profile: (a) M; (b) FeAl PM.(Kurian, & Sugunan, 2006).

1.6.3 Thermal Analysis (TGA/DTG)

Thermal analysis is a group of techniques in which the physical property of a substance is measured as a function of temperature, while the substance is subjected to a controlled temperature program. These include change in weight [Thermogravimetry (TG)], temperature difference [(Differential Thermal Analysis (DTA)] and heat flux difference [(Differential Scanning Calorimetry (DSC)].

Lack of thermal stability is the common drawback attributed to pillared clays. In order to find out thermal stability of prepared systems, it was subjected to thermogravimetric analysis in the temperature range of 30-800°C. The weight losses were occurred in three steps for pillared clays. The first step (100 -120°C) is related to lose of surface water and also the DTA profile of the clay shows an endotherm at 120°C. The second step (200-500°C) demonstrate the weight losses regarding the dehydration of pillar agents. The third step is between 500 and 800°C. In this step, the decomposition of the pillar agents and dehydroxylation are occured for that reason, the pillared structure might be loosened due to the pillar agent deformation.

1.7 Preparation, characterization and swelling behaviors of poly (acrylic acid)/Pillared clays, superabsorbent composites

Superabsorbent hydrogels are a type of loosely crosslinked hydrophilic polymer that can swell, absorb and retain a large volume of water or other biological fluid. Superabsorbents may have found many application fields owing to the water absorbing characteristics. Some of their applications include novel moisture sensors, fire protection materials, hygienic products, horticulture, gel actuators, drug-delivery systems, as well as water blocking tapes and coal dewatering (Li, Zhang, & Wang, 2005; Yao, & Zhou, 1994; Zhou,, Yao, & Kurth, 1996; Tsubakimoto, Shimomura, & Kobabyashi, 1987; Miura, et.al, 1991; Tanaka, 1992; Walker, 1987; Colombo, 1993; Dong, & Hoffman, 1991).

Recently, research on the use of superabsorbents as water managing materials for the renewal of arid and desert environment has attracted great attention, and encouraging results have been observed as they can reduce irrigation water consumption, improve fertilizer retention in soil, lower the death rate of plants, and increase plant growth rate (Zhang, Li, & Wang, 2005).

Additionally superabsorbents have negative features in some application fields because of high production cost and low gel strength. To overcome these negative points, inorganic fillers can be used as low cost material and developer the strength properties in polymer matrixes.

In the superabsorbent field, much attention has been paid to layered silicate recently for the preparation of superabsorbent composites because of developing mechanical and materials properties of superabsorbents. Clays, such as kaolin (Wu, Wei, Lin, & Lin, 2003), montmorillonite (Lee, & Yang, 2004; Kabiri, & Zohuriaan-Mehr, 2004), attapulgite (Li, Wang, & Chen, 2004), mica (Lin, Wu, Yang, & Pu, 2001), bentonite and sercite (Wu, Lin, Zhou, & Wei, 2000), have all been used for the preparation of

superabsorbent composites. Pillared clays are modified clays that protect the layered silicate structure.

In this thesis study pillared clays were used as inorganic materials for developing the properties of superabsorbent hydrogels. It was reported that the intercalation of certain metal oxides on 2:1 clay minerals significantly led to an increase in the sorption capacity (Lothenbach, Furrer, & Schulin, 1997). High temperature calcination of intercalated clays results in 'pillared' materials, where the polyhydroxo cationic species are irreversibly fixed to the layers. Al- pillared montmorillonite KSF (Al-KSF) and Al-pillared montmorillonite K10 (Al-K10) and Zr- pillared montmorillonite KSF (Zr-KSF) were pillared clays that used as inorganic fillers. The introduction of pillars (Keggien ion), besides increasing the material's resistance and stability, provides porosity, a greater surface area, access to acid areas existing in natural clay, and the presence of potentially active species for a specific reaction (Ding, Zhu, Greenfield, & Lu, 2001; Ding, Kloprogge,& Frost, 2001).

1.8 Objectives and Scope of the Thesis Study

Pillared clays have reached considerable interest as catalysts and catalysts supports over the past years. Their porosity, reactivity and thermal stability are being widely applied in adsorption and catalysis (Mrada, et. al, 1997; Kikuchi, & Matsuda, 1988).

Pillared clays with different inorganic compounds have drawn much attention. Numerous cations (hydroxyl aluminum (Kikuchi, & Matsuda, 1988), zirconium (Burch, & Warburton, 1987), and iron (Tzou, 1983)) have been used for the preparation of pillared clays.

In this thesis study, synthesis of aluminum, zirconium and iron pillared clays were prepared in various experimental conditions. In the preparation, drying processes were achieved by freeze dry and oven dry. The synthesized pillared clays have been

characterized using gas adsorption analysis (BET), X-ray diffraction (XRD), scanning electron microscopy (SEM) and FTIR techniques.

Additionally, the present work investigated the efficiency of aluminum-pillared-layered K10 and KSF montmorillonites (Al-PILCs) for the removal of Trimethoprim (TMP) which is one of common used antibiotics from aqueous solutions under kinetic and equilibrium conditions. In order to identify the mechanisms of TMP sorption on pillared montmorillonites, aluminium pillared layered montmorillonite KSF and montmorillonite K10 were prepared and then the adsorption conditions were varied and tested in sorption experiments.

In this thesis study, the prepared pillared clays were used inorganic fillers for synthesis of superabsorbent hydrogels. The performance of the inorganic fillers on the properties of the superabsorbents was compared each other in detail. Additionally, the synthesis of pillared clays containing acrylic-based superabsorbent hydrogel composites and the characterization performed by XRD, FTIR, and SEM were represented.

CHAPTER TWO

MATERIAL AND METHOD

2.1 Properties of clay samples

In this study, Montmorillonite KSF and Montmorillonite K10 will be used as clay samples.

KSF montmorillonite (KSF) and K10 montmorillonite (K10) supplied from Fluka Company were utilized as precursor material of pillared clays. Chemical composition of KSF Montmorillonite is %55.0 SiO_2, %18.0 Al_2O_3, %4.0 Fe_2O_3, %3.0 MgO, %3.0 CaO, %<0.5 Na_2O, %1.5 K_2O, %5.0 Sulphate and %10.0 loss on ignition. KSF has a surface area of 20-40 m^2/g. Chemical composition of K10 is %69.0 SiO_2, %14.0 Al_2O_3, %4.5 Fe_2O_3, %2.0 MgO, %1.5 CaO, %<1.5 Na_2O, %1.5 K_2O and % 7.0 ignition loss. K10 has a surface area of $197m^2/g$.

2.2 Preparation of Aluminum pillared clays (Al- PILCs)

The $AlCl_3 \cdot 6H_2O$ and NaOH procured from Merck were used to prepare the pillaring solution.

The first step in the pillaring process is to prepare a pillaring agent. Pillaring was achieved using aluminium hydroxide solution as pillaring agent. The pillaring solution was prepared by titrating aqueous 0.1 M NaOH with aqueous 0.1 M $AlCl_3 \cdot 6H_2O$ until the OH/Al ratio was equal to 2.0. At this hydrolysis ratio, Al_{13} is a major species in solution. The pillaring solution was aged for 2 h at 60 °C and then kept overnight at 30 °C. After aging, the resulting solution was reacted with a proper amount of aqueous suspension of KSF and K10 clay, keeping an Al / clay ratio of 10 mmol g^{-1}. The slurries were maintained at 60 ºC for 2 h followed by an aging period of 7 days at room

temperature, then washed by centrifugation and dialysis till the absence of chloride and oven-dried at 80 ºC for 18h and calcined at 250 °C for 2 h. On the other hand drying process was achieved by using freeze dryer.

2.3 Preparation of Zirconium pillared clays (Zr- PILCs)

Zr-pillared clays were prepared from zirconyl chloride solutions. In a first set of preparations, 0.2 M $ZrOCl_2$. 8 H_2O solution was previously refluxed at 95 °C for 5 and 24 h. The solution re- fluxed for 5 h remained limpid, but it turned turbid after refluxing for 24 h. The solutions were added dropwise to 2 wt% (%50 acetone %50 H_2O) suspensions of KSF and K10 montmorillonite at a rate of 10 mequiv. Zr g^{-1} clay. The final suspensions were stirred for 24 h at room temperature. Samples were further aged for 10 days. The pillared clays were washed by centrifugation and oven-dried. After this period, the samples were calcined at 250 °C for 2 h.

2.4 Preparation of Iron pillared clays (Fe- PILCs)

A typical Fe-PILC synthesis procedure was began by preparing pillaring solution. For this purpose, $FeCl_3.6H_2O$ was added to NaOH solution to obtain OH/Fe molar ratio of 2. In order to avoid precipitation of Fe species, the pH was kept constant at 2.5. A proper amount of deionized water was added to solution. The resulting solution was aged for 24h with stirring at room temperature. The pillaring solution was then slowly added to a suspension of KSF and K10 in deionized water. The Fe / clay ratio was keeping 10 mmol g^{-1}. The mixture was stirred and allowed to react. Finally, the solid was obtained by centrifugation and dialysis with deionized water until it was chloride free (conductivity <6 mS/cm). The aim of this stage was to remove excess chloride ions which could prevent the diffusion of polyoxocations within the interlayer space (Palinko, Lazar, Hannus, & Kirisci, 1996). The resulting products were oven-dried at 60 ºC for 24h and calcined at 250 °C for 2 h.

2.5 Synthesis of poly (acrylic acid)/Pillared clays, superabsorbent composites

Acrylic acid (AA) and the crosslinker N, N′-methylene–bisacrylamide (MBA) purchased from Fluka were used without further purification. Ammonium persulfate (APS), sodium metabisulfite (SMBS) and potassium hydroxide (KOH) (all from Merck) were used as received.

Acrylic acid (20 g) was neutralized with potassium hydroxide solution (12.1 g KOH + 10.0 g H_2O). Then crosslinker (MBA) solution (0.013 g MBA + 3.0 g H_2O) was added to the monomer solution. The mixture was poured into a 600-mL beaker, which was equipped with a magnetic stirrer and thermometer. 0.05g of Al-KSF and Al-K10 and 0.05, 0.10 and 0.20 g of Zr-KSF were added to stirring solutions and stirring was continued for five minutes until homogeny mixtures were obtained. To start polymerization reaction, the APS solution (0.05 g APS +1.5 g H_2O) and the SMBS solution (0.063 g SMBS + 2g H_2O) were added to the mixture. The temperature of mixture was increase rapidly to almost 100°C within a few minutes. Prior to hardening the products, the mixtures were pour into the Petri dish to obtain thin films. Samples were dried in a vacuum oven at 70°C for 24 h and then a few amount of water was dropped to film and after 1 h, the film was removed from Petri dish and cut into an appropriate size (~1cm x 1cm) . After all, samples were dried again.

2.6 Swelling measurements of poly (acrylic acid)/Pillared clays, superabsorbent composites

Water absorbency measurement was performed weighing the initial mass of composite (m_0) and mass determined at time t (m_t) of gel that was immersed in the distilled water at room temperature. Swollen samples were then separated from unabsorbed water by using tissue paper until reaching the swelling equilibrium. The

percent swelling values were calculated by the following equation. Data points are means of three measurements.

$$\%Swelling = 100\left[\frac{(m_t - m_0)}{m_0}\right]$$

2.7 Characterization Techniques

2.7.1 XRD analysis

X-ray powder diffraction patterns were obtained by Rigaku Dmax 2200/ PC model instrument with Cu K_α radiation (40 kV, 40 mA). Clays, pillared clays and superabsorbent samples for X-ray diffraction measurement were processed to powder form and film form for pillared clays and superabsorbents, respectively. The space of the layer is calculated by this formula $2d\sin\theta=n\lambda$ (Xie, Zhao, & Zhang,1980). X-ray diffraction (XRD) reveals the basal spacing of the pillared clays before and after in-situ incorporation indicating the morphology of the superabsorbent (exfoliated, intercalated or only dispersed).

2.7.2 FTIR analysis

The FTIR spectra of the samples were recorded on a Perkin Elmer FTIR spectrophotometer (Spectrum BX-II). 100 mg of fine KBr powder was dried at 110 ºC and mixed with 1 mg of samples. The samples were kept in the desiccators. For analysis of pillared clays, KBr pellets were prepared. Infrared spectra were carried out in the region 4000–400 cm^{-1}. The background spectrum of each KBr pellet was obtained by subtracting it from the sample spectra. The FTIR spectra of the superabsorbent composite were recorded on a FTIR Perkin Elmer Spectrum BX-II) using ATR probe at ambient conditions for film of composite.

2.7.3 Thermal analysis

Thermal behavior of pillared clays was determined by using Perkin-Elmer Diamond TG/DTA Analyzer. TGA measurements were carried out in porcelain pans at 10 °C/min heating rate in the range of 30–1000°C under nitrogen atmosphere with a flow rate of 50 ml/min.

2.7.4 BET Specific Surface Area Analysis

As a result of pillaring, surface area and pore volume increases drastically. For this reason, firstly surface area and pore volume of the precursor clay minerals are determined by BET specific surface area analysis to understand the increase.

The BET isotherms are plotted by volume versus relative pressure.

BET surface area (S_{BET}), total pore volumes (V_{total}) and average pore diameter (lp) were obtained from N_2 adsorption–desorption isotherms at 77 K, measured on SORPTOMATIC 1990 after a degassing under vacuum for 3 h at 150 ºC by using MILES-200 Advanced Data Processing Sorption Software Version 3.00. For porosity analysis, the BJH method (Barrett, Joyner, & Halenda, 1951) and the Dollimore–Heal method were used (Dollimore, Heal, 1964).

The Horvath- Kawazoe (H-K) method was used to determine the micropore surface area and volume (Horvath & Kawazoe, 1983). The Barrett, Joyner and Halenda (BJH) method was used to determine the mesopore- size distribution (Barrett, Joyner, & Halenda, 1951). Surface area measurements have an error of ± 3%.

2.7.5 SEM Measurements

SEM micrographs and elemental analysis were performed by a scanning electron microscope (SEM; Jeol JSM 60) operating at the accelerating voltage of 20 kV. The clays, pillared clays and the film of composite samples were dried before gold sputter-coated for SEM analysis. For SEM, photographs were taken at different magnifications (between 1000X and 10000X).

2.8 Adsorption experiments

Adsorption study was carried out using Trimethoprim antibiotic as adsorbate and Al-K10 and Al-KSF as adsorbents, respectively. Trimethoprim (TMP) was purchased from Sigma (Cat. No. T 788) and used without further purification. TMP solution was prepared by using certain proportion of ethanol and distilled water to enhance the solubility of TMP.

The batch experiments were carried out in a 50 ml stoppered flasks where 0.01 g of Al- K10 and 0.1 g of Al-KSF and 25 mL of TMP solution at desired initial concentration were added. The solution pH adjusted to the desired value by adding HCl and NaOH as required. The flasks were subsequently capped and shaken in a temperature controlled shaking water bath at 150 rpm for desired temperature. Preliminary kinetic experiments demonstrate that adsorption equilibrium was reached within 2 h for Al-K10 and 3 h for Al-KSF. After this period, a portion of the supernatant layers of suspensions were taken and centrifuged at 5000 rpm for 15 min and then analyzed for the concentration of TMP remaining in the solution by Spectrophotometric method. Spectrophotometric measurements were carried out using a Shimadzu UV–Visible 1601 model spectrophotometer at λ_{max} = 271 nm at ambient temperature. The adsorption capacities were calculated from the difference between initial concentration and equilibrium concentration of TMP.

The same procedures were carried out at solution temperatures of 303, 311, and 318 K to find adsorption isotherms and thermodynamic parameters. The effect of contact time, pH, initial concentration, temperature, and adsorbent dose was studied. In addition, some experiments were performed at various time intervals to determine the kinetic parameters. The pH was varied from 2.6 to 11.0, the initial concentration from 4.0×10^{-5} to 20.0×10^{-5} mol L^{-1}, and the amount of adsorbent was varied from 0.4 to 10 g L^{-1}.

CHAPTER THREE

RESULTS

3.1 Characterization of pillared clays

3.1.1 XRD analyses of pillared clays

In this study, Montmorillonite KSF, Montmorillonite K10 clays were used as precursor materials for synthesis of pillared clays. In order to clarify differences between clays and pillared clays, XRD analyses performed for both clays and pillared clays.

The XRD traces of the clays and pillared samples were shown as the follows. The XRD pattern of the parent clay exhibits a peak at 2θ whith a d value of ~5-6Å, which is commonly assigned to the basal 001 reflection (d_{001}). The d_{001} values of untreated montmorillonite KSF and K10 were 12.55 Å at 6.99 (2θ) and 14.83 Å at 5.94 (2θ), which correspond to the main montmorillonite component. In pillared clays, the d_{001} peak was found to shift towards the lower 2θ region, which is a clear indication of the enlargement of the basal spacing of the clay. The sharpest and the most intense peak, suggests that the intercalation process is homogeneous (Sanchez, & Montes, 1998). The less intense and broader peaks suggest that a fraction of clay remained unpillared (Gonzalez, Pesquera, Blanco, Benito, & Mendioroz, 1992) and/or delamination has occurred (Katdare, Ramaswamy, & Ramaswamy, 2000). 2θ and d_{001} basal spacing of clays and pillared clays were summarized in Table 3.1 and 3.2 as shown follows. OH/M molar ratio of all pillared clay is 2.0 and symbol of M indicates metal of pillaring agent such as Al, Fe and Zr. Calcinations were performed at the temperature of 250°C. Pillaring achieved an increase in the distance of layers of montmorillonite. The increase in d-spacing was as expected since the pillaring causes an expansion in the interlayer spacing. Subtraction of the thickness of the 2:1 layer of 9.60 Å (Manohar, Noeline, & Anirudhan, 2006) yields interlayer separations of all pillared clays and these results were

indicated in the Tables 3.1 and Table 3.2. Interlayer separations were between 4.42 and 10.0 Å. Zirconium pillared KSF series have higher interlayer separations than the other pillared KSF series. This was indicated as Zr-KSF > Al-KSF > Fe-KSF for interlayer separation. As seen pillared K10 series, Al-K10-OD*20x had the highest enlargement between interlayer. The interlayer separation of pillared K10 was increased in order of Zr–K10, Fe–K10, and Al–K10. Additionally, XRD data was reflected the main structure of precursors of pillared clays (KSF, K10).

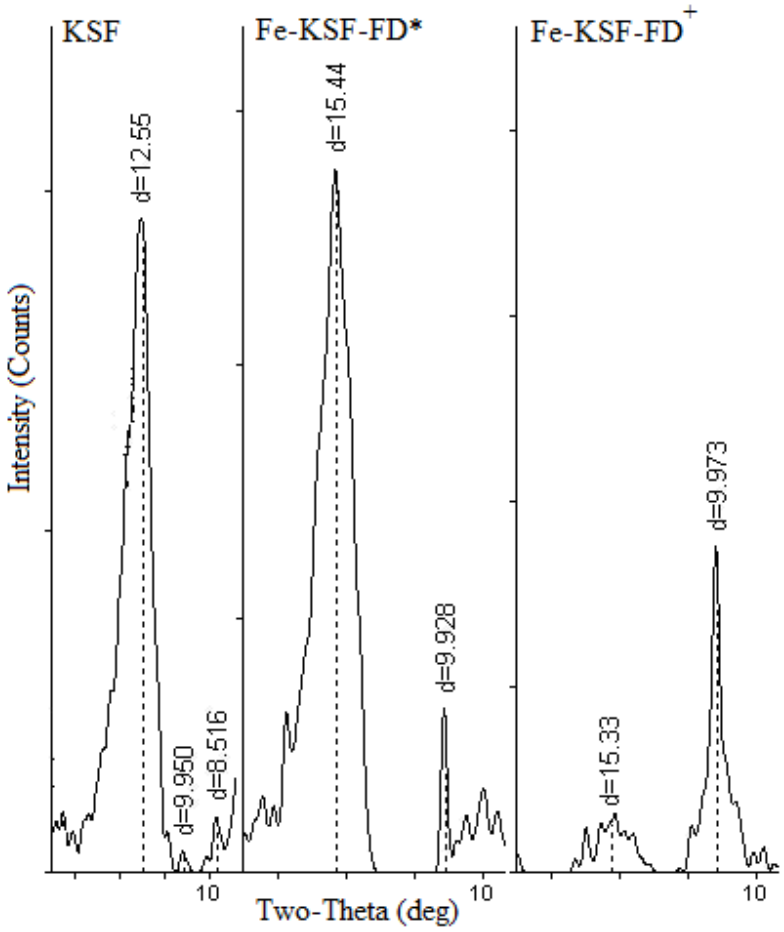

Figure 3.1 Comparison of XRD traces between the angles 0°-10° of KSF, Fe-KSF-FD* and Fe-KSF-FD^{+}.

Table 3.1 XRD results of montmorillonite KSF and its pillared clays

	Samples										
	KSF	Fe-KSF-FD*	Fe-KSF-FD^{+}	Zr-KSF-OD*	Zr-KSF-OD^{+}	Zr-KSF-FD^{+}	Al-KSF-OD* 20x	Al-KSF-OD^{+} 20x	Al-KSF-FD*	Al-KSF-FD^{+}	Al-KSF-OD^{+}
2θ	6.99°	5.73°	5.73°	4.60°	4.59°	4.60°	5.40°	5.54°	5.50°	5.54°	5.56°
d_{001} (Å)	12.55	15.44	15.33	19.49	19.15	19.13	16.40	15.82	15.99	15.82	15.88
d_{001}- 9.6(Å)[a]	-	5.84	5.73	9.89	9.55	9.53	6.80	6.22	6.39	6.22	6.28

[a] $d_{0\,0\,1}$ value of bone dry mineral, FD Freeze Dried, OD Oven Dried,* No calcination, $^{+}$ Calcination at 250°C, 20x 20 mmol Al/g clay and the other pillared clays are 10 mmol M/g clay.

Table 3.2 XRD results of montmorillonite K10 and its pillared clays

	Samples										
	K10	Fe-K10-FD*	Fe-K10-FD^{+}	Zr-K10-OD*	Zr-K10-OD^{+}	Zr-K10-FD^{+}	Al-K10-OD*20x	Al-K10-OD^{+} 20x	Al-K10-FD*	Al-K10-FD^{+}	Al-K10-OD^{+}
2θ	5.94°	4.90°	5.44°	5.70°	6.29°	5.21°	4.50°	4.80°	4.60°	6.05°	5.00°- 4.80°
d_{001} (Å)	14.83	18.56	16.29	15.45	14.02	16.93	19.60	18.78	19.35	14.56	17.67-18.46
d_{001}- 9.6 (Å)[a]	-	8.96	6.69	5.85	4.42	7.33	10.00	9.18	9.75	4.96	8.07-8.86

[a] $d_{0\,0\,1}$ value of bone dry mineral, FD Freeze Dried, OD Oven Dried,* No calsination, $^{+}$ Calsination at 250°C, 20x 20 mmol Al/g clay and the other pillared clays are 10 mmol M/g clay.

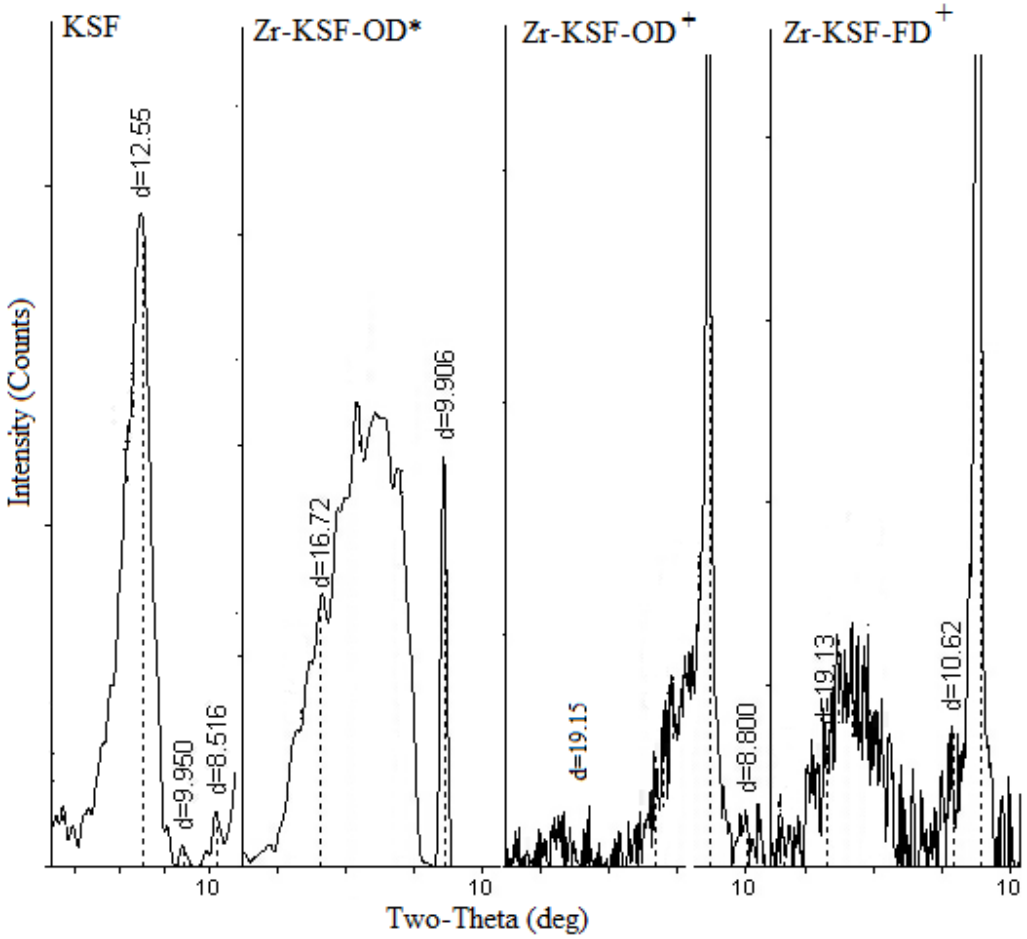

Figure 3.2 Comparison of XRD traces between the angles 0°-10° of KSF, Zr-KSF-OD*, Zr-KSF-OD^{+} and Zr-KSF-FD^{+}.

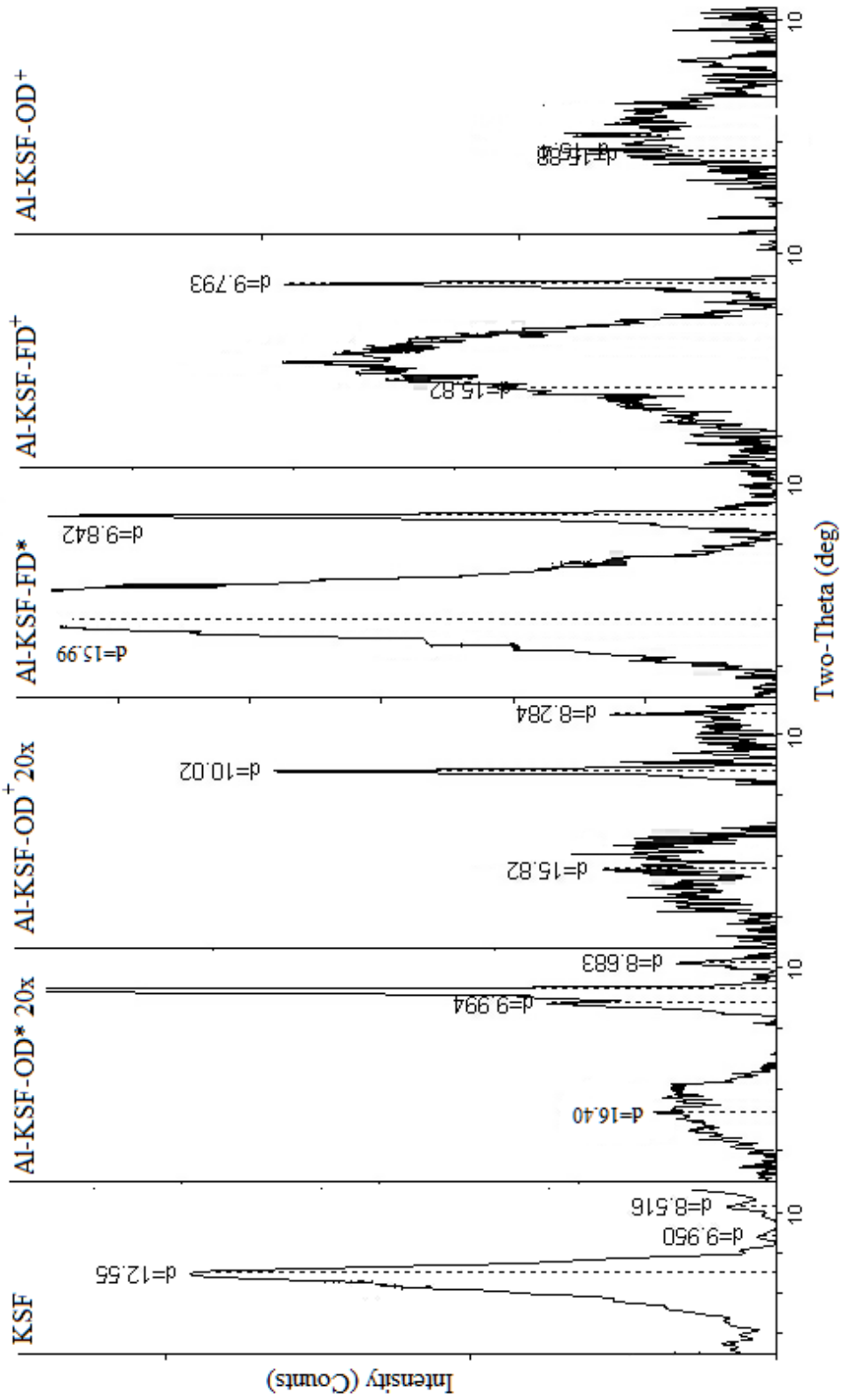

Figure 3.3 Comparison of XRD traces between the angles 0°-10° of KSF, Al-KSF-OD*20x, Al-KSF-OD^{+}20x, Al-KSF-FD*, Al-KSF-FD^{+} and Al-KSF-OD^{+}.

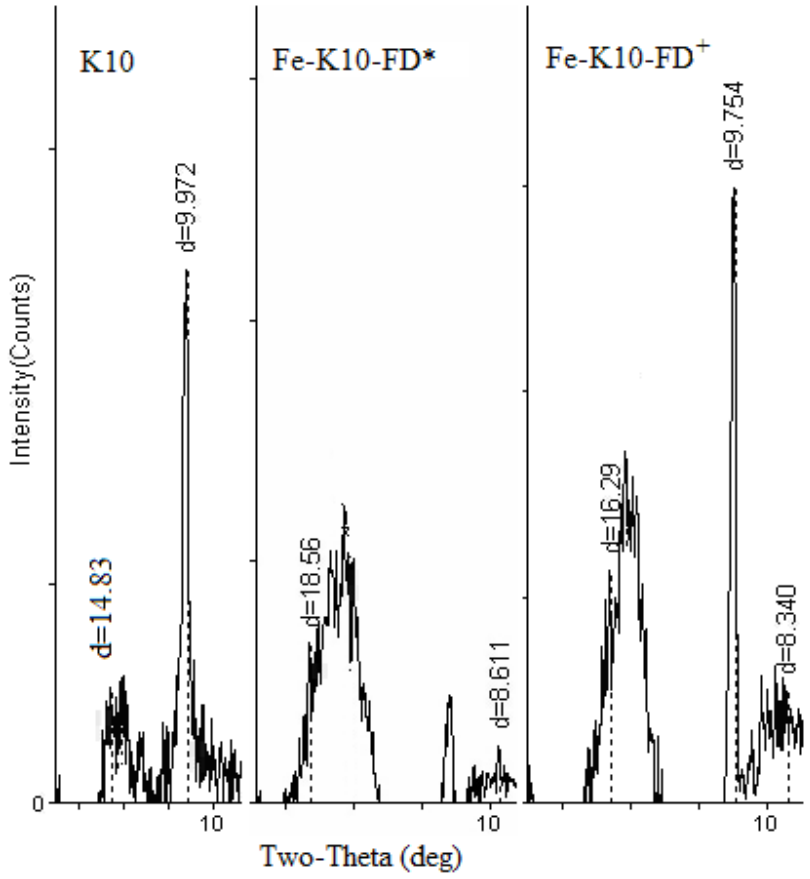

Figure 3.4 Comparison of XRD traces between the angles 0°-10° of K10, Fe-K10-FD* and Fe-K10-FD^{+}.

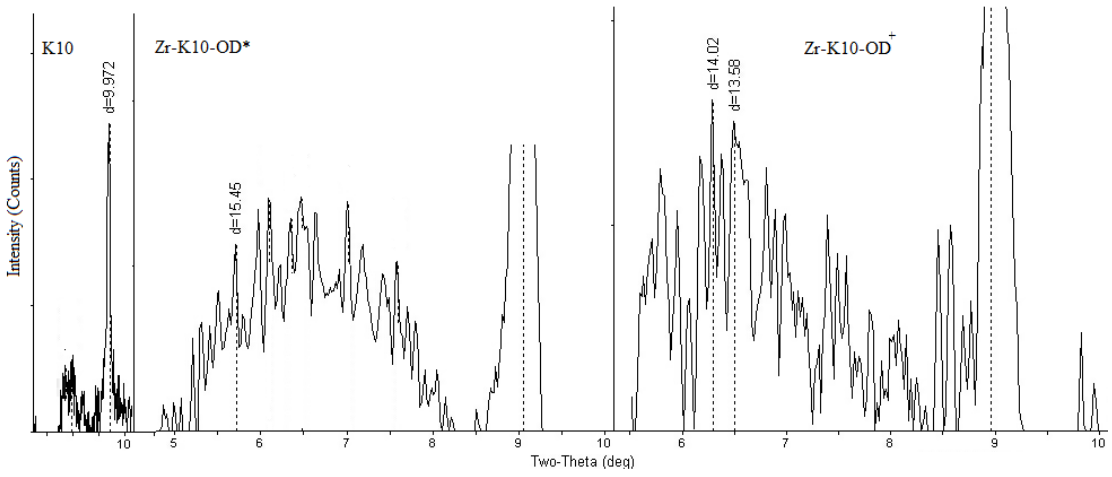

Figure 3.5 Comparison of XRD traces between the angles 0°-10° of K10, Zr-K10-OD* and Zr-K10-OD^{+}.

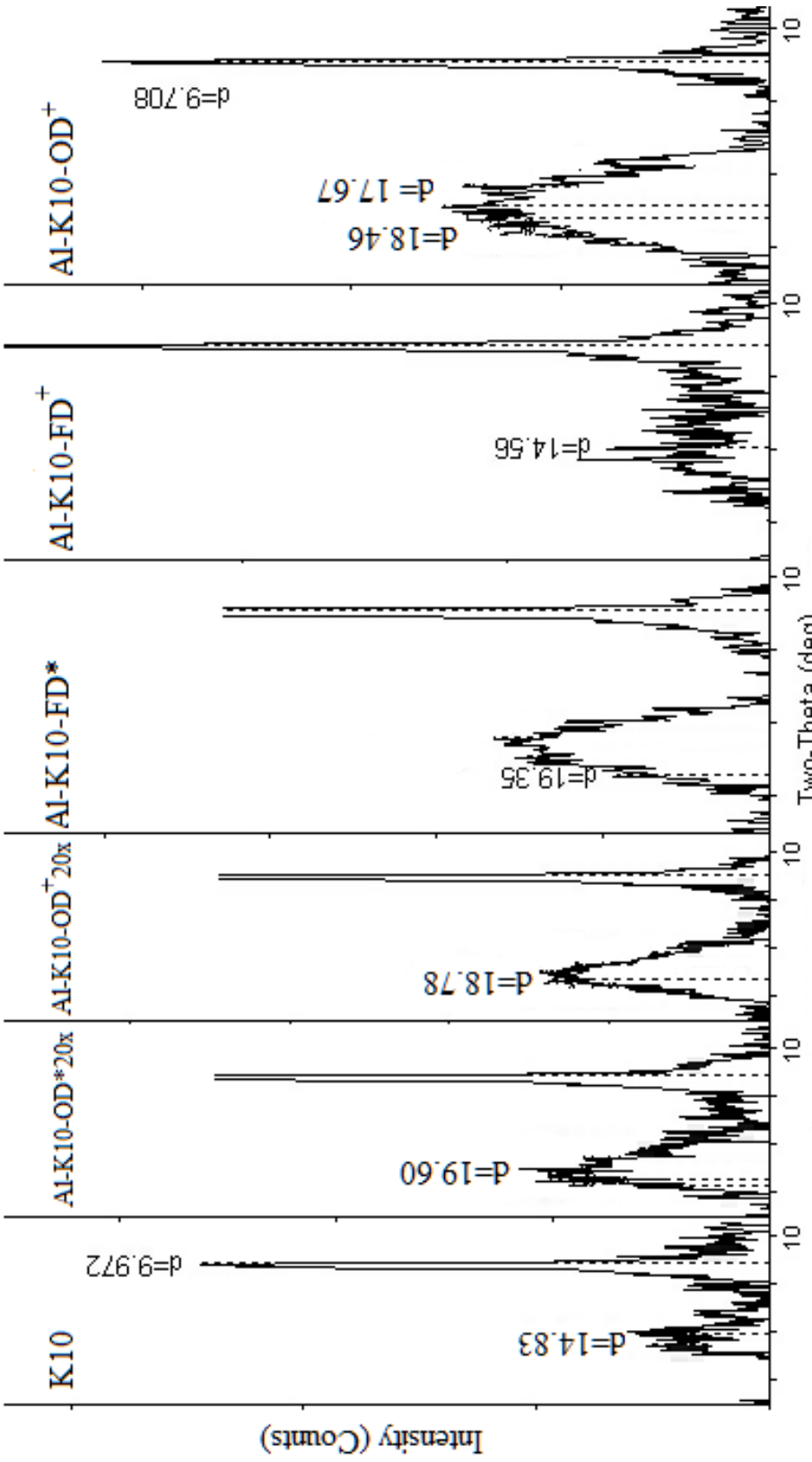

Figure 3.6 Comparison of XRD traces between the angles 0°-10° of K10, Al-K10-OD*20x, Al-K10-OD^{+}20x Al-K10-FD*, Al-K10-FD^{+} and Al-K10-OD^{+}.

3.1.2 FTIR analyses of pillared clays

The FTIR spectra results were summarized in Table 3.3 and 3.4. It can be observed that the two bands were observed around 3500 cm^{-1}, in the –OH stretching region. A broader band due to Al_2OH group of the octahedral layer was at about 3625 cm^{-1}. Stretching vibrations of water molecules may also contribute to –OH bands (3450 cm^{-1}). On pillaring, the band broadens due to the introduction of more –OH groups of the pillar, which is interpreted as an effect of pillaring. The broad absorption bands observed in clays and pillared clays at about 3625 cm^{-1} represent the fundamental stretching vibrations of different –OH groups present in Mg–OH–Al, Al–OH– Al and Fe–OH–Al units in the octahedral layer (Farmer, 1974). The decrease in intensity arises from the dehydration and dehydroxylation steps during pillaring. Band at around 1600 cm^{-1} is due to bending vibrations of water. Pillaring process replaces a large amount of interlayer cations that generally exist as hydrated and it decreases the intensity of –OH bands. PILCs have low amount of adsorbed/coordinated water due to the non-swellable nature. Thus, as a result of pillaring, intensity of the band around 1600 cm^{-1} decreases. The band around 1045 cm^{-1} is due to asymmetric stretching vibrations of SiO_2 (O–Si–O) tetrahedra. A band around 800 cm^{-1} is due to stretching vibration of Al_{IV} tetrahedra, when substitution of Al for Si is low; Al–OH–Al libration lies in the 915±950 cm^{-1} range. The weak band at about 690 cm^{-1} were assigned to O–Si–O asymmetric stretching and absorption at 526 cm^{-1} is due to bending vibration of Al–Si–O (cm^{-1}); the asymmetric bending mode of Si–O–Si band at 469 cm^{-1} as reported in silicate system (Olphen, Fripiat, 1979).

Concerning to pillared samples, an increase in the 3450 cm^{-1} /3625 cm^{-1} intensities ratio is visible with respect to the raw clay. This intensities increase in the 3450 cm^{-1} peak could be related to the presence of Al-polycations in the samples, forming pillars or not.

The retention of all bands as in parent montmorillonite in the framework region clearly shows that the basic clay layer structure remains unaffected on pillaring. These bands are slightly broader but their wavenumbers are almost the same as those of clays (the differences in their wavenumbers are not higher than 10 cm^{-1}). These results suggest that the complex is physically entrapped within the PILC structure.

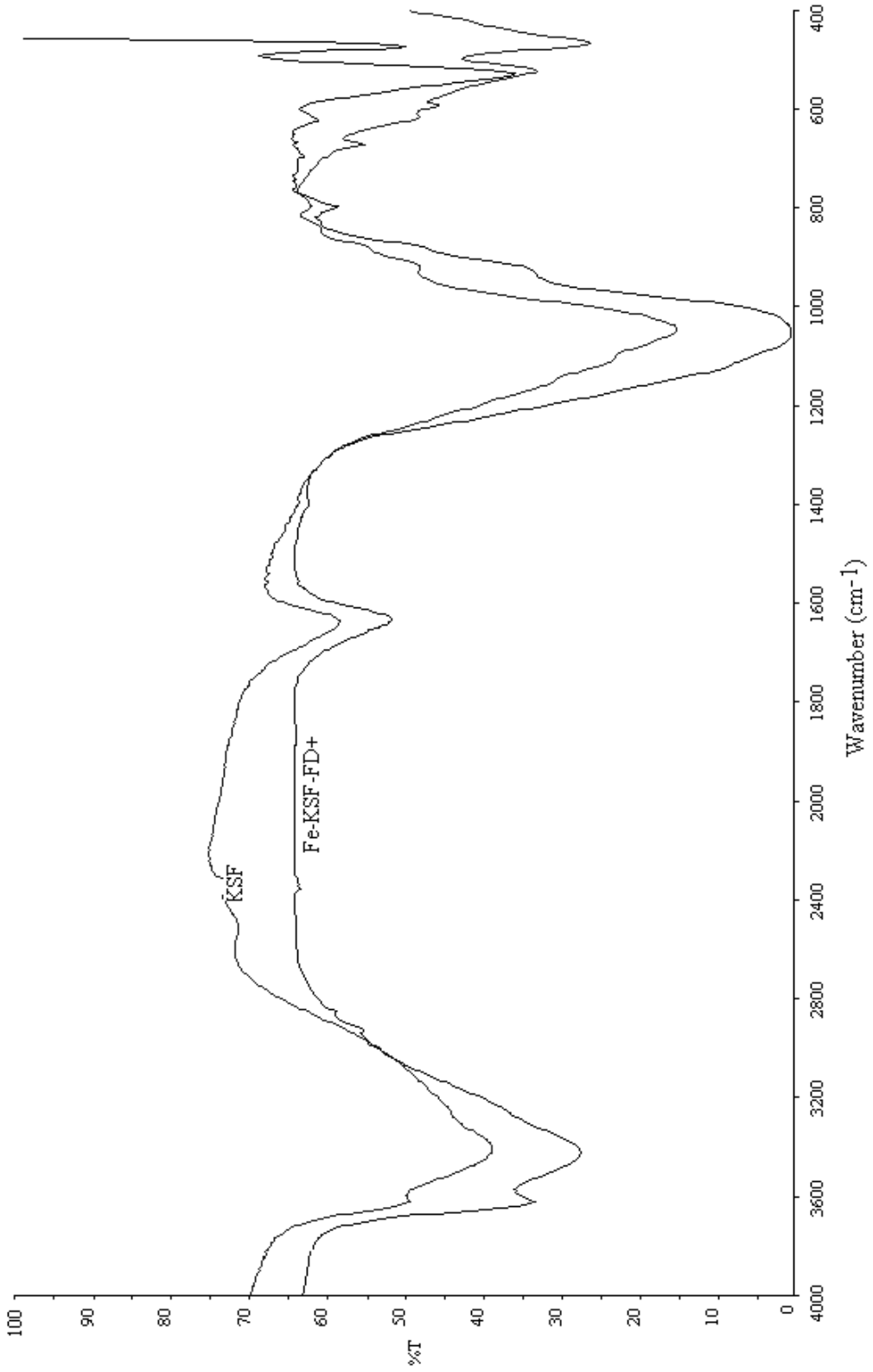

Figure 3.7 FTIR spectrum of KSF and Fe-KSF-FD^{+}

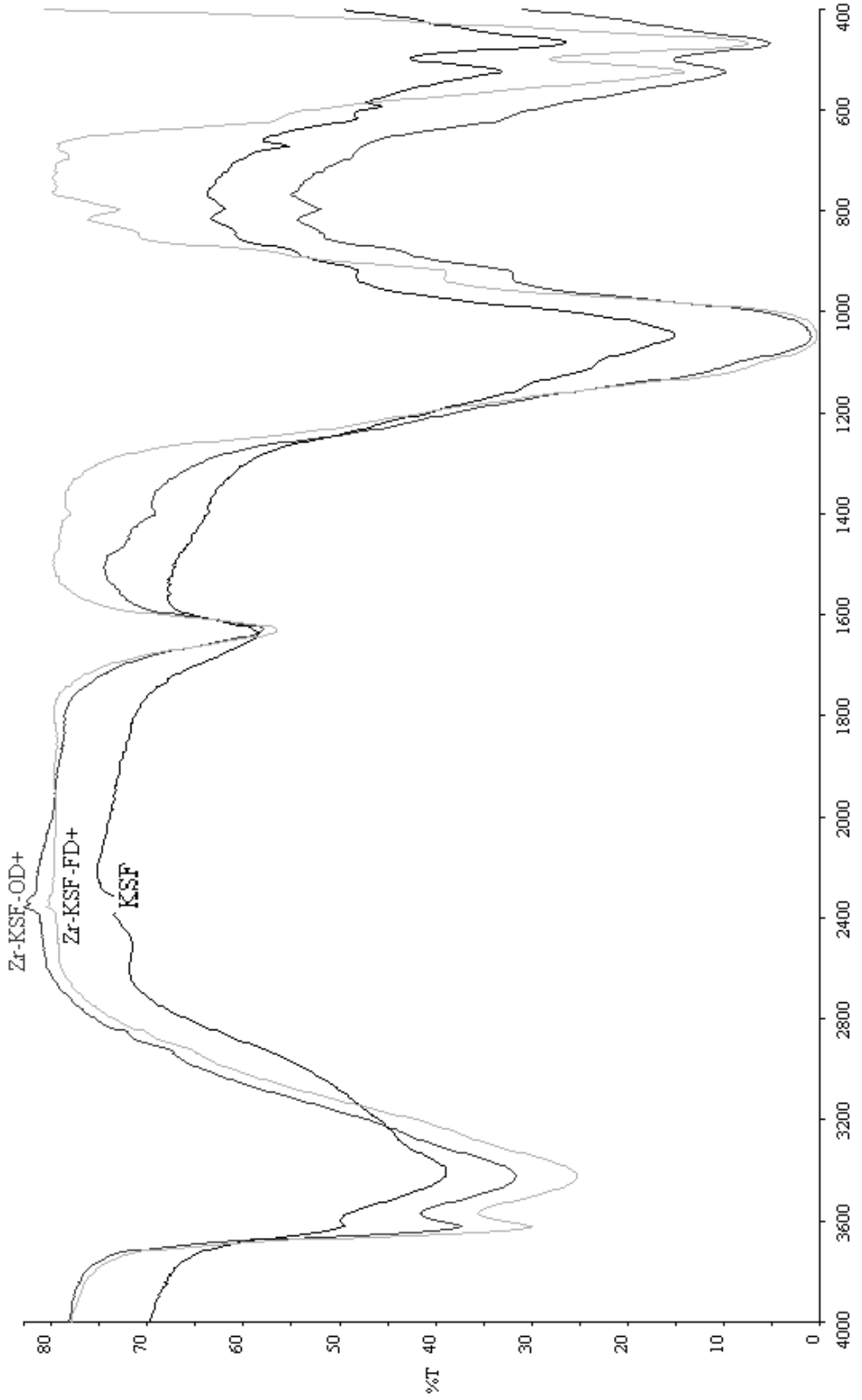

Figure 3.8 FTIR spectrum of KSF, Zr-KSF-FD^{+} and Zr-KSF-OD^{+}

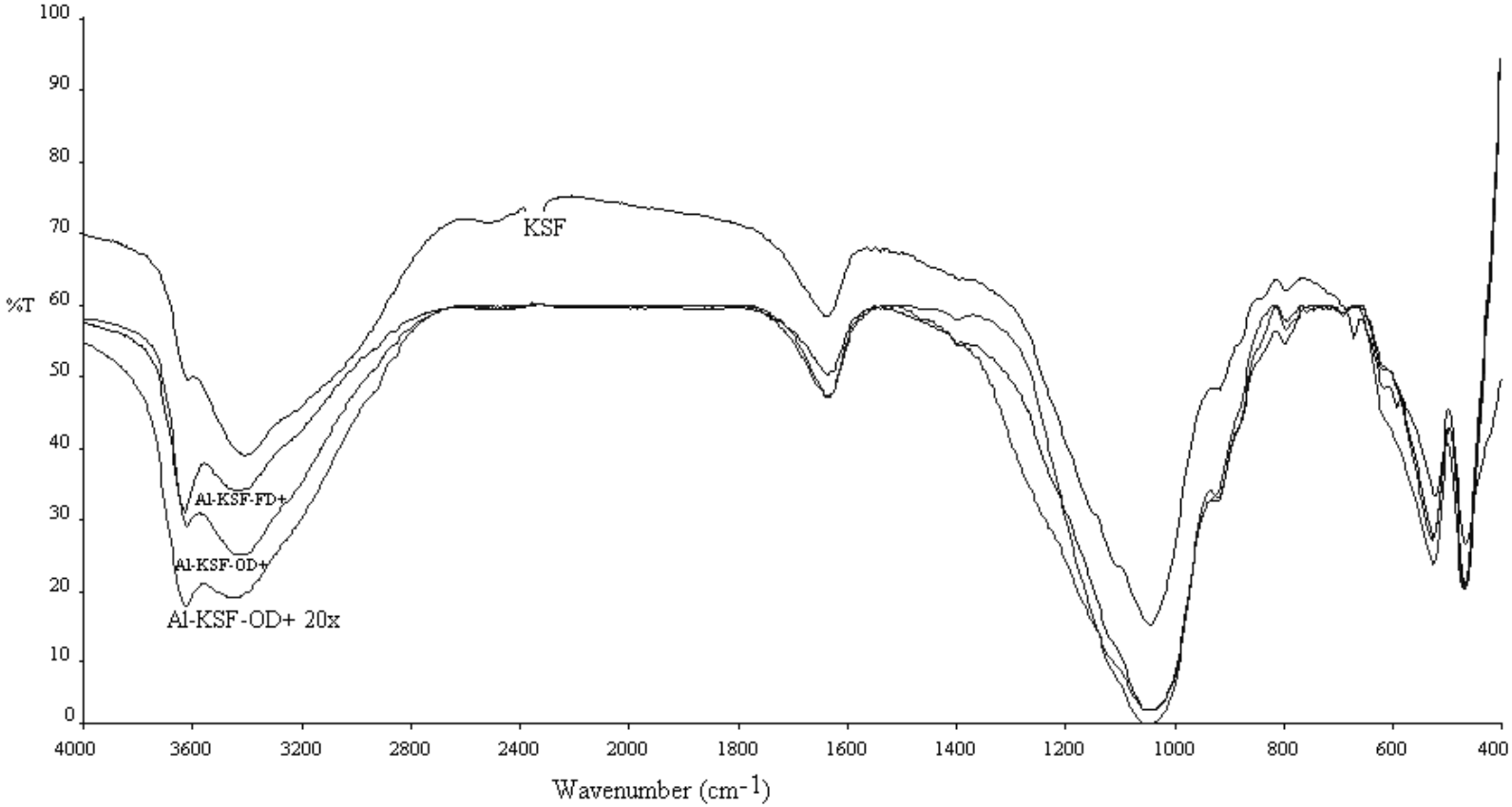

Figure 3.9 FTIR spectrum of KSF, Al-KSF-FD^{+}, Al-KSF-OD^{+} and Al-KSF-OD^{+} 20x

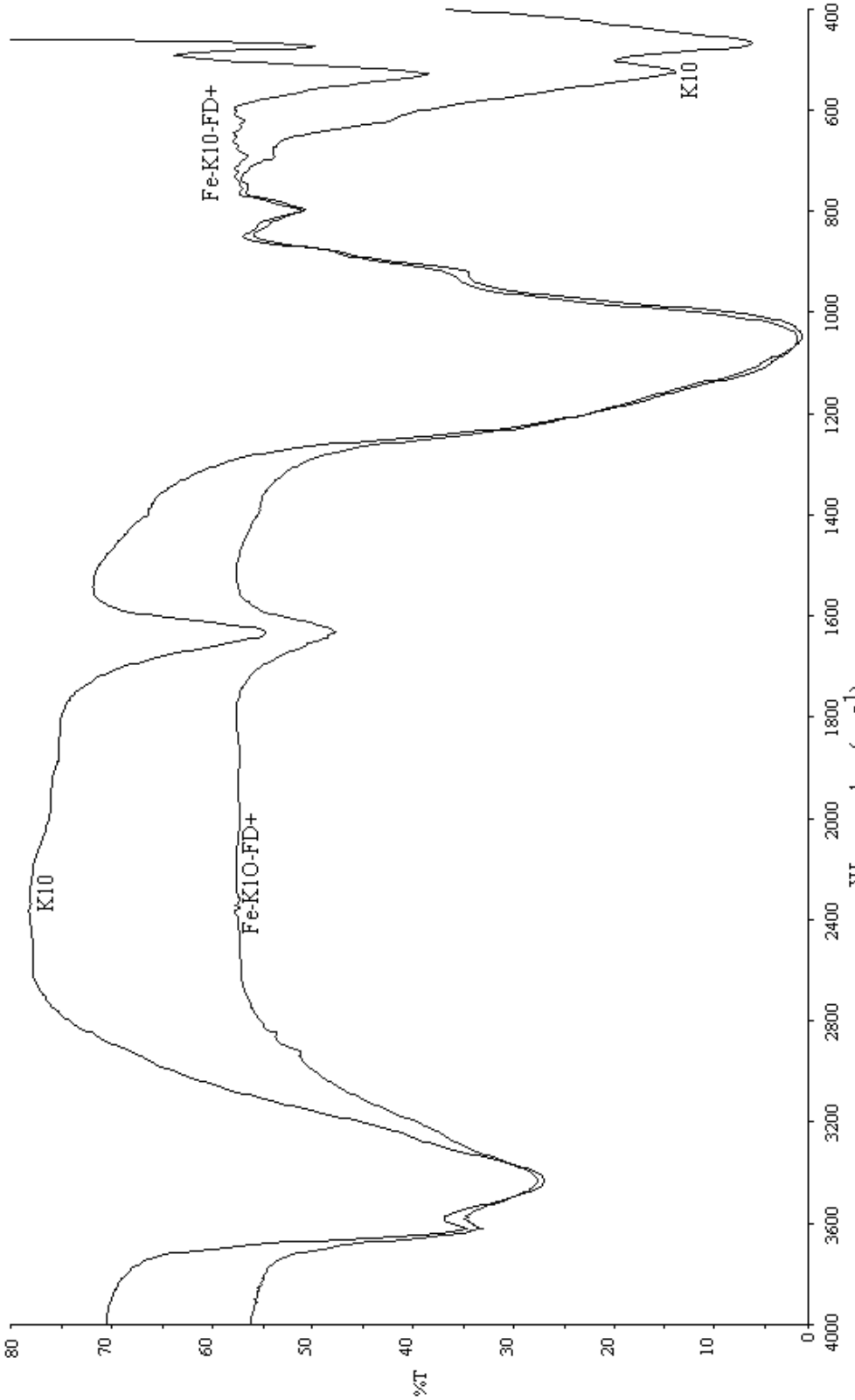

Figure 3.10 FTIR spectrum of K10 and Fe-K10-FD^{+}

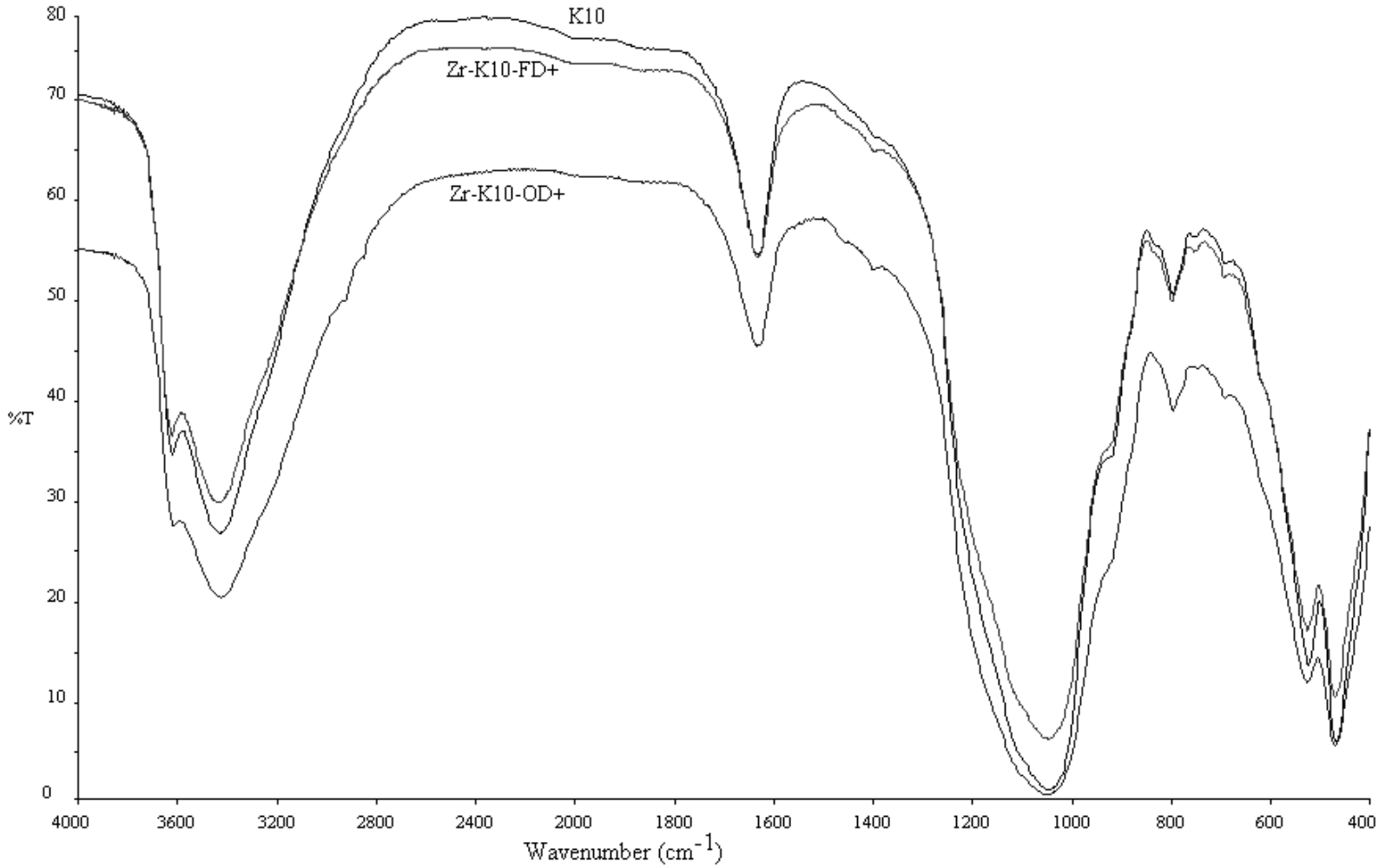

Figure 3.11 FTIR spectrum of K10, Zr-K10-FD^{+} and Zr-K10-OD^{+}

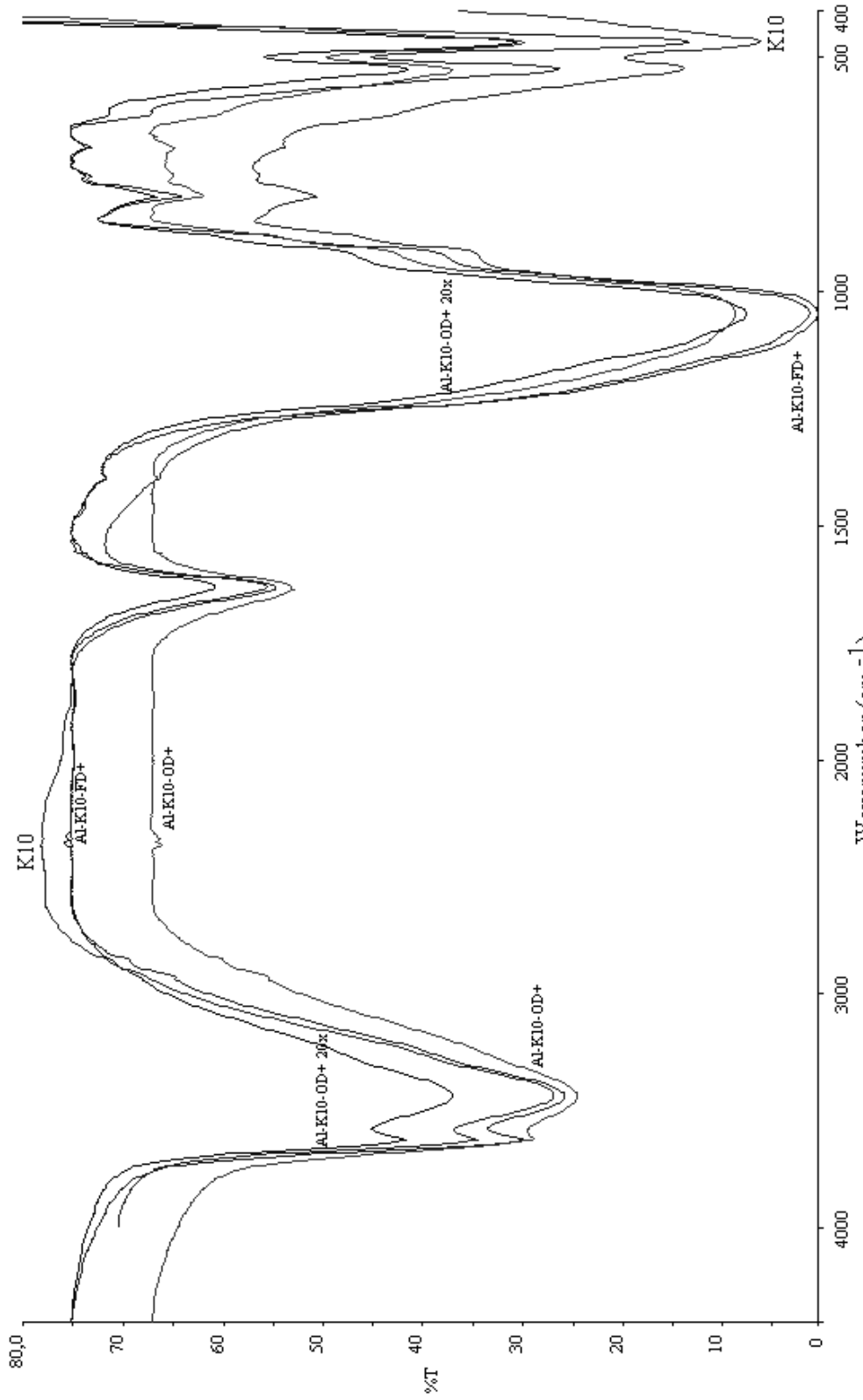

Figure 3.12 FTIR spectrum of K10, Al-K10-FD$^+$, Al-K10-OD$^+$ and Al-K10-OD$^+$ 20x

Table 3.3 The characteristic FT-IR data of KSF and its pillared clays

IR bands	Samples						
	KSF	**Fe-KSF-FD$^+$**	**Zr-KSF-OD$^+$**	**Zr-KSF-FD$^+$**	**Al-KSF-OD$^+$ 20x**	**Al-KSF-FD$^+$**	**Al-KSF-OD$^+$**
Al_2OH(octahedral layer) (cm^{-1})	3623	3626	3626	3626	3627	3630	3619
Streching vibrations of H_2O (cm^{-1})	3412	3428	3427	3429	3445	3436	3428
Bending vibrations of H_2O (cm^{-1})	1636	1634	1630	1630	1639	1637	1634
Asymmetric streching vibrations of SiO_2 tetrahedra (cm^{-1})	1043	1054	1048	1045	1048	1048	1050
Bending vibrations of Al_2OH (cm^{-1})	912	927	918	918	926	926	926
Streching vibration of Al^{IV} tetrahedra (cm^{-1})	795	799	795	795	794	797	798
Si–O–Si asymmetric stretching vibrations (cm^{-1})	674	692	692	692	69	671	690
Bending vibration of Al–Si–O (cm^{-1})	524	530	526	525	526	526	529
Bending vibration of Si–O–Si (cm^{-1})	468	474	470	469	469	468	472

Table 3.4 The characteristic FT-IR data of K10 and its pillared clays

IR bands	Samples						
	K10	**Fe-K10-FD$^+$**	**Zr-K10-OD$^+$**	**Zr-K10-FD$^+$**	**Al-K10-OD$^+$ 20x**	**Al-K10-FD$^+$**	**Al-K10-OD$^+$**
Al_2OH(octahedral layer) (cm^{-1})	3624	3619	3616	3624	3624	3623	3616
Streching vibrations of H_2O (cm^{-1})	3434	3434	3429	3436	3435	3436	3436
Bending vibrations of H_2O (cm^{-1})	1634	1633	1636	1633	1630	1630	1636
Asymmetric streching vibrations of SiO_2 tetrahedra (cm^{-1})	1048	1054	1054	1046	1048	1049	1047
Bending vibrations of Al_2OH (cm^{-1})	917	926	921	921	918	924	918
Streching vibration of Al^{IV} tetrahedra (cm^{-1})	798	799	797	798	798	798	796
Si–O–Si asymmetric stretching vibrations (cm^{-1})	694	693	692	692	695	693	692
Bending vibration of Al–Si–O (cm^{-1})	525	530	526	525	527	526	528
Bending vibration of Si–O–Si (cm^{-1})	469	474	472	469	470	470	471

3.1.3 SEM analyses of pillared clays

The SEM micrographs of pillared clays give information about only morphology; this information was supported the characterization by the other methods. SEM images of clays and pillared clays were illustrated in Figure 3.13 - 3.18.

Figure 3.13 showed representative micrographs of KSF (10000x magnification), Fe-KSF-FD* (5000x magnification), Fe-KSF-FD^{+} (10000x magnification). The KSF has a structure of abundant layers. The structure of the clay was retained in the pillared clays before and after calcinations at 250°C but the morphology of clay was influenced by pillaring. This suggestion was supported by the other characterization method for example by FTIR, XRD. The samples showed broad network structure.

The montmorillonites appears as corn flake like crystals with fluffy appearance revealing its extremely fine platy structure. After pillaring, clay has become fluffier. Similar changes were observed on morphology of the precursor clay by pillaring when examined the micrographs of the pillared clay. To clarify the effect of freeze drying on the Zr pillared clay, SEM micrographs cleared that freeze drying might caused the compact structure than oven dried. As seen in Figure 3.15, while the amount of pillaring agent was increased, the layered structure of clay became more tightly. When examined Figure 3.18(e), porous structure of freeze dried Aluminium pillared K10 calcinated at 250°C was determined more clearly. Consequently, for our observation, more tightly structure was obtained by dried by freeze drying. Otherwise, fluffy appearance was seen at pillaring clays by oven drying. Pillared clays prepared by using K10 were made up of more pieces than of KSF.

When the EDS analyses of pillared clays were examined, the pillaring agent ratio was increased by pillaring.

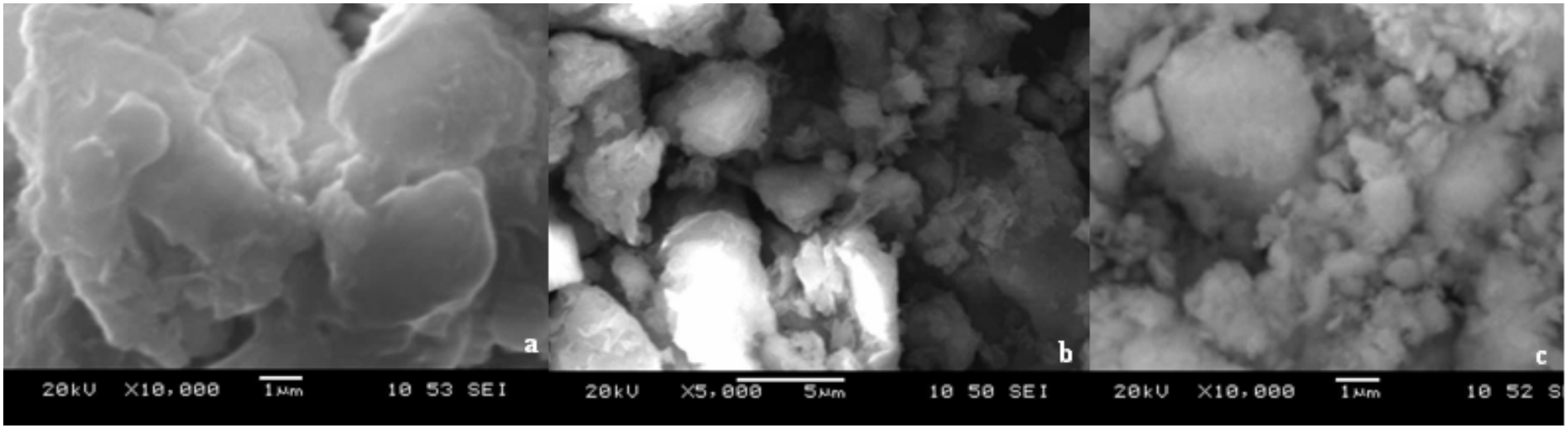

Figure 3.13 SEM micrographs of (a) KSF (10000x magnification) (b) Fe-KSF-FD* (5000x magnification) (c) Fe-KSF-FD^{+} (10000x magnification)

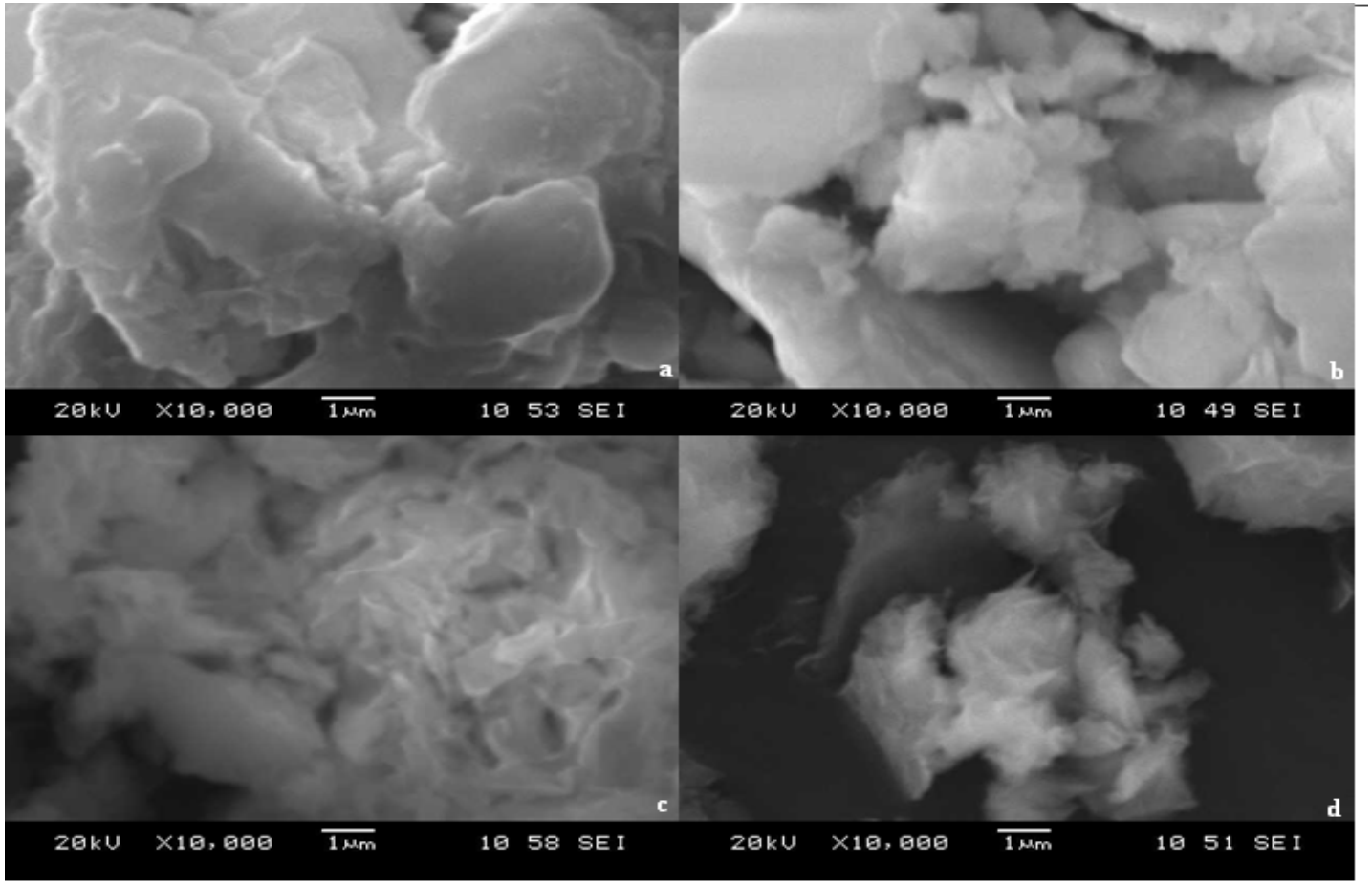

Figure 3.14 SEM micrographs of (a) KSF (10000x magnification) (b) Zr-KSF-OD* (10000x magnification) (c) Zr-KSF-OD^{+} (10000x magnification) (d) Zr-KSF-FD^{+} (10000x magnification)

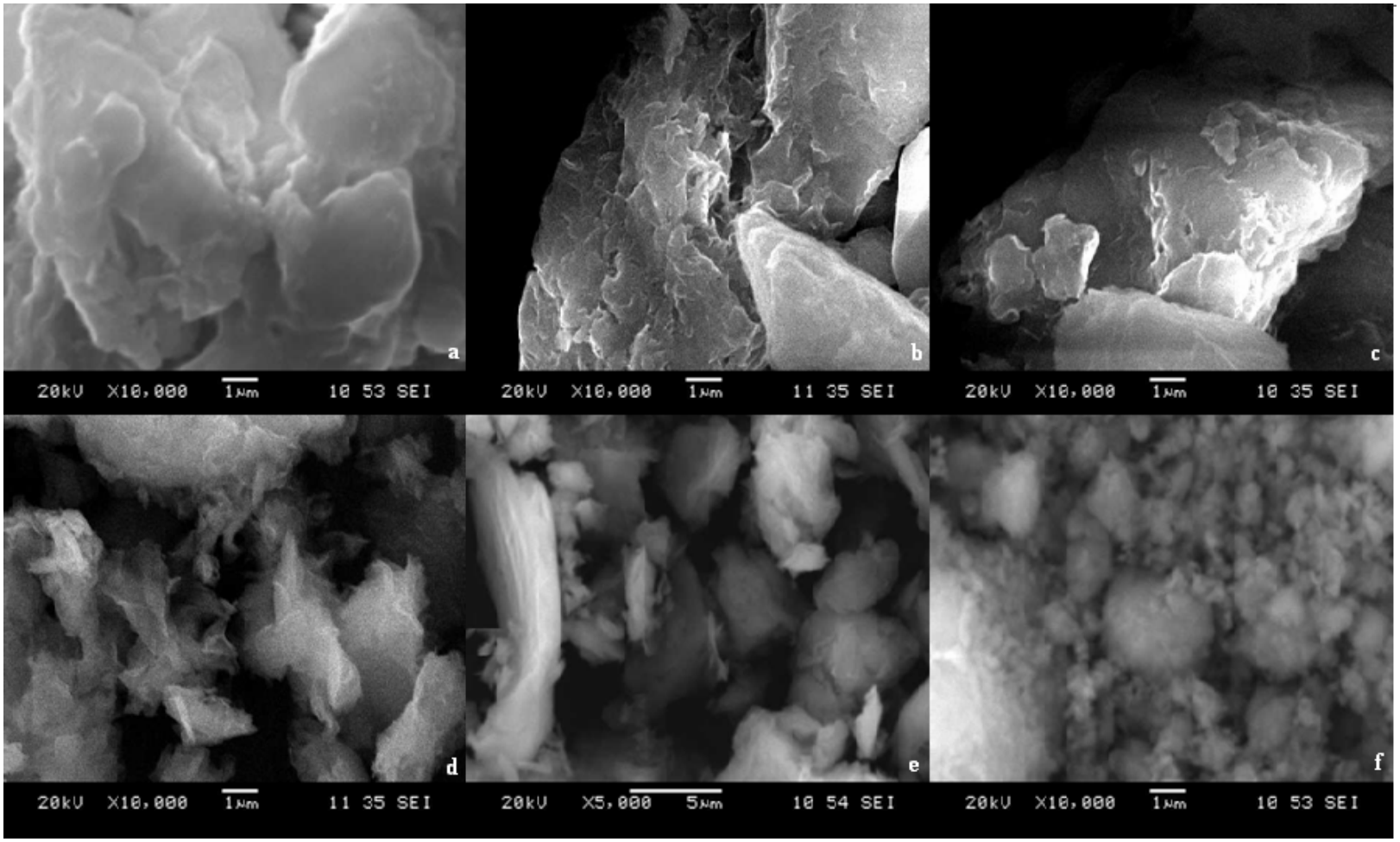

Figure 3.15 SEM micrographs of (a)KSF (10000x magnification) (b)Al-KSF-OD*20x (10000x magnification) (c)Al-KSF-OD^{+}20x (10000x magnification) (d)Al-KSF-FD* (10000x magnification) (e) Al-KSF-FD^{+} (5000x magnification) (f)Al-KSF-OD^{+} (10000x magnification)

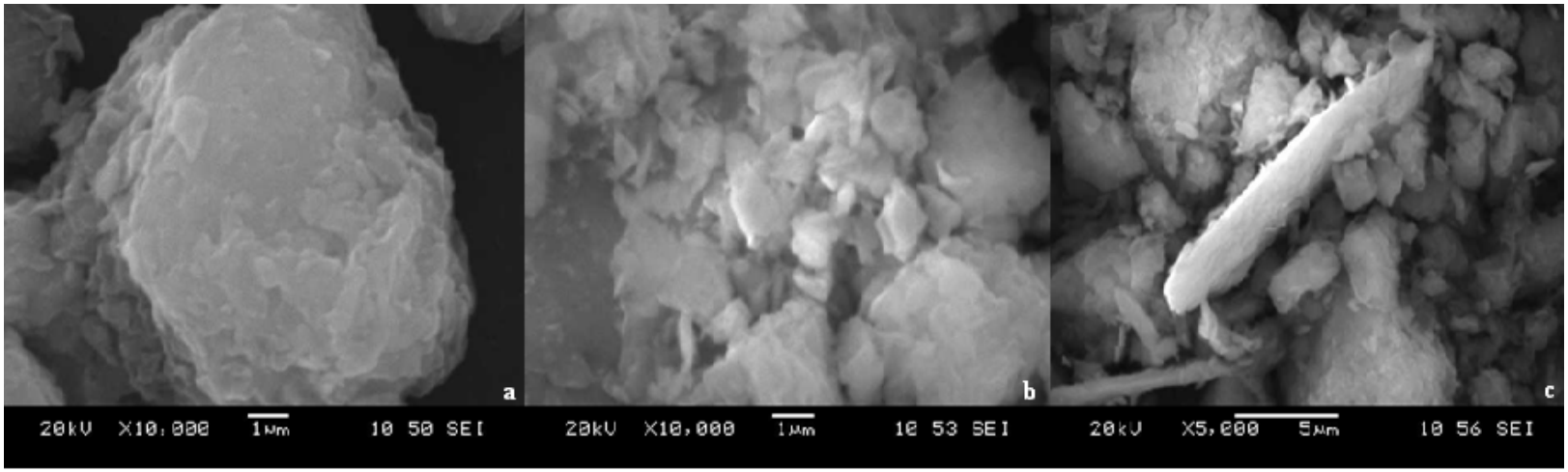

Figure 3.16 SEM micrographs of (a) K10 (10000x magnification) (b) Fe-K10-FD* (5000x magnification) (c) Fe-K10-FD^{+} (10000x magnification)

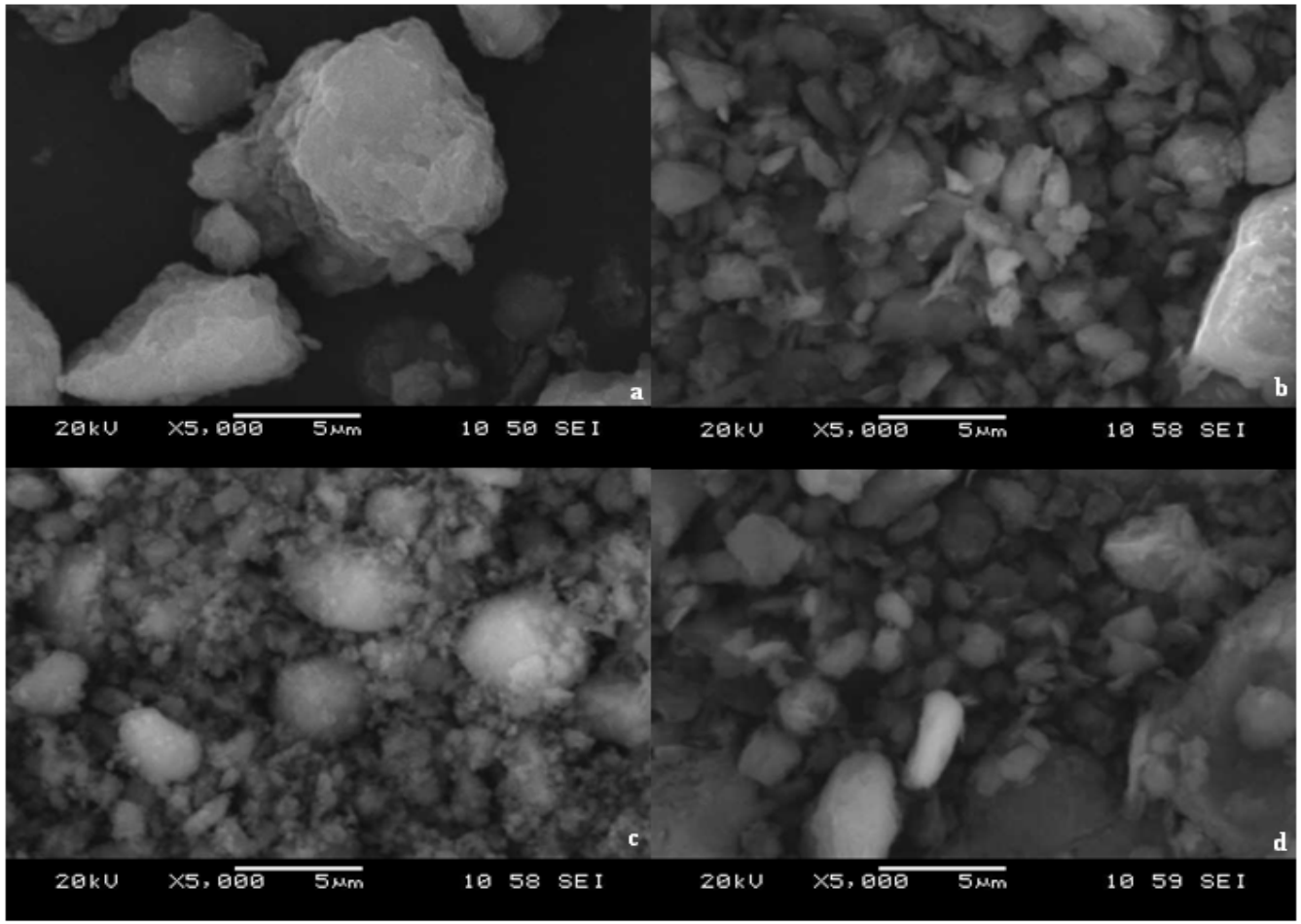

Figure 3.17 SEM micrographs of (a) K10 (5000x magnification) (b) Zr-K10-OD* (5000x magnification) (c) Zr-K10-OD^{+} (5000x magnification) (d) Zr-K10-FD^{+} (5000x magnification)

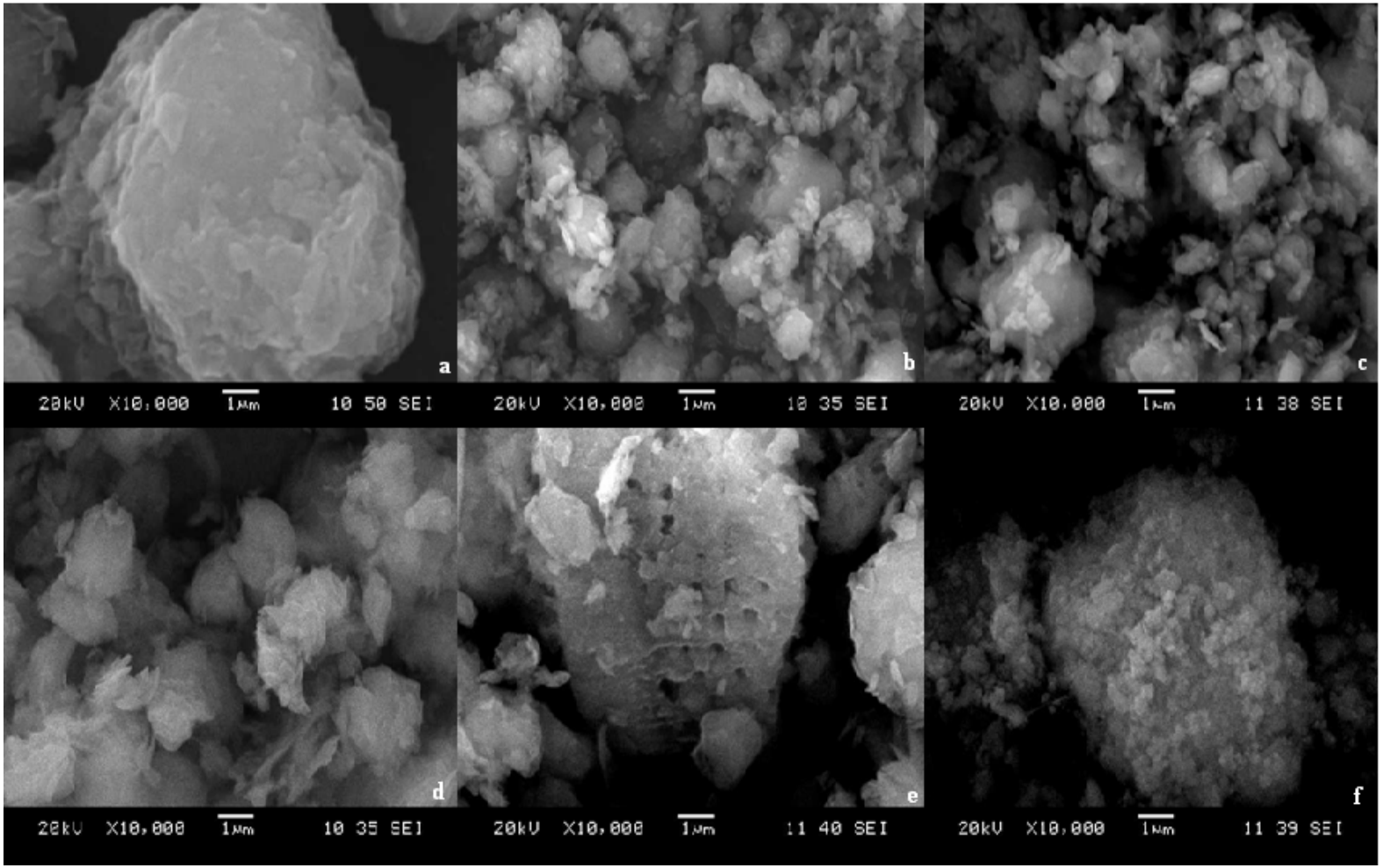

Figure 3.18 SEM micrographs of (a)K10 (10000x magnification) (b)Al-K10-OD*20x (10000x magnification) (c)Al-K10-OD^{+}20x (10000x magnification) (d)Al-K10-FD* (10000x magnification) (e) Al-K10-FD^{+} (10000x magnification) (f)Al-K10-OD^{+} (10000x magnification)

3.1.4 N_2 adsorption–desorption isotherms of pillared clays

Figures of 3.19-3.30 showed the nitrogen adsorption–desorption isotherms of pillared clays. The BET surface areas were measured. The nitrogen adsorption–desorption isotherms of all pillared clays exhibit type IV of the BDDT classification, with a well defined H4 hysteresis loop (Sing et al., 1972). This shape corresponds to narrow slit-like pores. The textural characteristics of the samples obtained from the analysis of these isotherms are given in Table 3.5. The BET surface areas (S_{BET}), Total pore volumes (V_{total}) and average pore diameter (l_p) were summarized in Table 3.5.

Table 3.5 The structure characteristics of aluminum pillared clay

Sample	**S_{BET} (m^2/g)**	**V_{total} (ml/g)**	**l_p (nm)**	**l_{DH} (nm)**
Fe-KSF-FD$^+$	135	0.254	7.502	3.933
Zr-KSF-OD$^+$	99	0.140	5.642	4.176
Zr-KSF-FD$^+$	117	0.173	5.886	3.934
Al-KSF-OD$^+$ 20x	46	0.063	5.501	4.165
Al-KSF-FD$^+$	77	0.123	6.402	4.172
Al-KSF-OD$^+$	28	0.090	12.78	4.164
Fe-K10-FD$^+$	244	0.361	5.913	3.709
Zr-K10-OD$^+$	223	0.314	5.638	3.710
Zr-K10-FD$^+$	237	0.336	5.676	3.715
Al-K10-OD$^+$ 20x	130	0.238	7.302	3.711
Al-K10-FD$^+$	234	0.364	6.208	3.715
Al-K10-OD$^+$	216	0.348	6.438	3.709

Fe-KSF-FD$^+$ had the highest BET surface area, total pore volume and average pore diameter between the pillared KSF samples. This might be affected the freeze drying and pillaring agent. When textural characteristics of all samples were examined, pillared clays freeze dried had the high surface areas than pillared clays oven dried. As can be

seen from Table 3.5 that freeze drying was more effective compared with the oven drying. Fe-K10-FD^+ had higher BET surface area than of Fe-KSF-FD^+ due to the precursor clays. Pillared clays which were synthesized by using K10 montmorillonite had higher textural characteristics because KSF and K10 had a surface area of 20-40 m^2/g and 197m^2/g, respectively. Fe-K10-FD^+ had the highest BET surface area than all pillared clays. Fe-K10-FD^+ and Al-K10-FD^+ had highest total pore volume. Otherwise Al-KSF-OD^+ had the highest average pore diameter. Al-KSF-OD^+ 20x had higher BET surface area than Al-KSF-OD^+ because of carrying keggin ion two times than Al-KSF-OD^+. But this approach was not ruled for Al-K10-OD^+ 20x and Al-KSF-OD^+. Pore size distribution analysis data which was obtained from N_2 adsorption–desorption experiments on the samples and evaluated according to the Dollimore–Heal method (Dollimore, Heal, 1964) showed that all the samples had a pore width of ~4 nm. Al-K10-OD^+ 20x had smaller surface area than precursor clay of K10. It might be result of coke formation which might be filled the pores or closed the pore openings during calcinations or not properly decomposing of precursors. It can be seen that the average pore diameters were about 5-13 nm, which was an obvious mesoporous layered structure. As a result of N_2 adsorption–desorption isotherms, it was concluded that pillared clays had much greater surface areas than K10 and KSF. It was beneficial for catalysis and adsorption studies.

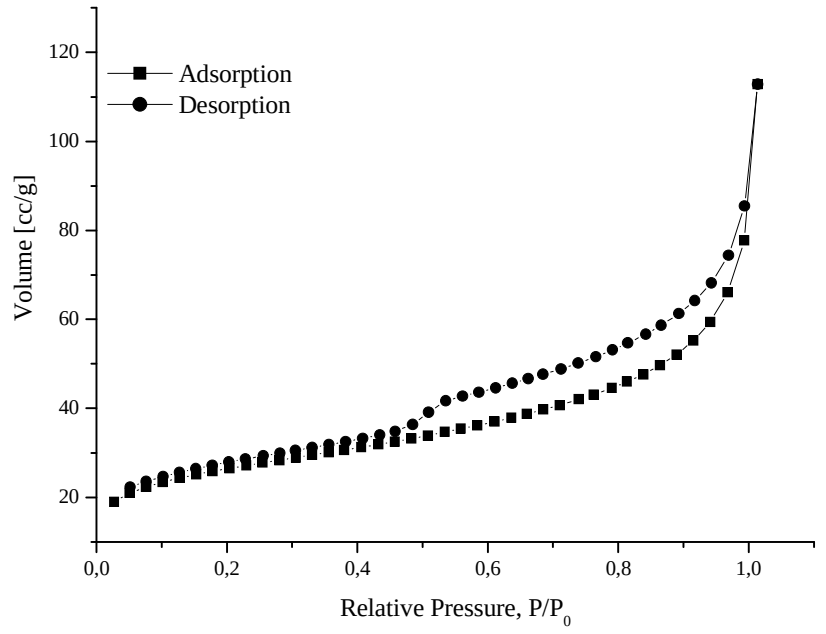

Figure 3.19 The N_2 adsorption–desorption isotherms at 77 K for Fe-KSF-FD$^+$

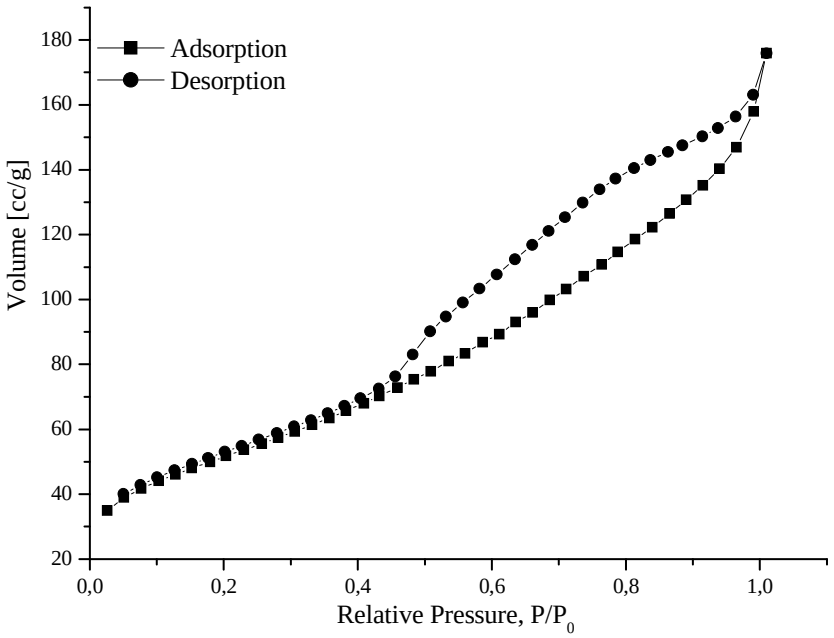

Figure 3.20 The N_2 adsorption–desorption isotherms at 77 K for Fe-K10-FD$^+$

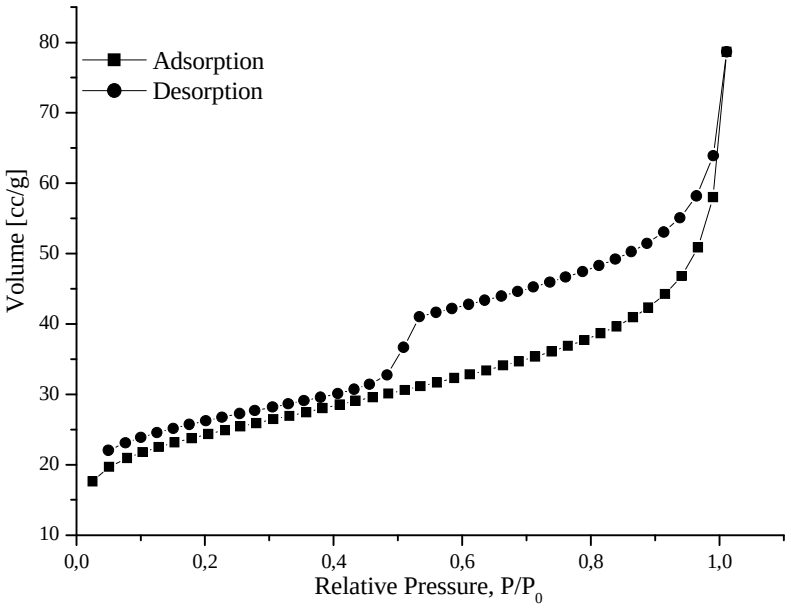

Figure 3.21 The N_2 adsorption–desorption isotherms at 77 K for Zr-KSF-OD^+

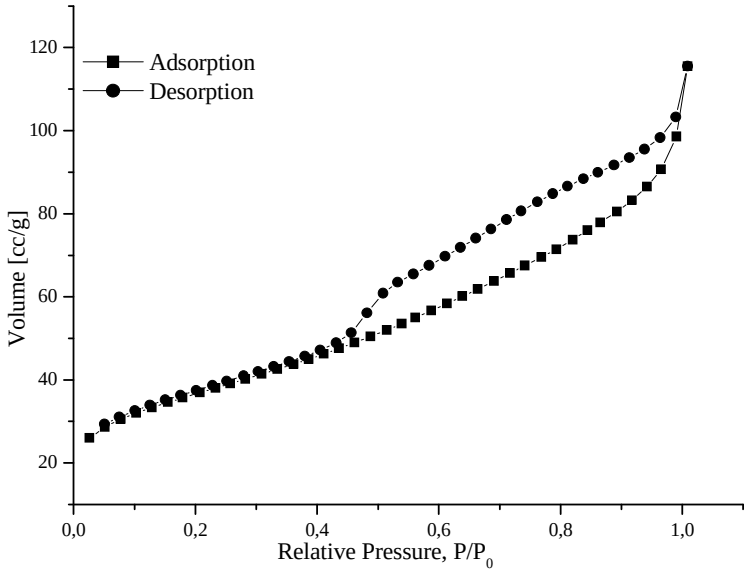

Figure 3.22 The N_2 adsorption–desorption isotherms at 77 K for Zr-K10-OD^+

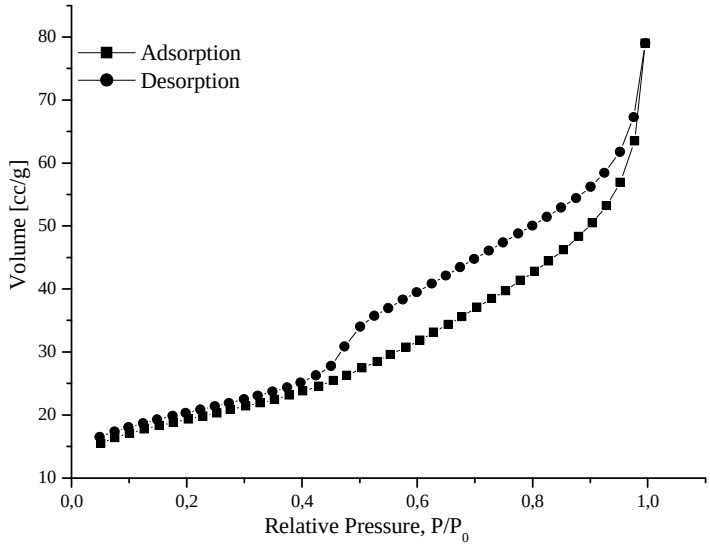

Figure 3.23 The N_2 adsorption–desorption isotherms at 77 K for Al-K10-OD^+ 20x

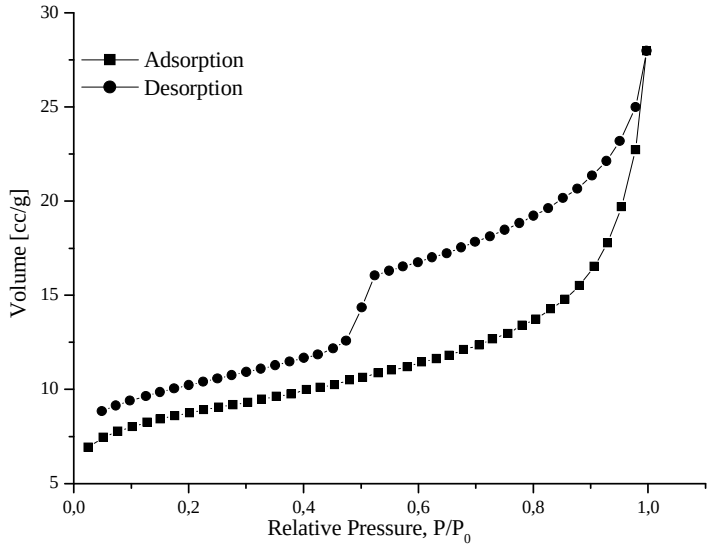

Figure 3.24 The N_2 adsorption–desorption isotherms at 77 K for Al-KSF-OD^+ 20x

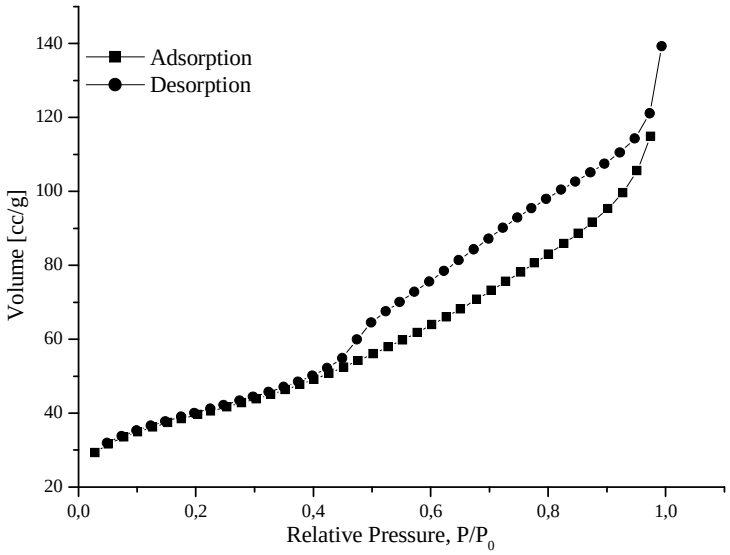

Figure 3.25 The N_2 adsorption–desorption isotherms at 77 K for Al-K10-FD^+

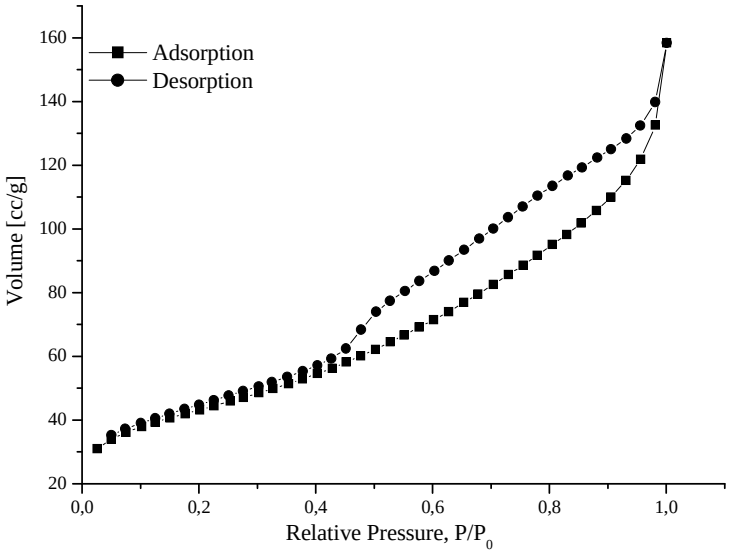

Figure 3.26 The N_2 adsorption–desorption isotherms at 77 K for Al-K10-OD^+

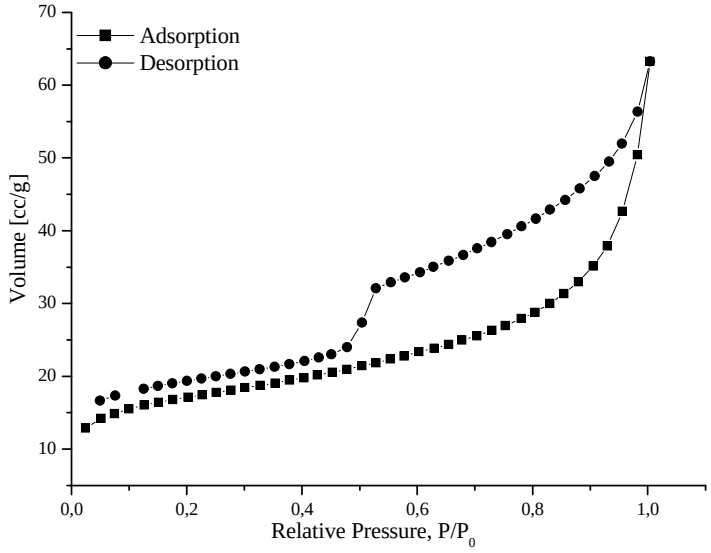

Figure 3.27 The N_2 adsorption–desorption isotherms at 77 K for Al-KSF-FD^+

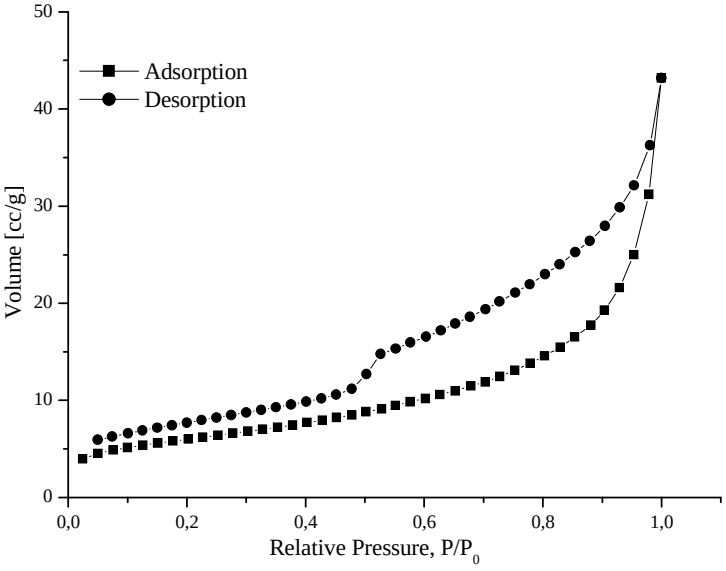

Figure 3.28 The N_2 adsorption–desorption isotherms at 77 K for Al-KSF-OD^+

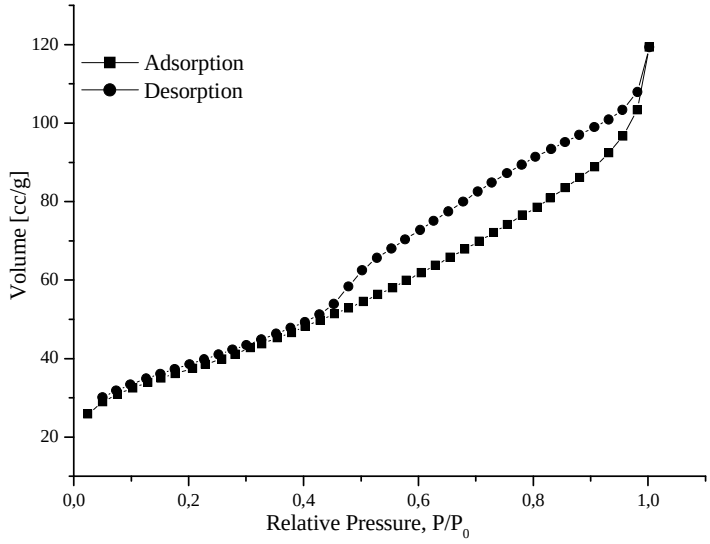

Figure 3.29 The N_2 adsorption–desorption isotherms at 77 K for Zr-K10-FD$^+$

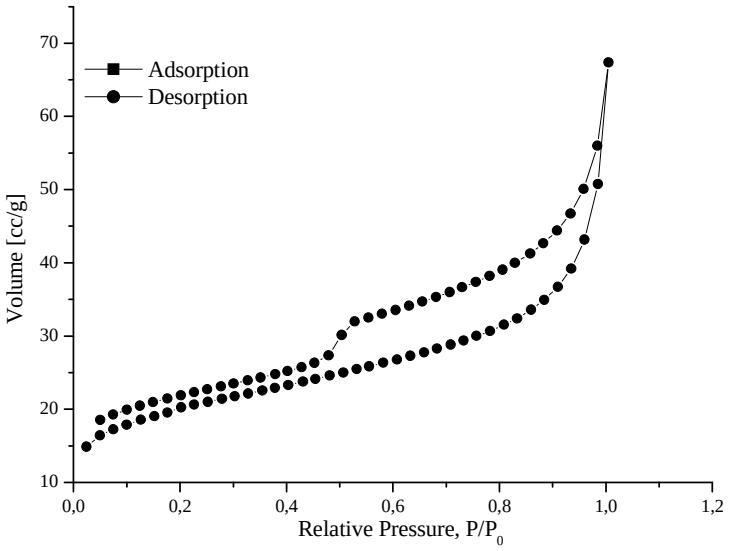

Figure 3.30 The N_2 adsorption–desorption isotherms at 77 K for Zr-KSF-FD$^+$

3.1.5 TGA analyses of pillared clays

The thermogravimetric analysis curves of pillared clays and parent clays were shown in Figures 3.31-3.40. Weight loses and inflection points were summarized in Table 3.6 in detail for all samples. The thermogravimetric analysis of clays and pillared clays revealed a weight loss on heating in the range of 20 to 300°C which can be attributed to elimination of physical adsorbed water. The first step mass losses might be assigned to desorption of water, the second step can be related to the dehydroxylation of OH groups on the internal and/or external surface of the samples. On the other hand, the weight losses in the second stage have been assigned to the removal of chemisorbed water, water molecules coordinated to the pillars and dehydroxylation of the pillars. The weight loss corresponding to the latter process is found to be occurring in the temperature range of 425 °C–650 °C (Binitha, Sugunan, 2006). Likewise, inflection points were found after 800°C for both raw clays and pillared clays due to the collapse of the clay structure. Most of the lost water was water adsorbed at the surface, being lost at temperatures lower than 200°C. The water associated with the micropore structure of the PILC (dehydroxylation of hydroxide groups associated with interlayer pillars) was occurred after this temperature. Between 500 and 900°C, an additional amount of water was lost with a low weight change above 800°C. As shown in thermogravimetric curves of clays and pillared clays, the decomposition of clay only occurred up to 800 °C. It was understood from the Table 3.6, pillared clays based on montmorillonite K10, the weight losses were higher than the unpillared form of clay. Higher weight losses were due to the –OH of pillaring agent. It was supported the pillaring of K10. When examined the pillaring clay based KSF montmorillonite, weight losses upon the physical adsorbed water were increased by pillaring. Furthermore the weight losses related to chemical adsorbed water or hydroxyl groups of interlayer pillars were decreased for Fe-KSF-FD* and Zr-KSF-OD*. The value of dehydroxylation temperatures of pillared clays were nearly in the same range. The stability of the pillared clays was related to the dehydroxylation of hydroxide groups associated with interlayer pillars. This was

affected the calcination temperatures of pillared clays. For that reason thermogravimetric analysis were beneficial for thermal stability of pillared clays.

Table 3.6 The thermal analysis parameters of clays and pillared clays

Samples	**%Weight Loss (0-300ºC)**	**%Weight Loss (300–1000ºC)**	**%Total Weight Loss**	**Dehydroxylation Temperature (ºC)**	**Collapse temperature (ºC)**
KSF	10.7	13.0	23.7	597	899
Fe-KSF-FD*	12.6	4.0	16.6	670	932
Zr-KSF-OD*	8.6	5.6	14.2	658	-
Al-KSF-OD* 20x	15.0	14.5	29.5	500	930
Al-KSF-OD*	10.0	7.5	17.5	623	917
K10	6.1	4.1	10.2	662	947
Fe-K10-FD*	11.9	3.1	15.1	660	941
Zr-K10-OD*	7.3	4.6	11.9	641	-
Al-K10-OD* 20x	12.7	5.0	17.8	617	-
Al-K10-OD*	8.0	4.6	12.6	649	-

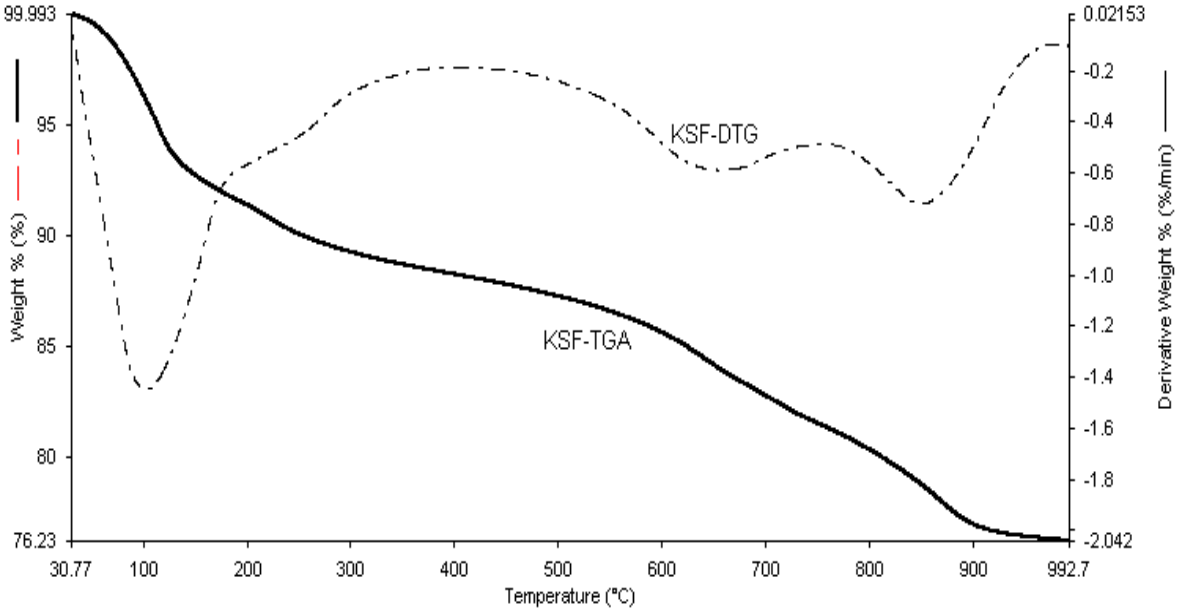

Figure 3.31 Thermogravimetric analyses (TGA) and differential thermogravimetric analyses (DTG) of KSF

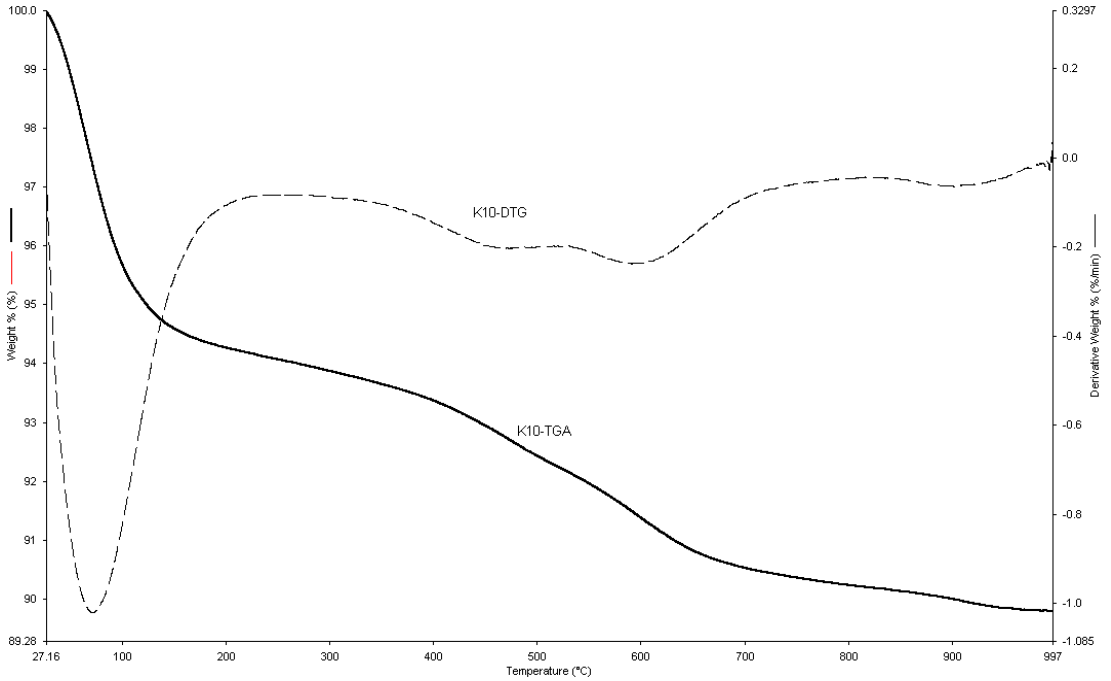

Figure 3.32 Thermogravimetric analyses (TGA) and differential thermogravimetric analyses (DTG) of K10

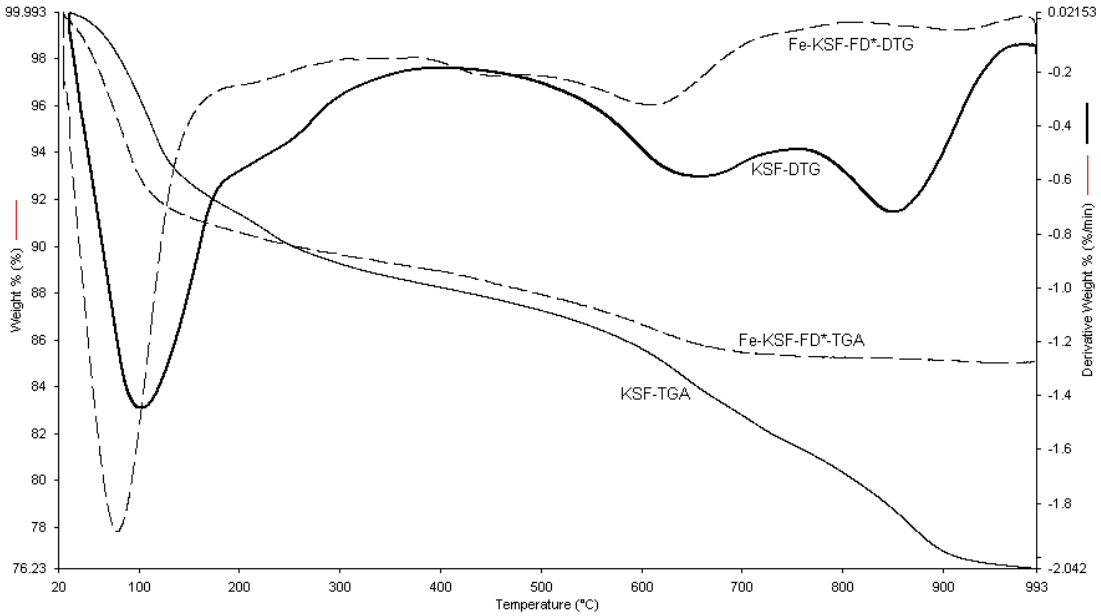

Figure 3.33 Thermogravimetric analyses (TGA) and differential thermogravimetric analyses (DTG) of KSF and Fe-KSF-FD*

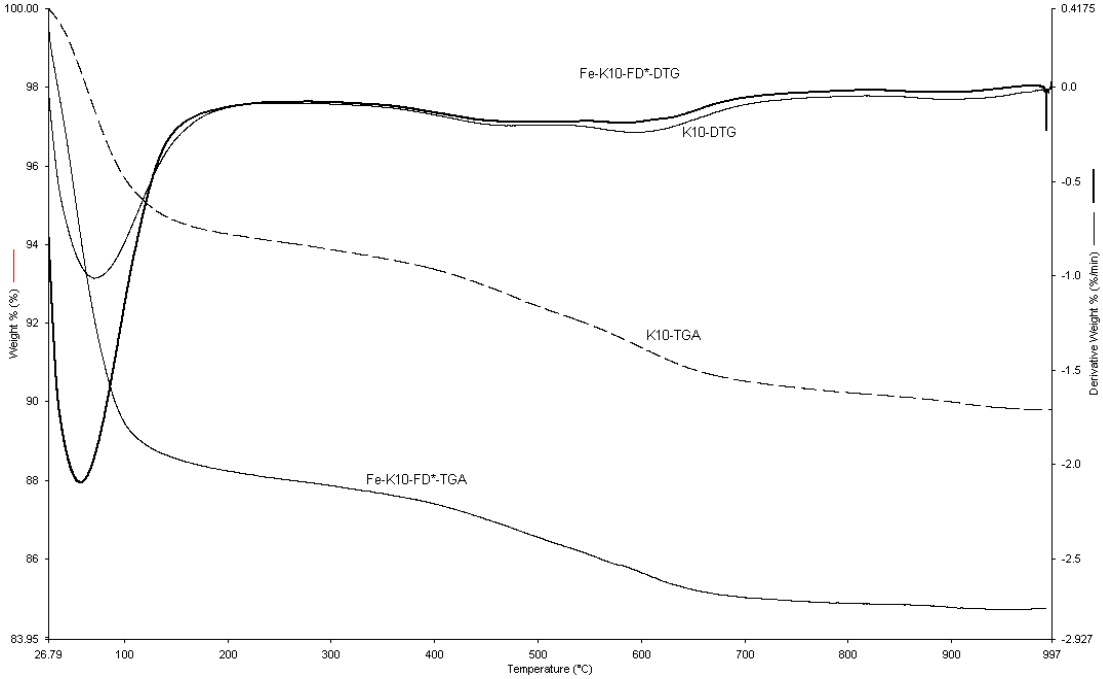

Figure 3.34 Thermogravimetric analyses (TGA) and differential thermogravimetric analyses (DTG) of K10 and Fe-K10-FD*

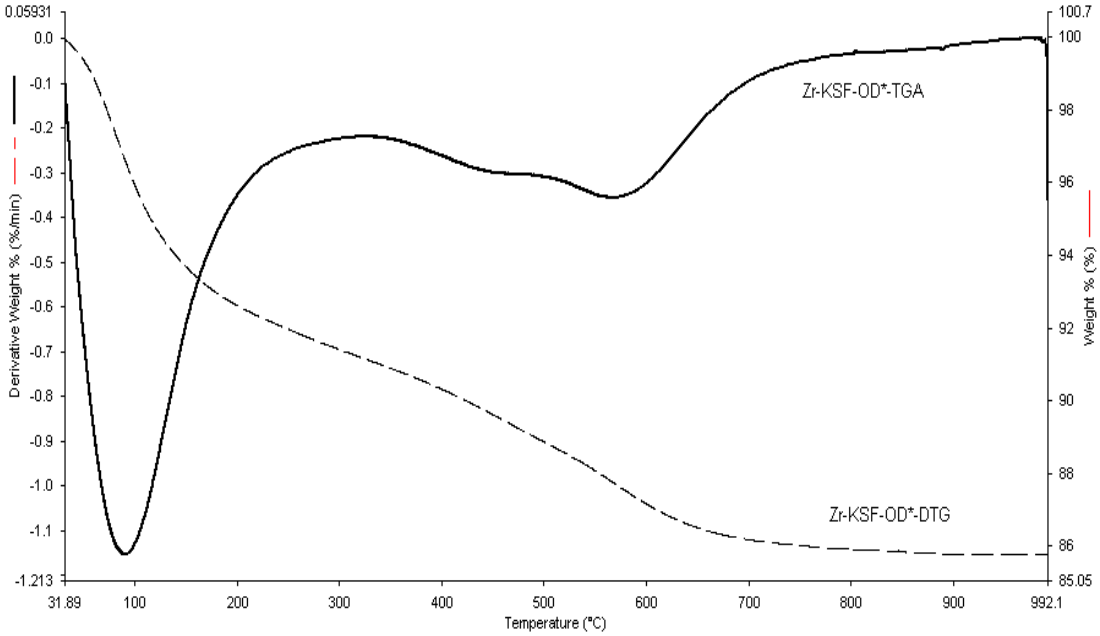

Figure 3.35 Thermogravimetric analyses (TGA) and differential thermogravimetric analyses (DTG) of Zr-KSF-OD*

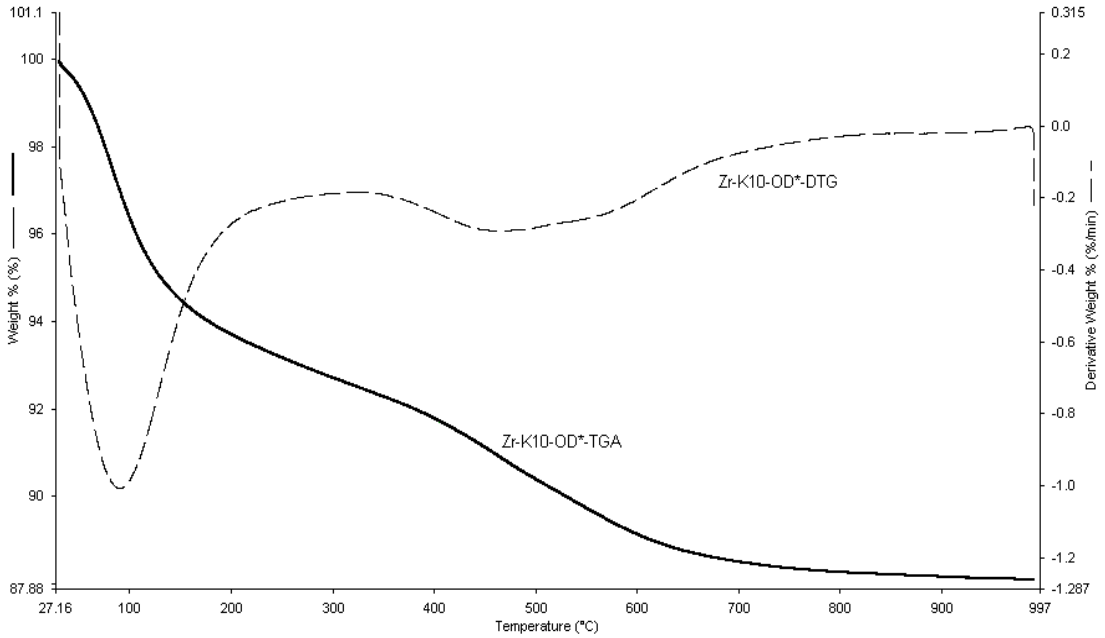

Figure 3.36 Thermogravimetric analyses (TGA) and differential thermogravimetric analyses (DTG) of Zr-K10-OD*

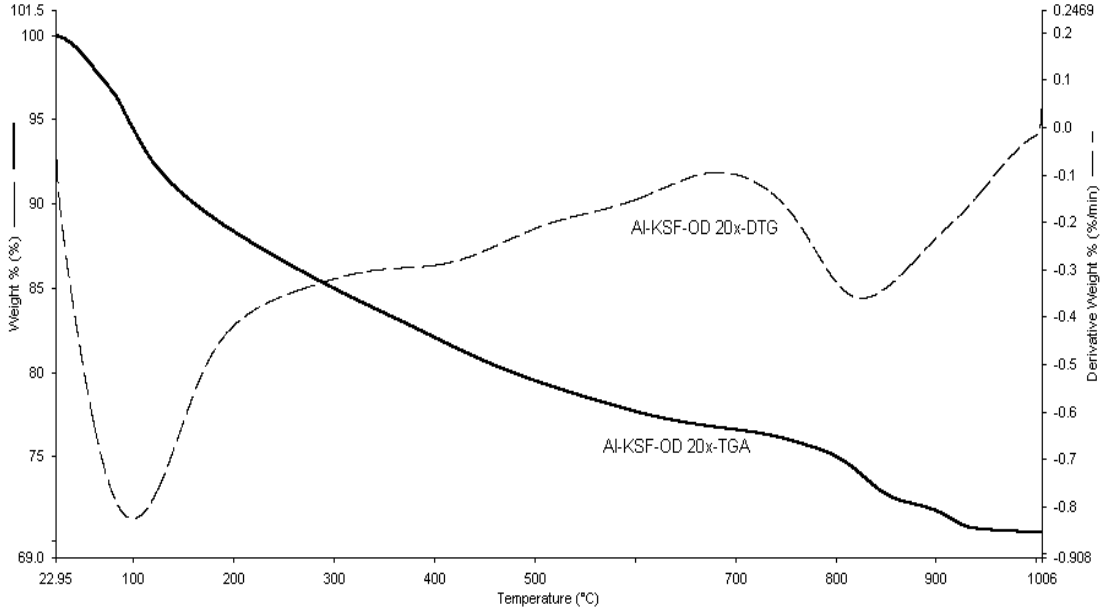

Figure 3.37 Thermogravimetric analyses (TGA) and differential thermogravimetric analyses (DTG) of Al-KSF-OD* 20x

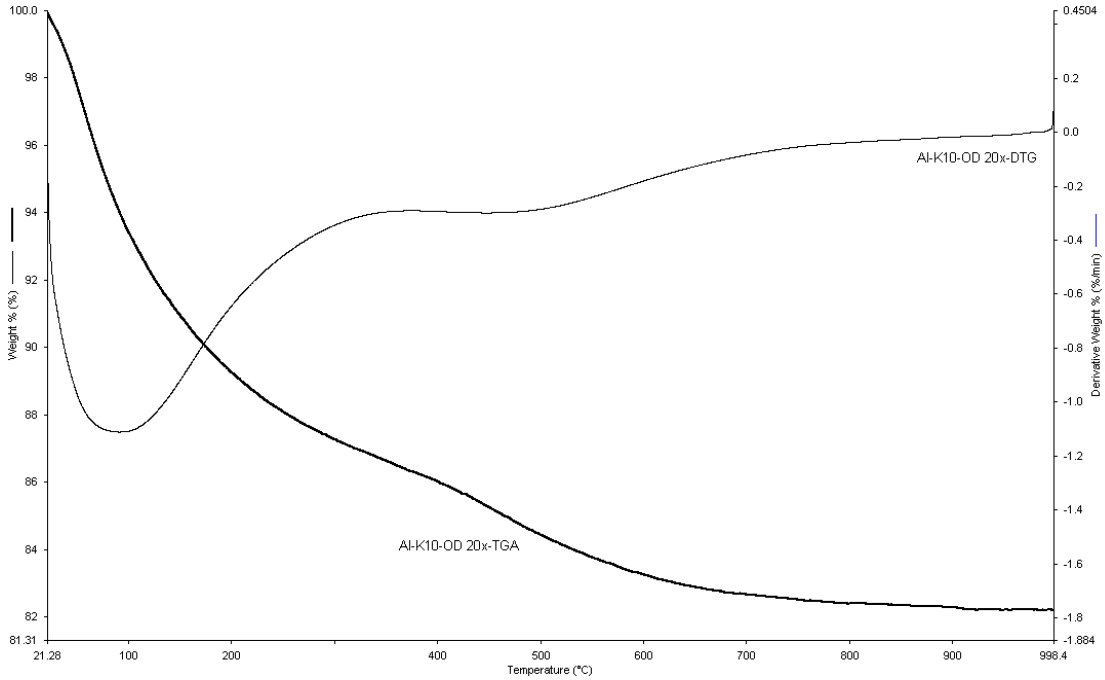

Figure 3.38 Thermogravimetric analyses (TGA) and differential thermogravimetric analyses (DTG) of Al-K10-OD* 20x

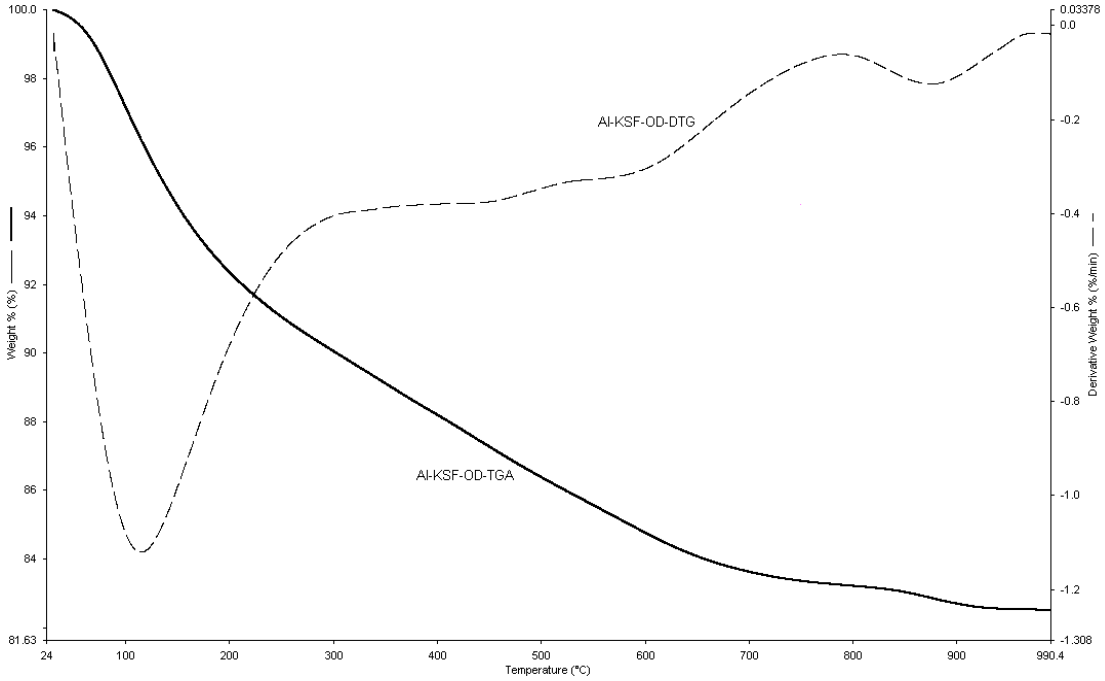

Figure 3.39 Thermogravimetric analyses (TGA) and differential thermogravimetric analyses (DTG) of Al-KSF-OD*

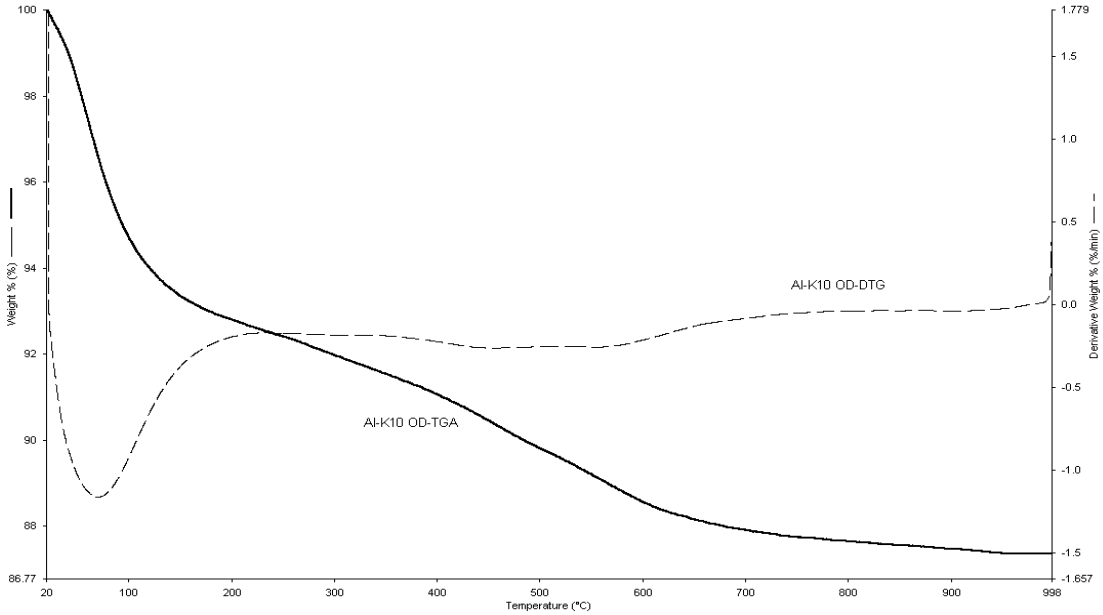

Figure 3.40 Thermogravimetric analyses (TGA) and differential thermogravimetric analyses (DTG) of Al-KSF-OD*

3.2 Characterization and swelling behaviors of poly (acrylic acid)/Aluminium pillared Montmorillonite K10 and KSF

3.2.1 XRD analysis of Al-KSF and Al-K10 based superabsorbents

The change of the interlayer distance can be detected by XRD. The X-ray diffraction patterns of Al-K10, Al-KSF, Al-K10-SA and Al-KSF-SA are shown in Figure 3.41 and Figure 3.42. There is intense diffraction for KSF, K10, Al-KSF and Al-K10 at 2θ=6.50° approximately while no diffraction peak appears for Al-K10-SA and Al-KSF-SA, suggesting that clay sheets are exfoliated and uniformly dispersed in organic network. These peaks are assigned to the 001 lattice spacing of montmorillonite. The lattice spacing of K10, KSF, Al-K10 and Al-KSF are 14.83 Å at 2θ=5.94°, 12.55Å at 2θ=6.99°, and 17.67-18.46Å at 2θ=5.00-4.80° and 15.88Å at 2θ=5.56°, respectively. The distance between the layers for Al-K10 is higher than the distance between the layers for Al-KSF. This shows that the orientation of Al_xO_y (pillaring agent) is different in interlayer of K10 and KSF. 001 lattice spacing of clays were increasing by pillaring. These data supported that clays were pillared by Keggion ion. After polymerization with pillared clays the diffraction peak corresponding to the montmorillonite is not observed. Pillared clay based composites presented a low swelling value. It is known that if the increase in the basal space is very high, the forces that keep the layers together are not enough to keep an intercalated structure generating an exfoliated structure. Layers of montmorillonite are completely dispersed in a continuous polymer matrix as single layers. The XRD patterns of Al-K10 and Al-KSF based composites showed three and two crystal peaks at 2θ of ~ 20° and 30°, respectively. These data support the presence of layers of clays.

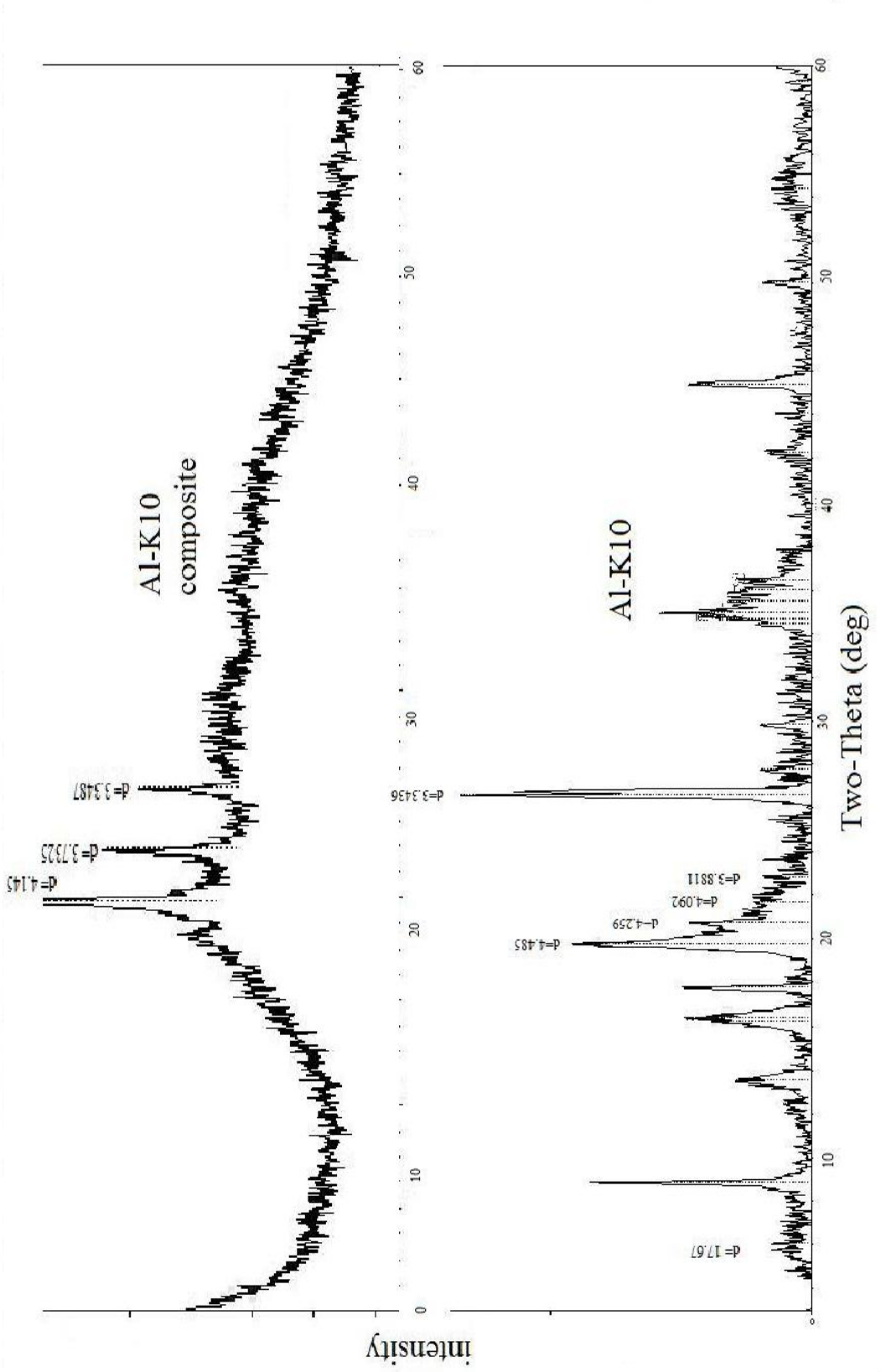

Figure 3.41 XRD patterns of Al-K10 and Al-K10-SA composite

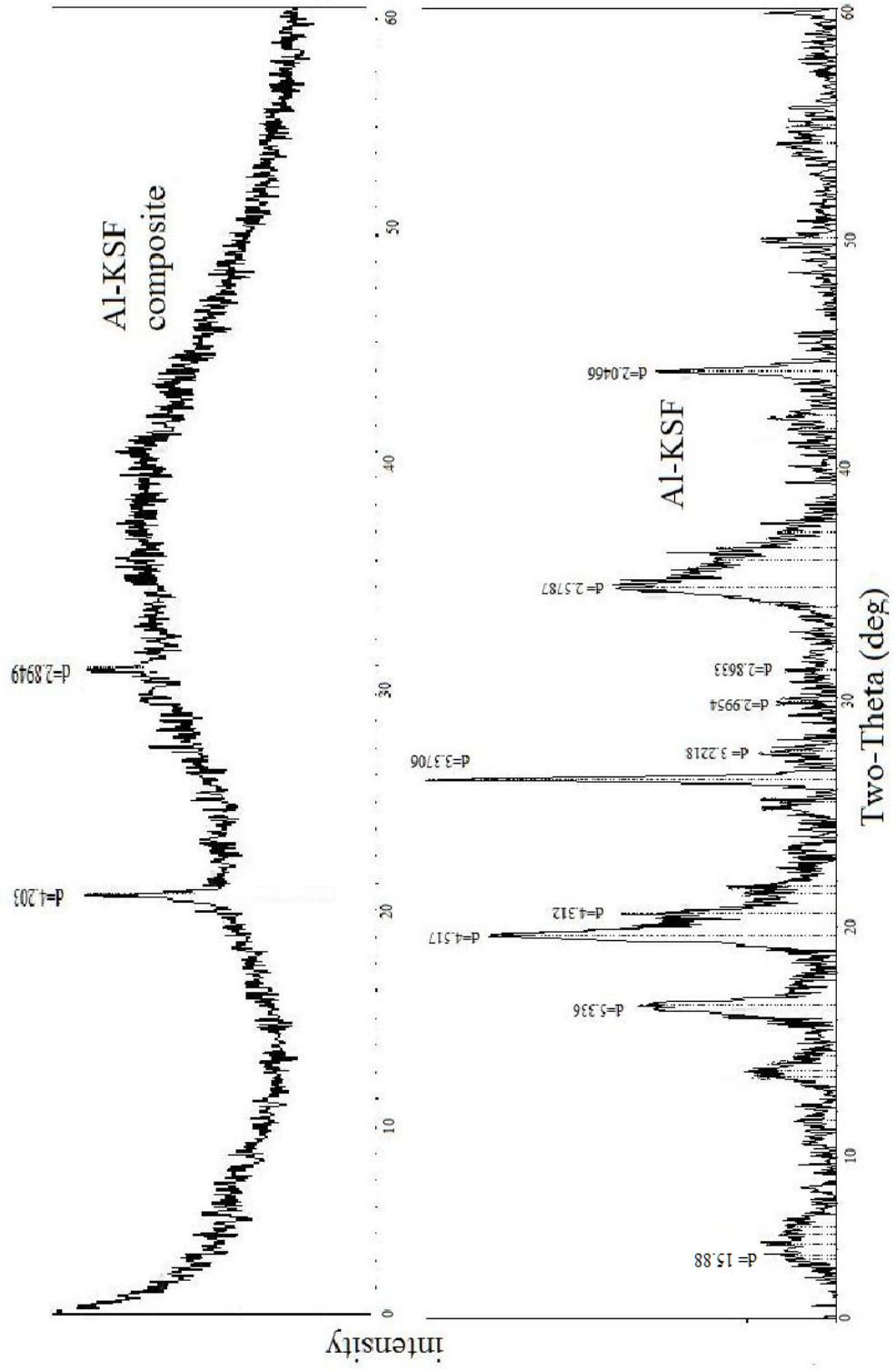

Figure 3.42 XRD patterns of Al-KSF and Al-KSF-SA composite

3.2.2 FT-IR analysis of Al-KSF and Al-K10 based superabsorbents

The structure of Al-KSF-SA and Al-K10-SA composites was confirmed by FTIR analysis. Table 3.7 lists the functional groups available in K10, Al-K10, Al-K10-SA, KSF, Al-KSF and Al-KSF-SA samples. OH stretching vibration of Al-K10 was in the range 3622-3647 cm^{-1}. After grafting of SA, this band shifted to 3647 cm^{-1}. It is interesting to note that, OH stretching vibration for Al-KSF was obtained at 3624 cm^{-1}. However, after fabricating Al-KSF-SA composite, this band slightly shifted to 3629 cm^{-1}. It can be said that a little interaction generates between OH groups of Al-KSF and SA. Thus formation of additional network occurs slightly. This means higher swelling ratio for Al-KSF-SA composite. The new absorption bands are appeared at 2988-2881 cm^{-1} for Al-K10-SA and 2956-2871 cm^{-1} for Al-KSF-SA due to -CH_2 stretching vibrations. Bending vibration of –CH_2 groups of Al-K10-SA and Al-KSF-SA were located at 1463 and 1445 cm^{-1}, respectively. Stretching vibration of C=O group was observed at 1750 cm^{-1} and 1722 cm^{-1} for Al-K10-SA and Al-KSF-SA respectively. This new band may be on account of ester formation. The carboxylate groups of the grafted poly(acrylic acid) may react with OH groups on the surface of Al-K10 and AL-KSF-SA leading to ester formation. Asymmetric and symmetric vibrations of R-COOK groups appear 1539 cm^{-1} and 1402 cm^{-1} for Al-K10-SA and 1554 and 1402 cm^{-1} for Al-KSF-SA, respectively. The band around 1045 cm^{-1} is due to asymmetric stretching vibrations of SiO_2 tetrahedral. After polymerization, stretching vibrations of SiO_2 tetrahedral was shifted to 1076 cm^{-1} and 1075 cm^{-1} for Al-K10 and Al-KSF based composites, respectively. It indicates the esterification of carboxylic acid with silanol. This mechanism was supported by shifting of the OH stretching vibration of clays and pillared clays. These results may confirm the grafting reaction between pillared clays and the acrylic network through ester formation. A band around 800 cm^{-1} is due to stretching vibration of Al_{IV} tetrahedral, when substitution of Al for Si is low; Al_2OH vibration lies in the 915±950 cm^{-1} range, and absorption at 526–469 cm^{-1} is due to bending of Si–O vibration. These IR characteristic bands of clay were observed and only little shifts were noticeable in pillared clays and the network of pillared clay based composites from Table 3.7. The

little shifts of these all bands showed that the basic clay layer structure remains unaffected on pillaring and polymerization. These results suggested that the pillaring agents physically entrapped within the PILC structure.

Table 3.7 The characteristic FT-IR data of the samples

IR bands	**Samples**					
	K10	Al-K10	Al-K10 composite	KSF	Al-KSF	Al-KSF composite
Al_2OH(octahedral layer) (cm^{-1})	3623	3622-16	3647	3620	3624	3629
Stretching vibrations of H_2O(cm^{-1})	3428	3436	3395-3345	3411-3389	3429	3439-3363
Stretching vibration of $-CH_2$ (cm^{-1})			2988-2881			2956-2871
Stretching vibration of C=O (cm^{-1})			1750			1722
Bending vibrations of H_2O(cm^{-1})	1633	1636	1682	1636	1633	1621
Asymmetric vibration of R-COOK (cm^{-1})			1539			1554
Bending vibration of $-CH_2$(cm^{-1})			1463			1445
Symmetric vibration of R-COOK (cm^{-1})			1402			1402
Asymmetric stretching vibrations of SiO_2 tetrahedra(cm^{-1})	1046	1041	1076	1046	1041	1075
Bending vibrations of Al_2OH(cm^{-1})	920	921	915	917	921	914
Stretching vibration of Al^{IV} tetrahedra(cm^{-1})	798	796	800	794	794	806
Bending vibration of Si-O(cm^{-1})	524 468	528 471	524 469	523 467	526 471	520 482

3.2.3 SEM images of Al-KSF and Al-K10 based superabsorbents

SEM micrographs of Al-K10, Al-K10-SA and Al-KSF, Al-KSF-SA were shown in Figure 3.43 (a-b) and Figure 3.44 (a-b), respectively. Water absorbency capacity of superabsorbents might be related to the porosity of clays as used as fillers and level of crosslinking. As seen in the micrograph of Al-K10, it was clear that the pores were observed on the surface of the clay structure. After graft polymerization with Al-K10, Al-K10 was dispersed homogenous on hydrogel. Presumably, it may be claimed that homogenous dispersion of pillared clay particles may be contributed to more crosslinking structure of Al-K10-SA. From SEM images of Al-KSF and Al-KSF-SA, it was deduced from the micrograph of Al-KSF based composite that the homogenous dispersion of pillared clay was lower than Al-K10 based composite and the pores were not observed clearly from the morphology of Al-KSF. It may indicate less crosslinking structure for Al-KSF-SA. In other words, it was expected that the water absorbency of Al-KSF based composite was higher than Al-K10-SA. Water molecules might easily diffuse because of low cross-linking ratio.

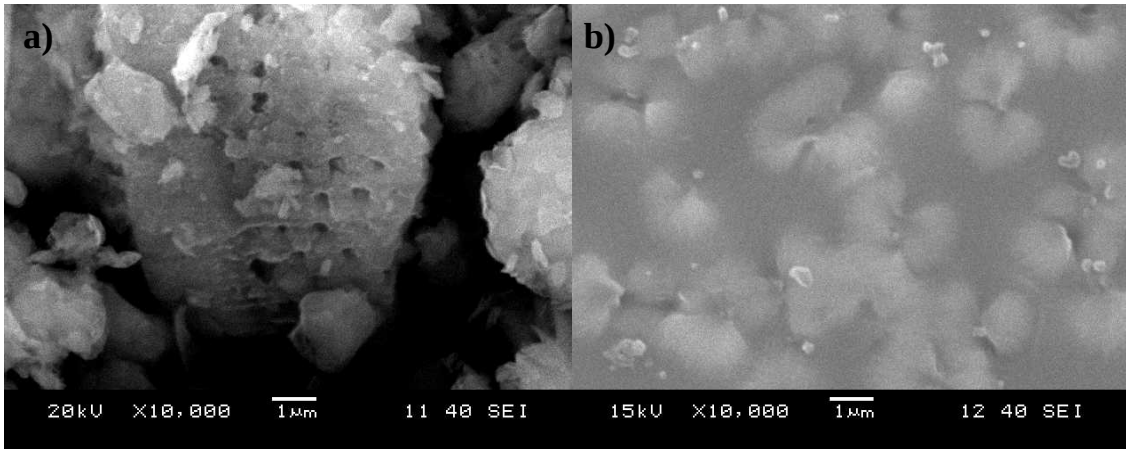

Figure 3.43 SEM micrographs of (a) Al-K10 (10000x magnification) (b) Al-K10 containing acrylic-based superabsorbent hydrogel composites.

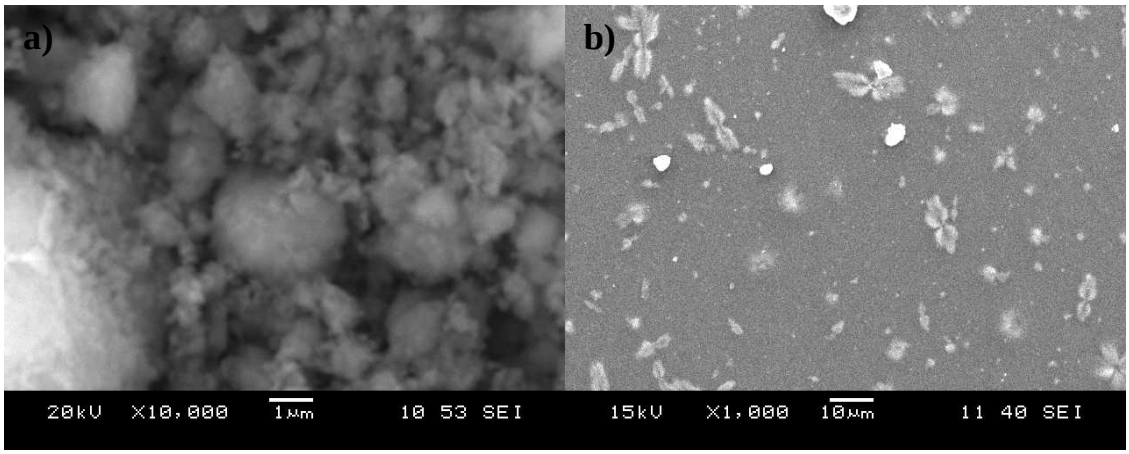

Figure 3.44 SEM micrographs of (a) Al-KSF (10000x magnification), (b) Al -KSF containing acrylic-based superabsorbent hydrogel composites (1000x magnification).

3.2.4 Swelling capacity of Al-KSF and Al-K10 based superabsorbents

Figure 3.45 shows swelling values of the Al-KSF and Al-K10 based superabsorbents in distilled water. Al-KSF and Al-K10 based superabsorbents (Al-KSF-SA and Al-K10-SA) reached equilibrium within 100 min. The percentages of equilibrium swelling values were at about %7900 for Al-KSF-SA and at about %5700 for Al-K10-SA. As shown from Figure 3.45, Al-KSF based composites had greater equilibrium swelling values than Al-K10 based superabsorbent. This might be due to network of superabsorbent. In addition, crosslink density and elasticity of polymer network might be affected the water absorption of hydrogels. Seki, Torgürsül, & Yurdakoç, 2007, determined that water absorbency values for iron rich smectite superabsorbent were about 230 times the weight of the superabsorbent hydrogel under normal atmospheric conditions. The value which is obtained in this study can be considered as low values. It is probable that pillared clays may function as a crosslinking agent. If it is possible, carboxylate groups of the polyacrylate chains may react with OH groups of pillared clays. From Figure 3.45, it can be inferred that more crosslink points occur may Al-K10 pillared clay and SA. Because of the formation of additional network, the remaining space for water to enter reduces.

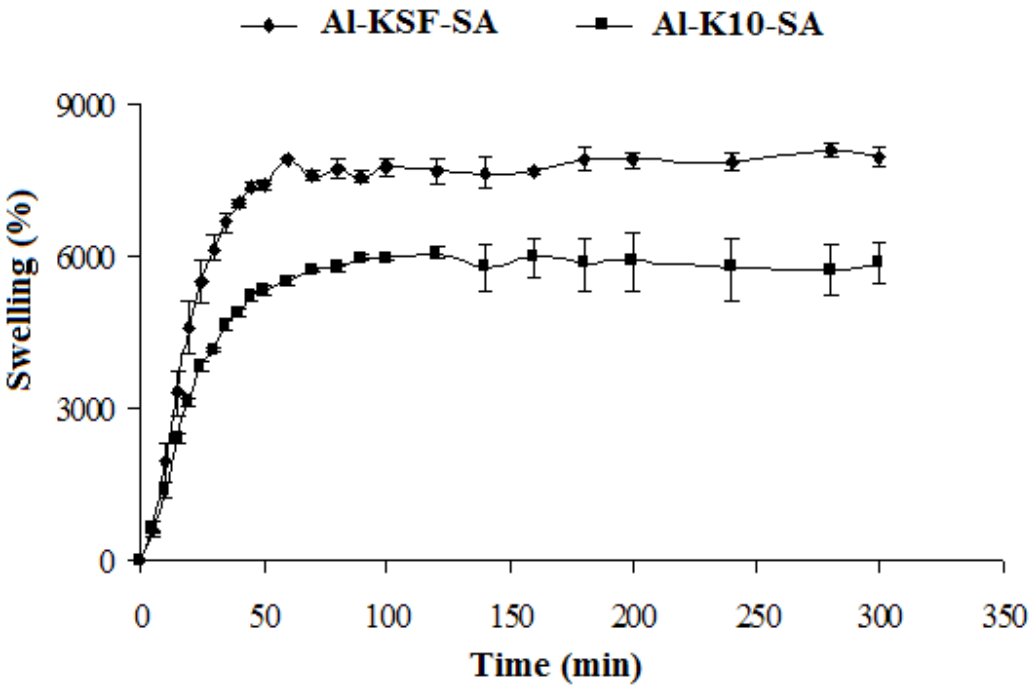

Figure 3.45 Swelling kinetics of superabsorbents composite in distilled water

3.2.5 pH-sensitivity of Al-KSF and Al-K10 based superabsorbents

pH sensitivity of superabsorbent were also evaluated by immersing films in different buffer solutions. Figure 3.46 was plotted so as to determine the effect of pH on equilibrium swelling. As observed from Figure 3.46, pH affected swelling values of superabsorbent and deswelling occurred. Equilibrium deswelling values were decreased with increasing of pH values until pH of 5.5. Beyond the pH value of 5.5, deswelling values were almost similar to each other. At low pH values, it was seen that Al-KSF based superabsorbent had slightly greater deswelling values than Al-K10 based superabsorbent. As a result, it had been reached that the swelling behavior of Al-KSF and Al-K10 based superabsorbent films seem to be pH dependent.

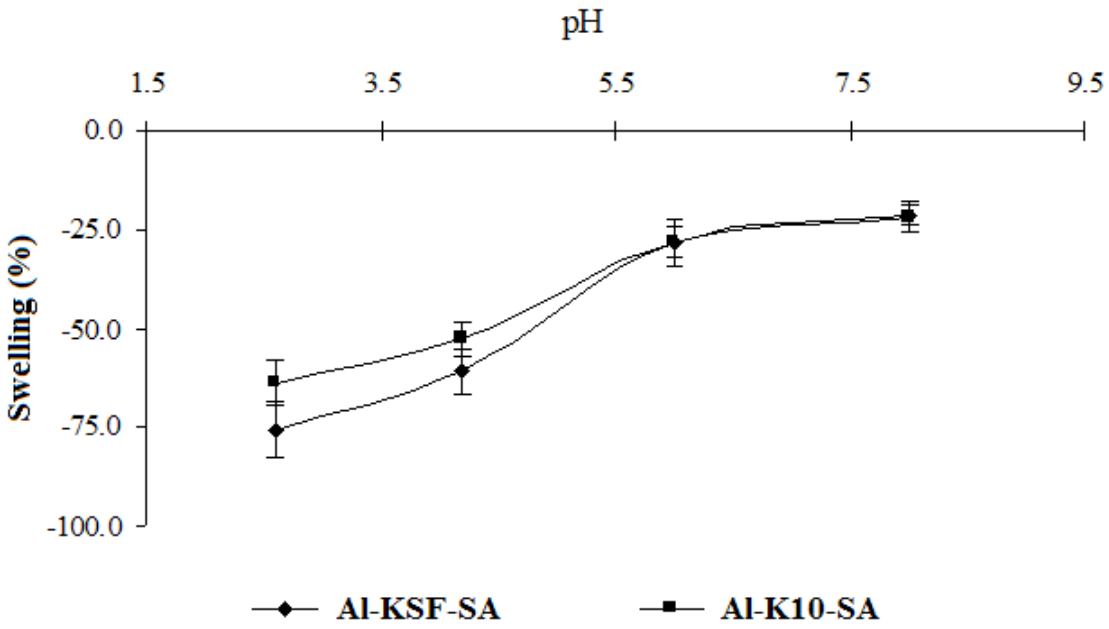

Figure 3.46 Effect of pH on the equilibrium swelling of superabsorbents

Higher hydration and distension could increase the interaction between polymeric network and clay, which increases crosslink density of obtained superabsorbent composite, and then decreases the equilibrium water absorbency. For example, Na^+-montmorillonite has the highest hydration and distension among the clays selected, and then the lowest equilibrium water absorbency of corresponding superabsorbent composites (Zhang, & Wang, 2007).

3.2.6 Swelling reversibility of Al-KSF and Al-K10 based superabsorbents

The swelling reversibility of superabsorbents was alternately conducted at pH 1.2 and 7.8. After superabsorbents were equilibrated at pH=7.8 and then alternated between solutions at pH=1.2 and pH=7.8, respectively. Superabsorbents were equilibrated at pH=7.8**,** then the samples were immersed in pH=1.2 for about 180 min. A shrinking was measured at about 80-90%. Then the films put into pH=7.8 for 180 min. and

approximately 55-60% swelling was determined. When the pH values were varied repeatedly, Al-KSF and Al-K10 based superabsorbents exhibited a reversible swelling behavior with relatively fast response. It can be added that reversible swell-shrink properties of Al-KSF and Al-K10 based superabsorbents would be beneficial characteristics for pH sensitive systems with controllable swelling ability.

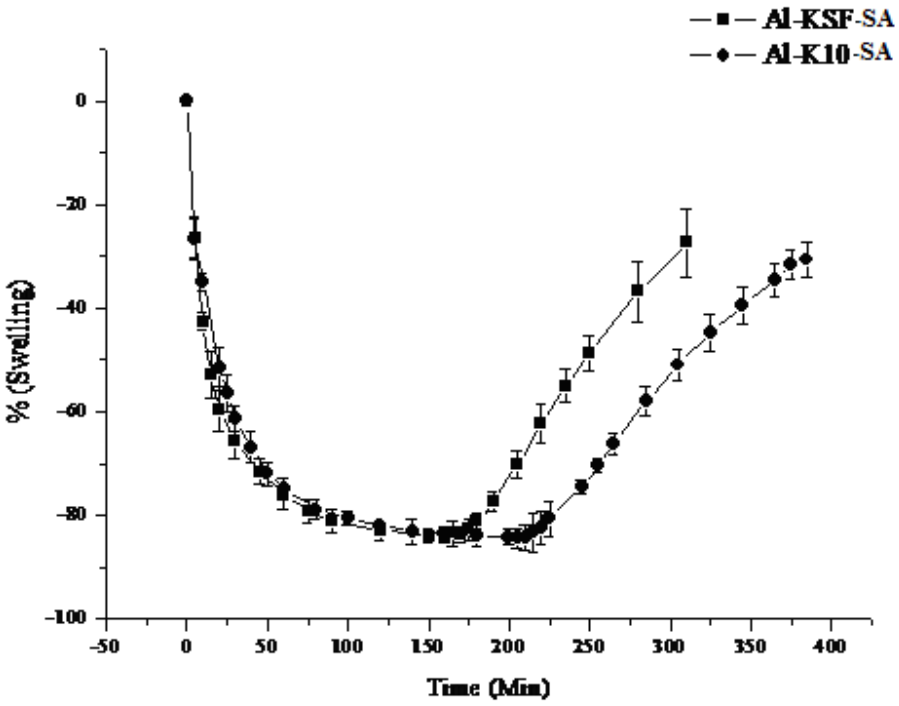

Figure 3.47 pH-dependent reversible swelling behaviour of superabsorbents (Superabsorbents equilibrated at pH=7.8, then alternated between solutions at pH=1.2 and pH=7.8)

3.3 Sorption experiments of Aluminium pillared Montmorillonite K10 and Montmorillonite KSF

3.3.1 Characterization of Al pillared clays for adsorption study

X-ray diffraction (XRD) reveals the basal spacing of the clays and aluminium pillared clays. 2θ and d_{001} basal spacing of clays and pillared clays were summarized in

Table 3.8. The d_{001} values of untreated montmorillonite KSF and K10 were 12.55 Å at 6.99 (2θ) and 14.83 Å at 5.94 (2θ), which correspond to the main montmorillonite component. In pillared clays, the d_{001} peak was found to shift towards the lower 2θ region, which is a clear indication of the enlargement of the basal spacing of the clay. OH/Al molar ratio of all pillared clay is 2.0. Pillaring achieved an increase in the distance of layers of montmorillonite. The increase in d-spacing was as expected since the pillaring causes an expansion in the interlayer spacing. Subtraction of the thickness of the 2:1 layer of 9.60 Å (Manohar, Noeline, & Anirudhan, 2006) yields interlayer separations of all pillared clays and these results were indicated in the Table 3.8. Al-K10 had the highest enlargement between interlayer. Additionally, XRD data was reflected the main structure of precursors of pillared clays (KSF, K10).

Table 3.8 XRD results of K10, KSF, Al-K10 and Al-K10

	Samples			
	KSF	**Al-KSF**	**K10**	**Al-K10**
2θ (°)	6.99	5.54	5.94	4.80
d_{001} (Å)	12.55	15.82	14.83	18.78
d_{001}- 9.6(Å)[a]	-	6.22	-	9.18

The BET surface areas (S_{BET}), Total pore volumes (V_{total}) and average pore diameter (l_p) were measured and summarized in Table 3.9. The N_2 adsorption–desorption isotherms at 77 K for Al-PILCs exhibit Type IV behaviors according to the IUPAC classification or BDDT classification (Sing & et al., 1985), characteristic of mesoporous adsorbents. It can be seen that the average pore diameter is about 5-7 nm for pillared clays, which is an obvious mesoporous layered structure. Specific surface area value of Al-KSF was greater than the surface area of KSF. On the other hand, the specific surface area of Al-K10 was lower than K10. This may be due to the filling the pores by coke which formed during calcination or precursors of pillars.

Table 3.9 The structure characteristics of aluminum pillared clay

Sample	S_{BET} (m^2/g)	V_{total} (ml/g)	l_p (nm)
Al-K10	130.50	0.238	7.302
Al-KSF	46.16	0.063	5.501

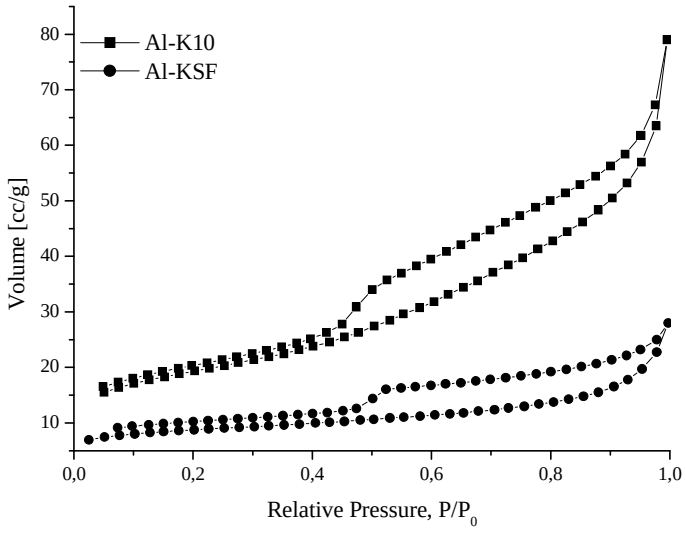

Figure 3.48 The N_2 adsorption–desorption isotherms at 77 K for Al-K10 and Al-KSF

The FTIR spectra results were shown in Table 3.10. It can be seen that the two bands were observed around 3500 cm^{-1}, in the –OH stretching region. A broader band due to Al_2OH group of the octahedral layer was at about 3625 cm^{-1}. Stretching vibrations of water molecules may also contribute to –OH bands (3450 cm^{-1}). On pillaring, the band broadens due to the introduction of more –OH groups of the pillar (Al-polycations), which is interpreted as an effect of pillaring. The broad absorption bands observed in, K10, Al-K10, KSF and Al-KSF at 3624, 3624, 3623 and 3627 cm^{-1}, respectively represent the fundamental stretching vibrations of different –OH groups present in Mg–OH–Al, Al–OH– Al and Fe–OH–Al units in the octahedral layer (Farmer, 1974). The decrease in intensity arises from the dehydration and dehydroxylation steps during pillaring. Band at around 1600 cm^{-1} is due to bending vibrations of water. Pillaring

process replaces a large amount of interlayer cations that generally exist as hydrated and it decreases the intensity of –OH bands. PILCs have low amount of adsorbed/coordinated water due to the non-swellable nature. Thus, as a result of pillaring, intensity of the band around 1600 cm^{-1} decreases. The band around 1045 cm^{-1} is due to asymmetric stretching vibrations of SiO_2 (Si–O–Si) tetrahedra. A band around 800 cm^{-1} is due to stretching vibration of Al_{IV} tetrahedra, when substitution of Al for Si is low; Al–OH–Al libration lies in the 915±950 cm^{-1} range. The weak band at 684 cm^{-1} were assigned to O–Si–O asymmetric stretching and absorption at 526cm^{-1} is due to bending vibration of Al–Si–O (cm^{-1}); the asymmetric bending mode of Si–O–Si band at 469 cm^{-1} as reported in silicate system (Olphen, Fripiat, 1979).

The retention of all bands as in parent montmorillonite in the framework region clearly shows that the basic clay layer structure remains unaffected on pillaring. These bands are slightly broader but their wavenumbers are almost the same as those of clays (the differences in their wavenumbers are not higher than 10 cm^{-1}). These results suggest that the complex is physically entrapped within the PILC structure.

Table 3.10 The characteristic FT-IR data of the samples

IR bands	**Samples**			
	K10	**Al-K10**	**KSF**	**Al-KSF**
Al_2OH(octahedral layer) (cm^{-1})	3624	3624	3623	3627
Streching vibrations of H_2O (cm^{-1})	3434	3435	3412	3463
Bending vibrations of H_2O (cm^{-1})	1634	1630	1636	1640
Asymmetric streching vibrations of SiO_2 tetrahedra (cm^{-1})	1048	1048	1043	1047
Bending vibrations of Al_2OH (cm^{-1})	917	917	912	915
Streching vibration of Al^{IV} tetrahedra (cm^{-1})	798	798	795	792
Si–O–Si asymmetric stretching vibrations (cm^{-1})	694	674	674	692
Bending vibration of Al–Si–O (cm^{-1})	525	527	524	527
Bending vibration of Si–O–Si (cm^{-1})	469	470	468	470

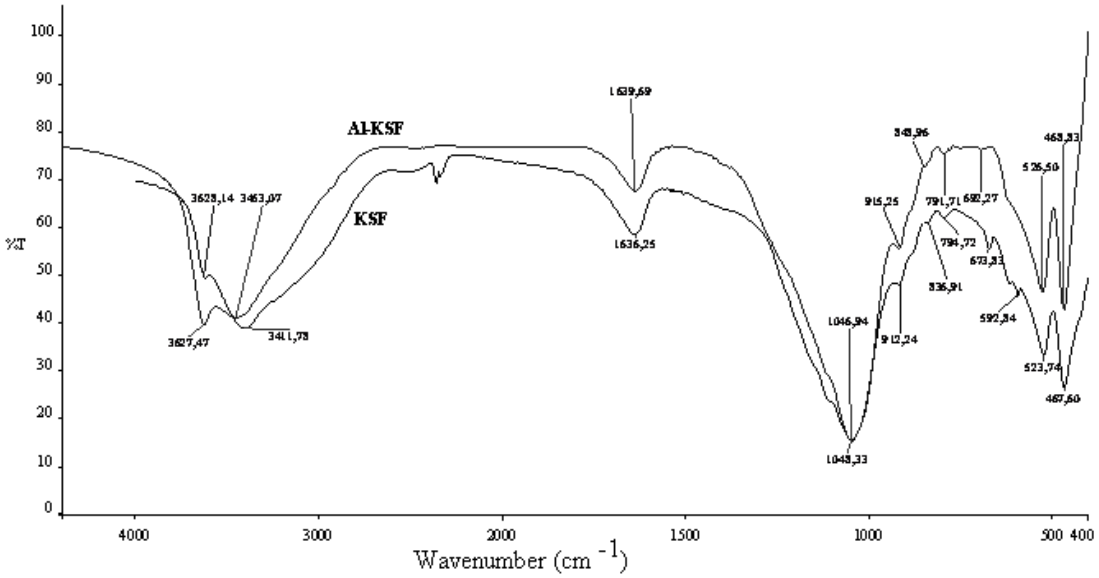

Figure 3. 49 FTIR spectrum of KSF and Al-KSF

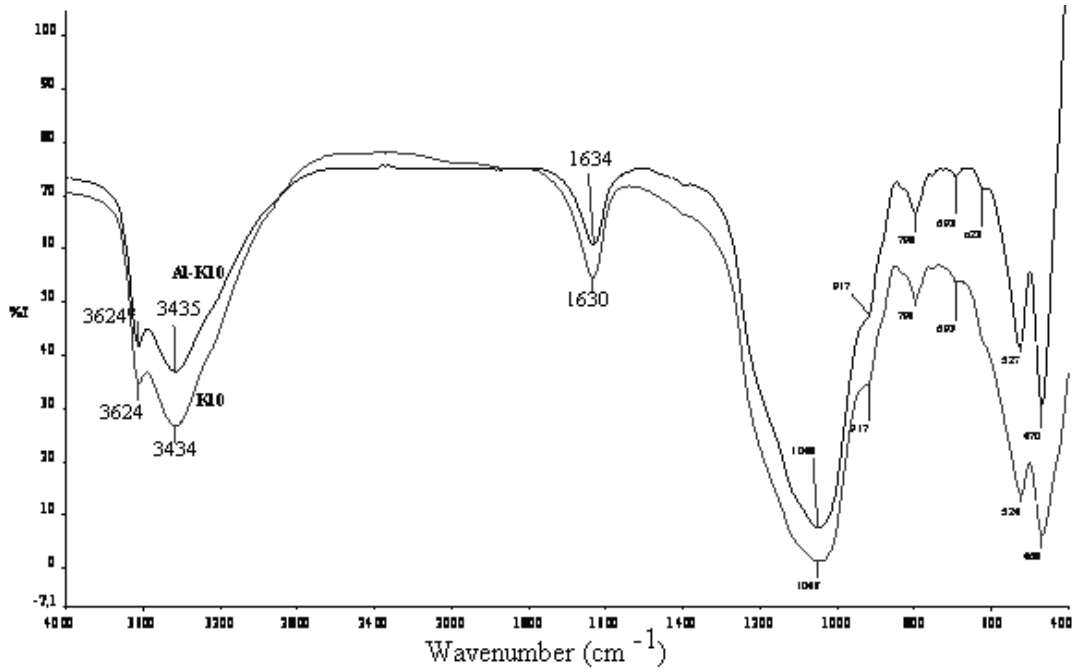

Figure 3.50 FTIR spectrum of K10 and Al-K10

Thermogravimetric analysis curves for KSF, K10, Al-KSF and Al-K10 were shown in Figure 3.55-3.58. For clays and PILCs, the weight loss occurs in two steps. The first step over the temperature range 25-300ºC exhibits a cumulative of about 10.755, 6.133,

15.091, and 12.480 wt% for, KSF, K10, Al-KSF and Al-K10, respectively. This weight loss is corresponding to the physically adsorbed water. The losts between 300 and 1000ºC were due to dehydroxylation of the clay structure. The decomposition takes place between 300 and 1000 °C with a weight loss of 13.01%, 4.07%, 14.36% and 5.06% respectively for KSF, K10, Al-KSF and Al-K10. The inflection points were seen clearly in Figure 3.55-3.58. The collapse of the structures of KSF, K10, Al-KSF and Al-K10 are nearly at 597, 654, 782 and 679 ºC. These values were obtained from DTG curves of them. The TGA curves showed that PILCs lose more weight than their unpillared counterpart during calcinations. About 50% of the lost water was water adsorbed at the surface, being lost temperatures lower than 150 ºC. It is well known that the stability of pillars is related to their dehydroxylation. The water associated with the micropore structure of the PILC (dehydroxylation of hydroxide groups associated with interlayer pillars) began to be removed at this temperature.

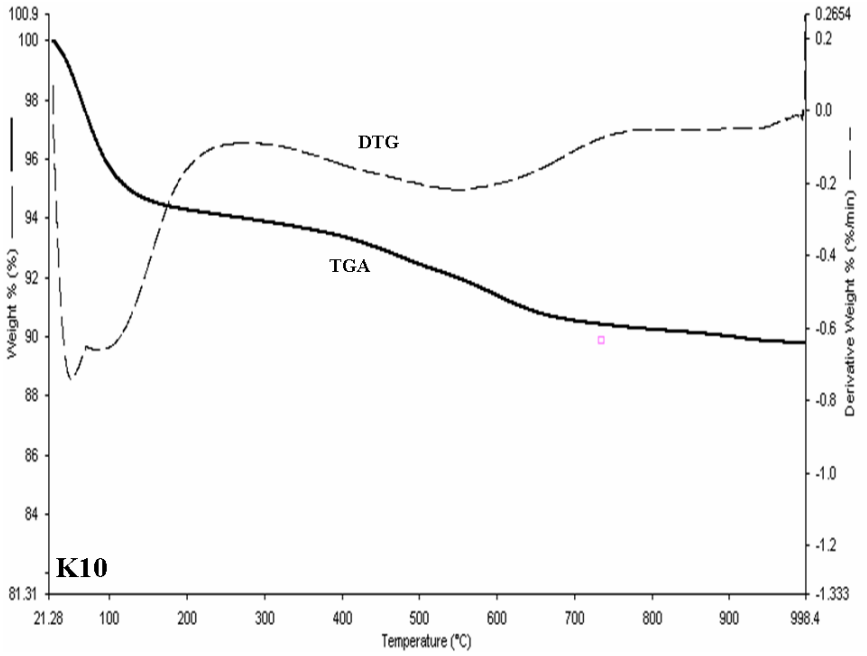

Figure 3.51 Thermogravimetric analyze (TGA) and differential thermogravimetric analyze (DTG) of K10.

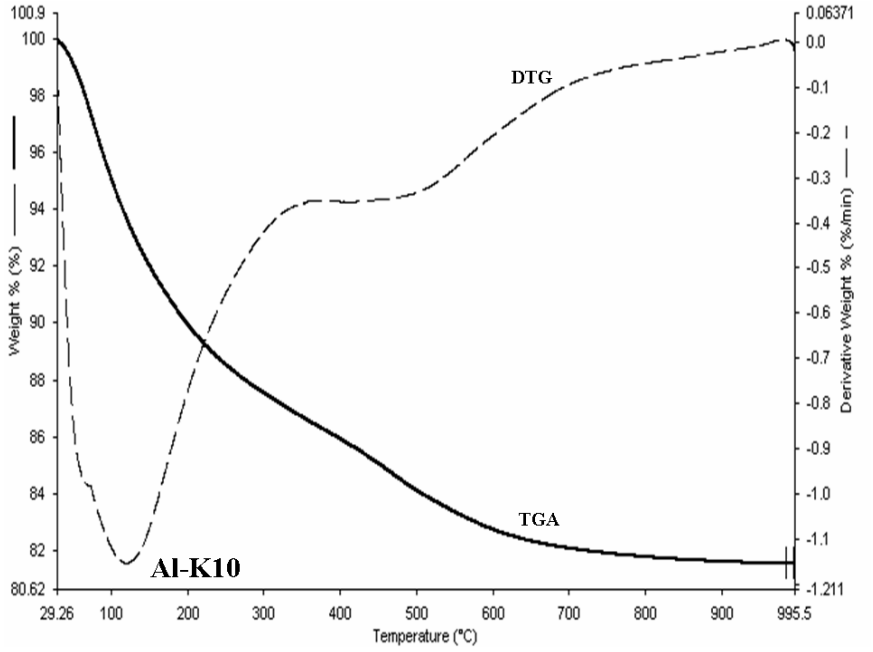

Figure 3.52 Thermogravimetric analyze (TGA) and differential thermogravimetric analyze (DTG) of Al-K10.

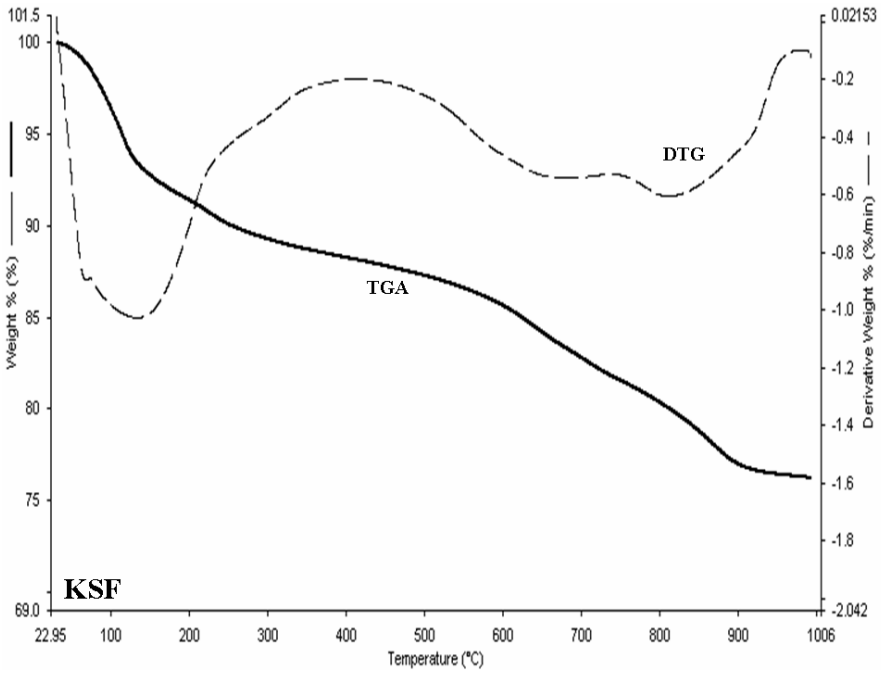

Figure 3.53 Thermogravimetric analyses (TGA) and differential thermogravimetric analyses (DTG) of KSF.

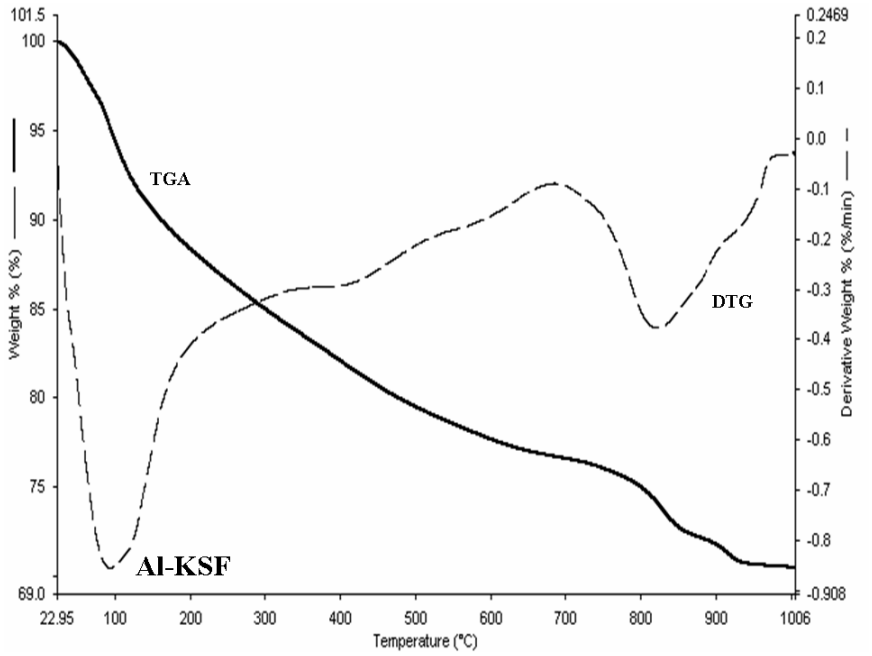

Figure 3.54 Thermogravimetric analyses (TGA) and differential thermogravimetric analyses (DTG) of Al-KSF.

The SEM micrographs of clays and aluminum pillared clays were shown in Figure 3.55 to clarify the change in morphological features. The surface morphology of montmorillonites is different from that of Al-PILCs. The montmorillonites appears as corn flake like crystals with fluffy appearance revealing its extremely fine platy structure. After pillaring, clay has become more porous and fluffy.

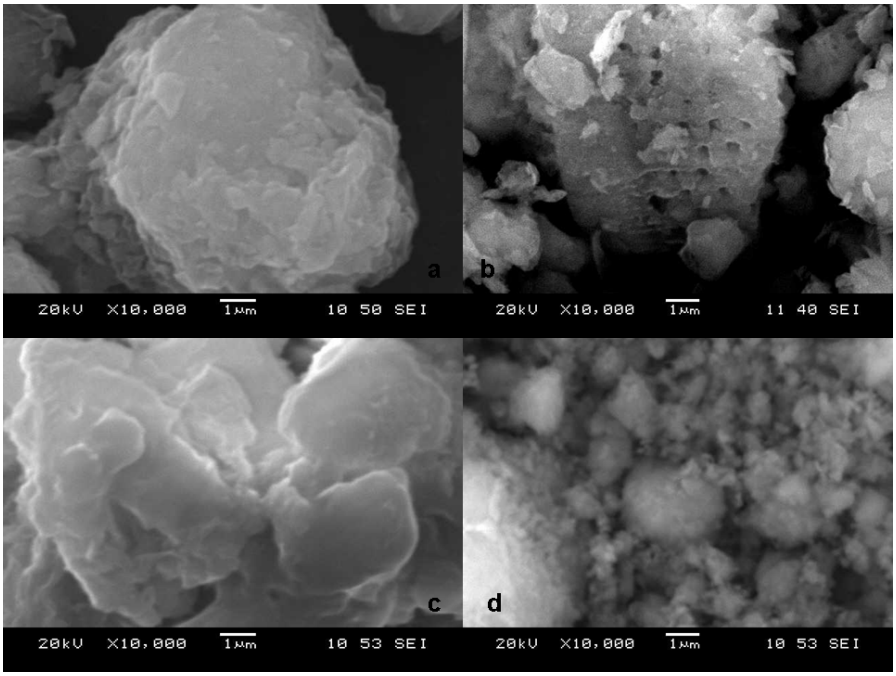

Figure 3.55 SEM micrographs of K10 (a), Al-K10 (b), KSF (c) and Al-KSF (d)

3.3.2 Adsorbent dose effect

The amount of adsorbent is an important parameter because this determines the capacity of an adsorbent for a given initial concentration of the adsorbate. The preliminary investigation on the effect of adsorbent dose on adsorption of Trimethoprim shows that Al-K10 exhibits higher removal capacity of TMP at lower adsorbent dosages in comparison with Al-KSF. The effect of adsorbent concentration on TMP adsorption was shown in Figure 3.56, it was noticed that uptake per unit mass of the Al-K10 was higher when its concentration was lower. Such performance on the adsorbent may be attributed to the fact that some of the adsorption sites remain unsaturated during the adsorption process. On the contrary, the adsorption percentage of Al-KSF increased with increasing adsorbent dosages because of the increase in the number of reaction sites available to TMP. Almost 73% and 33% removal of TMP from 25 mL solution was possible with 250 mg of Al-KSF and 10 mg of Al-K10, respectively. This indicates that

10 mg of Al-K10 and 250 mg of Al- K10 is more effective than the other dosages of adsorbents for the removal of TMP from aqueous solutions. As such subsequent adsorption experiments with TMP were performed only on 10 mg and 100 mg of Al-K10 and Al-KSF, respectively.

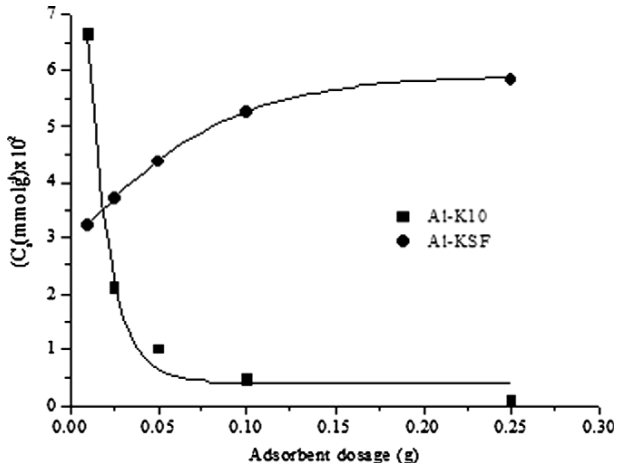

Figure 3.56 The effect of adsorbent dose on the adsorption of TMP onto Al-K10 and Al-KSF (C_0=0.8x10^{-4}molL^{-1})

3.3.3 pH effect on adsorption

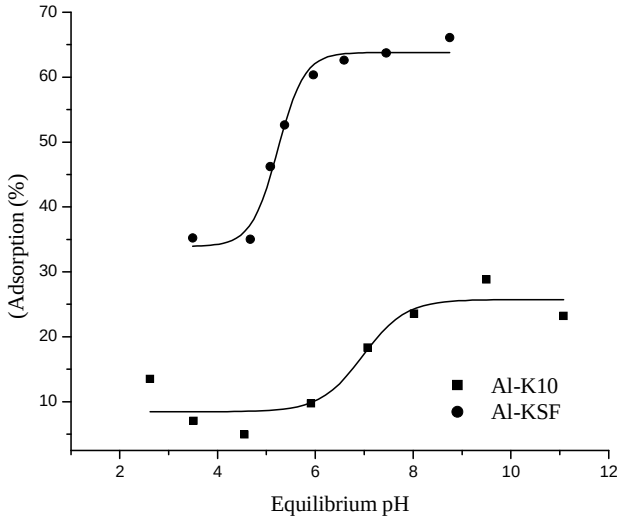

Figure 3.57 pH effect on adsorption of TMP onto 100 mg of Al-K10 and Al-KSF (C_0=10^{-4}molL^{-1})

The pH of the aqueous solution is an important variable that controls adsorption onto surfaces of Al-PILCs. The effect of pH on removing TMP by Al-PILCs for the equilibrium pH nearly between 2.5 and 11.0 is represented in Figure 3.57. It is easily understood from the Figure 3.57 that the adsorbent surface and TMP were affected with an increase of pH. For that reason, the removal percentage of TMP was changed because of increasing pH.

TMP adsorption onto Al-K10 increase nearly between 5 and 9 attains a maximum value around 8.7 and does not change considerably for higher pH values. With an increase of pH of the solution from 5.0 to 9.0, the removal capacity increased from 8.6% to 25.6%. It can be seen that in the pH range 3.5–6.6, TMP removal percentage by adsorption onto Al-KSF is from 35.2 to 63.7 and it is much greater than the removal by Al-K10.

TMP is a weak base with a pKa value of 7.3. At low pH conditions, all of the TMP (T:) is in the protonated form:

$TH^+ \leftrightarrow T: + H^+$

Protonated form of the drug doesn't prefer the adsorbent surface which has positive charge. TMP and the adsorbent surface, both carrying positive charges at acidic pH values may explain the poor adsorption of TMP on the surfaces of Al-PILCs. In contrast, the percentage of adsorption is increased with an increase in pH. The observed increase of sorption with increasing pH can be attributed to the decrease of the competition of the hydronium ions for PILCs' sites at higher pH values. Positively charged surface site on the adsorbent favors the adsorption of deprotonated form than protonated form of drug. The adsorption studies were carried out at pH 4.55 for Al-K10 and at pH 5.08 for Al-KSF.

3.3.4 Effect of contact time

The effect of contact time in the adsorption of TMP by Al-PILCs for different temperatures (303, 311 and 318 K) can be seen in Fig. 3.58 and 3.59. The adsorption of trimethoprim increased with increasing contact time and become almost constant nearly after 120 min and 240 min for Al-K10 and Al-KSF, respectively. These results represent the time at which an equilibrium TMP concentration is presumed to have been attained. According to the results, the equilibrium time was fixed at 120 min and 240 min for the rest of the Al-K10 and Al-KSF batch experiments to make sure that equilibrium is reached.

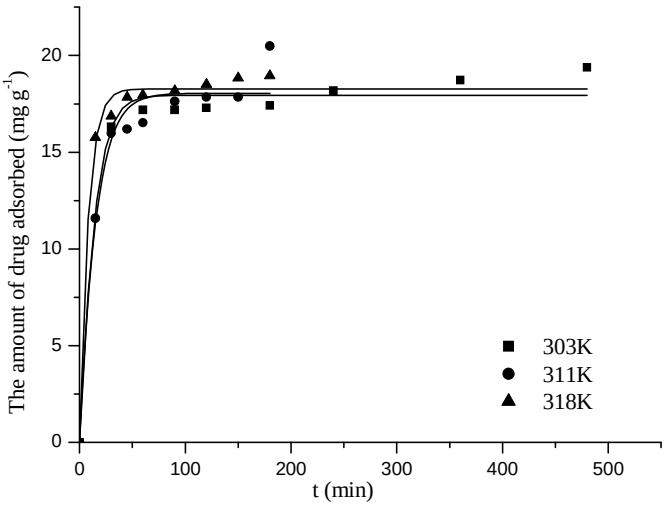

Figure 3.58 Effect of contact time of TMP adsorption onto Al-K10

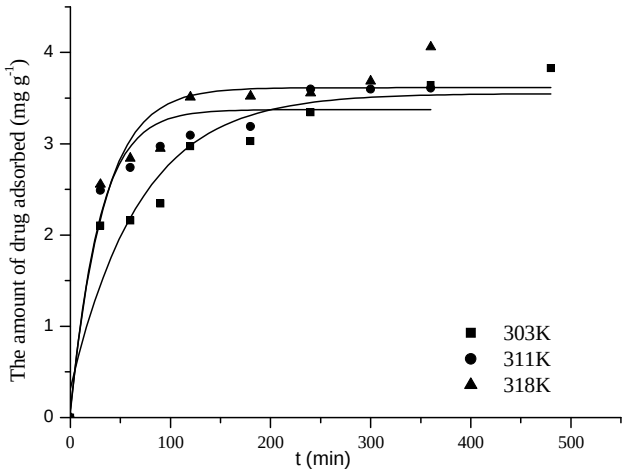

Figure 3.59 Effect of contact time of TMP adsorption onto Al-KSF

The decreasing removal rate towards the end suggests formation of a monolayer of TMP on the outer surface of Al-PILCs and intraparticle diffusion onto the inner surface of the adsorbent particles through the film (Manohar, Noeline, & Anirudhan, 2006). The equilibrium times were found to be approximately the same for all the temperatures studied. The percentage adsorption increases with increasing temperature.

3.3.5 Adsorption kinetics

In order to quantify the changes in adsorption with time and also to evaluate kinetic parameters, three models were applied. These models are pseudo-first-order kinetic model, pseudo-second-order kinetic model and intraparticle diffusion model.

A pseudo-first-order kinetic model of Lagergren (Lagergren, 1898) is given by:

$$\frac{1}{q_t} = \left(\frac{k_1}{q_1}\right)\left(\frac{1}{t}\right) + \frac{1}{q_1} \qquad (1)$$

where

q_t is the amount of trimethoprim adsorbed (mg g^{-1}) on Al-PILCs at various time t ,q_1 is the maximum adsorption capacity (mg g^{-1}), k_1 is rate constant for the adsorption process (min^{-1}) for the pseudo-first order adsorption. Kinetic parameters (q_1 and k_1) were obtained from the intercept and slope of the pseudo-first order straight line. These parameters and correlation coefficients (R_1^2) were summarized in Table 4, R_1^2 are between 0.756- 0.954 for Al-K10 and between 0.756-0.883 for Al-KSF at 303, 311 and 318K, respectively.

Table 3.11 Kinetic parameters for TMP adsorption onto Al-PLCs at 303, 311 and 318K

	Al-K10			Al-KSF		
Temperature / K	303	311	318	303	311	318
Pseudo-first-order kinetic model						
R_1^2	0.75	0.89	0.95	0.75	0.88	0.86
k_1 (min^{-1})	3.77	5.50	4.16	24.99	14.94	17.17
q_1 (mg g^{-1})	18.22	18.47	19.26	3.52	3.60	3.86
Pseudo-second-order kinetic model						
R_2^2	1.0	1.0	1.0	0.98	1.0	0.99
k_2 (g $mg^{-1}min^{-1}$)	0.004	0.005	0.012	0.008	0.011	0.013
q_2 (mg g^{-1})	19.59	19.49	19.31	3.80	3.86	4.03
Intraparticle diffusion model						
R_p^2	1.0	0.92	0.98	0.98	0.98	0.99
k_i (mg $s^{-1/2}g^{-1}$)	0.18	0.32	0.18	0.12	0.09	0.10
C	15.35	14.20	16.62	1.36	2.04	2.06

The pseudo second – order adsorption kinetic rate equation is expressed as

$$\frac{dq_t}{d_t} = k_2(q_2 - q_t)^2 \qquad (2)$$

where k_2 is the rate constant (g $mg^{-1}min^{-1}$), q_2 is the maximum adsorption capacity (mg g^{-1}) for the pseudo second order adsorption kinetic model. Integrating and applying boundary conditions ($q_t = 0$ at $t = 0$ and $q_t = q_t$ at $t = t$), we have a linear form as

$$\left(\frac{t}{q_t}\right) = \frac{1}{k_2 q_2^{\,2}} + \frac{t}{q_2} \qquad (3)$$

To calculate the values of k_2 and q_2 at various temperatures, the intercept and the slope of the linear plots of (t/q_t) versus t were obtained. In general, the correlation coefficients of the first-order kinetic model were was lower than that of the second-order kinetic model. Therefore, the sorption of TMP on Al-PILCs was considered to be explained better by the second-order kinetic model. The experimental data fitted better to the second-order kinetic model as seen from Table 3.11. The maximum adsorption capacities found from drug adsorption onto Al-KSF was increased with an increase in temperature. It implies that a high temperature favors TMP adsorption onto Al-KSF. In addition, the adsorption process is chemical and the movements of TMP from the bulk phase to solid phase (Al-KSF) with a rise in temperature of the solution. On the contrary, the decrease in q_2 values with increasing temperature was observed for adsorption of TMP onto Al-K10. It exhibits that a low temperature favors TMP adsorption onto Al-K10 and the type of adsorption can be considered as physical process. This result is supported by the parameters found from applying isotherm models in the next section.

An intraparticle diffusion model of Weber and Moris (Weber, Morris, & Sanit, 1963) is shown as:

$$q_t = k_{\mathrm{i}}\, t^{1/2} + C \qquad (4)$$

where q_t is the amount of drug adsorbed (mol/g) at time t, C is the intercept. The values of intercept give an idea about the boundary layer thickness, i.e. the larger intercept; the

greater is the boundary layer effect. k_i is the intra-particle diffusion rate constant (mg s^{-1} g^{-1}). k_i was obtained from the slope of q_t versus $t^{1/2}$. The plot may present multilinearity, indicating that a fewsteps take place. The first, sharper portion is attributed to the diffusion of adsorbate through the solution to the external surface of adsorbent or the boundary layer diffusion of solute molecules. The second portion describes the gradual layer adsorption stage, where intraparticle diffusion is rate limiting. The third portion is attributed to the final equilibrium stage. Second, the plots of q_t versus $t^{1/2}$ for intraparticle diffusion model given in Eq. (4) is shown in Fig. 3.60 and 3.61. The external surface sorption (stage 1) is absent because of completion before 5 min. The plots of q_t versus $t^{1/2}$ are found to be straight line (stage 2). The straight line refers to intraparticle diffusion effects (Ayyappan, Carmalin, Swaminathan, & Sandhya, 2005). The k_i values for Al-K10 and Al-KSF are determined and shown in Table 3.11.

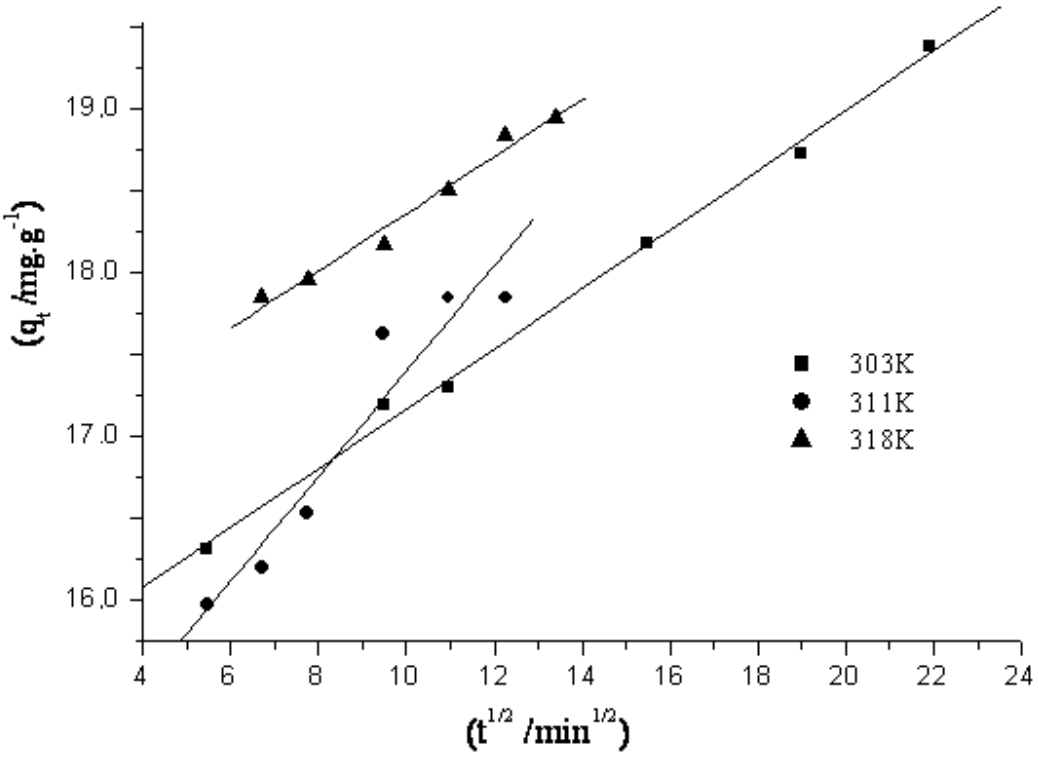

Figure 3.60 Intraparticle Diffusion Plot for TMP onto Al-K10 at 303K, 311K and 318K

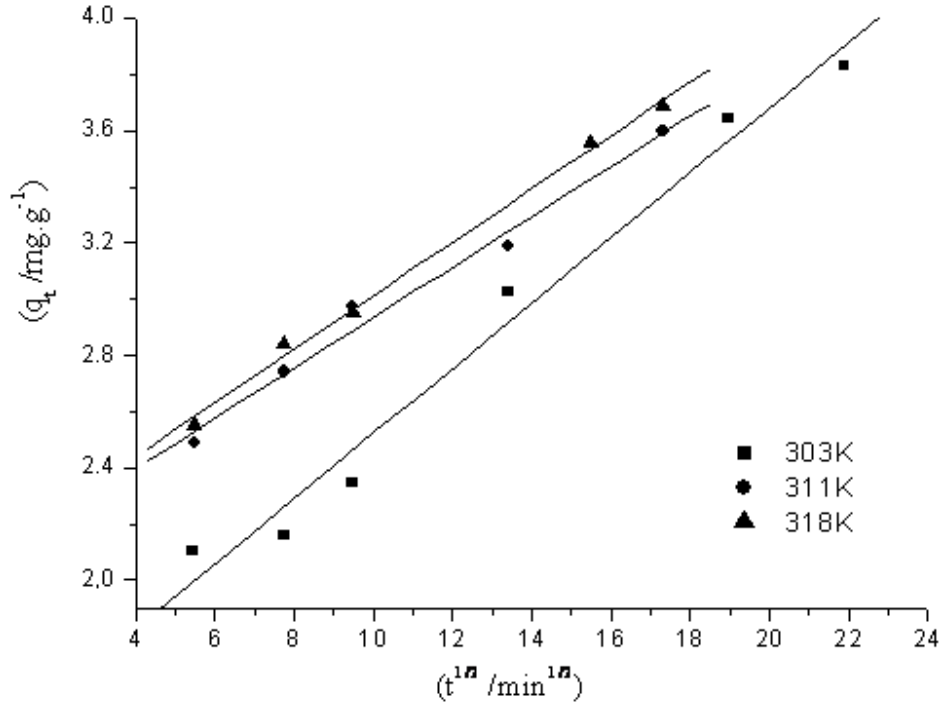

Figure 3.61 Intraparticle Diffusion Plot for TMP onto Al-KSF at 303K, 311K and 318K

The values of intercept, *C* give an idea about the boundary layer thickness, i.e., the larger the intercept, the greater is the boundary layer effect. *C* values are increasing with increase of temperature for Al-KSF. *C* values of Al-K10 are greater than the values obtained from Al-KSF adsorption studies. This indicates that boundary layer effect is not so much efficient for the adsorption of TMP onto Al-KSF than Al-K10. The curves reveal a linear characteristic that the intraparticle diffusion controls the adsorption process. The linear portions of the intraparticle diffusion curves do not pass through the origin, so it was proposed that in addition to intraparticle diffusion, other process may control the rate of adsorption.

In order to quantify the changes in adsorption with time and also to evaluate kinetic parameters, three models were applied. These models are pseudo-first-order kinetic model, pseudo-second-order kinetic model and intraparticle diffusion model.

3.3.6 Adsorption isotherm

The change in the adsorbed amount of TMP with equilibrium concentrations is given in Figure 3.62 and 3.63. C_s is the solid phase concentration (mmol g^{-1}) and C_e is the final concentration (mmol L^{-1}) in the supernatant at equilibrium for each initial concentration.

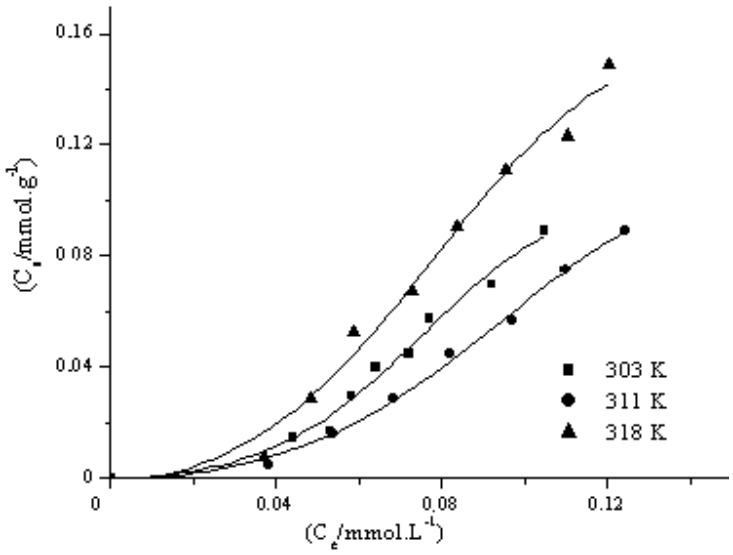

Figure 3.62 Adsorption isotherm for TMP on Al-K10 at 303K, 311K and 318K

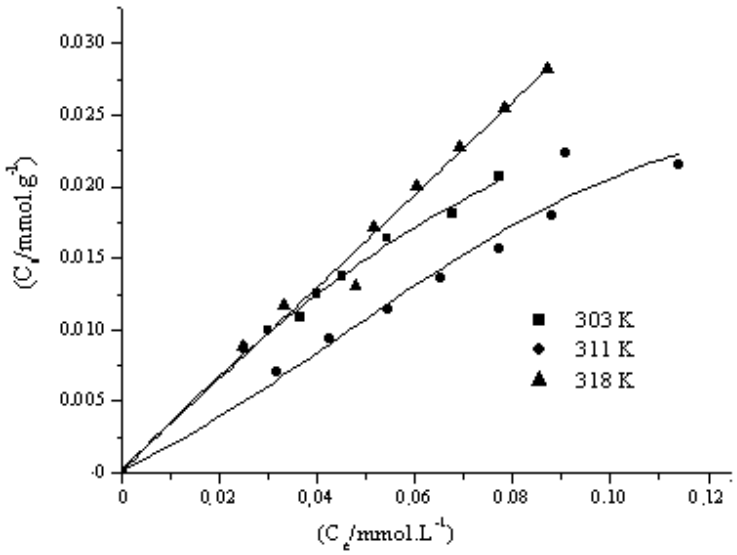

Figure 3.63 Adsorption isotherm for TMP on Al-KSF at 303K, 311K and 318K

In terms of the slope of initial portion of the Al-K10 and Al-KSF isotherm curves, the shapes of these isotherms correspond to S–type and C-type according to Giles classification, respectively (Giles, McEwan, Nakhwa, & Smith, 1960). Such isotherms are relatively rare and indicative of weak adsorbent–adsorbate interactions (Rouquerol, Rouquerol, & Sing, 1999).

Analysis of the isotherm data is important to develop equations that accurately represent the results and could be used for design purposes to remove trimethoprim (TMP) from wastewater treatment plant. In this concern, various isotherm equations have been used to describe the equilibrium nature of adsorption processes. In order to investigate the sorption isotherm, three models were analyzed. These models were the Langmuir, the Freundlich, and the Dubinin-Raduschkevich (DR) models. The Langmuir isotherm theory assumes monolayer coverage of adsorbate over a homogenous adsorbent surface (Langmuir, 1918). The adsorption data were first adjusted to the linear form of Langmuir adsorption model (Eq.5).

$$\frac{C_e}{C_s} = \frac{1}{C_m\, a_L} + \frac{C_e}{C_m} \tag{5}$$

The specific sorption (C_e/C_s) was plotted against the equilibrium concentration (C_e). C_s is the solid phase concentration (mmol g^{-1}) and C_e is the final concentration (mmol L^{-1}) in the supernatant at equilibrium for each initial concentration, C_m is the amount of drug necessary for the formation of the monolayer. a_L is a Langmuir constant related to the intensity of the adsorption and adsorption energy. From the slope and intercept coefficients of Eq. (5), for each temperature studied the values of the constants C_m and a_L were found.

The adsorption capacity C_m and energy of adsorption a_L are presented in Table 3.12. The essential characteristics of the Langmuir isotherm can be expressed in terms of a dimensionless constant separation factor R_L that is given by equation

$$R_L = 1/(1 + a_L C_0) \quad (6)$$

C_0 is the initial TMP concentration (mmol L^{-1}) and a_L is Langmuir constant. R_L values at different temperatures for both Al-K10 and Al-KSF are reported in Table 3.12. R_L values between 0 and 1 indicate favorable adsorption of TMP onto Al-KSF at the concentration studied. R_L values of Al–K10 are higher than 1. It indicates that unfavorable adsorption was occurred and also all C_m values are negative for Al-K10.

The correlation coefficients obtained by employing Langmuir equation are smaller than obtained by Freudlich equation. The Empirical Freundlich expression (Eq. (7)) is an exponential equation and therefore, assumes that as the adsorbate concentration increases so too does the concentration of adsorbate on the adsorbent surface. Theoretically, using this expression, an infinite amount of adsorption can occur (Freundlich, 1906).

Freundlich equation is based on a monolayer adsorption by the adsorbent with a heterogeneous energy distribution of active sites (Aksu, & Kabasakal, 2004).

$$C_s = K_f C_e^{\,nf} \quad (7)$$

Linearized form of the equation can be used to find the parameters K_f and n_f.

$$\ln C_s = \ln K_f + n_f \ln C_e \quad (8)$$

The slope and intercept coefficients of Eq. (8) give n_f and K_f, respectively, for each temperature studied. See Table 3.12 for the Langmuir and Freundlich adsorption parameters. n_f is a characteristic constant related to sorption intensity, C_s, C_e and K_f represent sorbed amount (mmol g^{-1}), residual concentration of sorbate in solution at equilibrium (mmol L^{-1}) and sorption capacity of sorbent (mmol g^{-1}), respectively. For Al-K10, K_f values decrease by increasing temperature. However K_f values obtained from

the studies in which Al-KSF was used increase by increasing temperature. All isotherm and kinetic models used in this study supported these results. All isotherm values are summarized in Table 3.12.

Table 3.12 Isotherm parameters for TMP adsorption onto Al-K10 and Al-KSF at various temperatures

	Al-K10			**Al-KSF**		
Temperature (K)	**303**	**311**	**318**	**303**	**311**	**318**
Langmuir model						
R_l^2	0.71	0.85	0.69	0.88	0.95	0.91
C_m (mmol g^{-1})	-0.03	-0.04	-0.10	0.06	0.10	0.20
L (gL^{-1})	-7.68	-5.58	-5.08	6.17	2.31	0.55
R_L	4.31	2.26	2.03	0.62	0.81	0.95
Freundlich model						
R_f^2	0.95	0.99	0.97	0.99	1.0	1.0
K_f ($mmolg^{-1}$)	14.57	6.58	5.50	0.14	0.15	0.26
n_f	2.21	2.04	1.69	0.76	0.87	0.92
DR model						
R_D^2	0.98	0.99	0.97	0.99	0.99	1.0
X_m ($molg^{-1}$)	0.80	0.61	0.22	0.66	0.80	1.52
E ($kJmol^{-1}$)	5.43	5.55	6.26	9.06	8.72	8.77

It can be seen that the Freundlich model yields a much better fit than the Langmuir model when the R^2 values are compared. This suggests that the boundary layer thickness is increased (Özcan, & Özcan, 2004). Furthermore, the value of n_f at equilibrium is bigger than 1 for Al-K10. It is noted that the values of n_f are bigger than 1, reflecting the unfavorable adsorption. These results indicate that Al-K10 hasn't a very strong adsorption capacity for TMP in the solution. n_f values obtained from the study in which Al-KSF was used are smaller than 1 thus this adsorption is favorable for removing TMP

from wastewater treatment plants. This result is deduced also from dimensionless separation factors.

The Dubinin–Radushkevich (D–R) isotherm model is more general than the Langmuir isotherm since it does not assume a homogeneous surface or constant sorption potential. It was applied to distinguish between the physical and chemical adsorption of metal ions (Lin, & Juang, 2002; Dubinin, & Radushkevich, 1947). The isotherm parameters were obtained from the linear form of Dubinin–Radushkevich isotherm equation.

$$\ln C_{sorb} = \ln X_m - \beta\varepsilon^2 \quad (9)$$

where C_{sorb} is the amount of ions sorbed onto the adsorbent ($molg^{-1}$), X_m represents DR monolayer capacity of the sorbent ($molg^{-1}$), β a constant related to sorption energy (mol^2/kJ^2) and ε Polanyi sorption potential, the amount of energy required to pull a sorbed molecule from its sorption site to infinity which is equal to:

$$\varepsilon = RT \ln (1+1/C_e) \quad (10)$$

where R is the gas constant in $kJmol^{-1}K^{-1}$; T is the temperature in Kelvin and C_e is the equilibrium concentration in solution ($mol\ dm^{-3}$). The Polanyi adsorption theory postulates fixed volume of sorption site close to sorbent surface and existence of sorption potential over these sites. The sorption potential is related to an excess of sorption energy over the condensation energy and is independent of temperature. The plot of lnC_{sorb} versus ε^2 follows linearity. The value of X_m is determined from the intercept and the value of β is derived from the slope. The sorption energy, E for ions onto adsorbent calculated using the expression:

$$E = -\frac{k^{-1/2}}{\sqrt{2}} \quad (11)$$

is the range of 8-16 kJmol^{-1} designated for ion exchange mechanism (Malik, Hasany, & Subhani, 2005). If the value of E is smaller than 8 kJmol^{-1}, this shows physical adsorption due to weak van der Waals forces (Singh, & Pant, 2004). The Dubinin–Radushkevich isotherm parameters are shown in Table 3.12. The maximum sorption capacities (X_m) of the applied adsorbents for TMP were decreased by increasing temperature for Al-K10 and increased by increasing temperature for Al-KSF. The values of porosity factors (β) for both Al-K10 and Al-KSF are less than unity and so imply the adsorbents to have fine micropores and indicate a surface heterogeneity may be arisen from the pore structure as well as adsorbate–adsorbent interactions (Singh, & Pant, 2004). The adsorption of TMP from aqueous solution onto Al-K10 is physical thus E values for Al-K10 were smaller than 8 kJmol^{-1}. Weak physical forces, such as van der Waals and hydrogen bonding may affect the sorption mechanism onto Al-K10. Furthermore E values for Al-KSF are higher than 8 kJmol^{-1} but not so much. It can be said that the adsorption mechanism of TMP onto Al-KSF is ion exchange.

3.3.7 Adsorption thermodynamic

The thermodynamic parameters of equilibrium constants (K_c), the enthalpy (ΔH^o), the Gibbs free energy (ΔG^o), and the entropy (ΔS^o) of the adsorption of TMP onto Al-PILCs were determined using the following equations (Vaishya, & Gupta, 2002).

$$\Delta G^\circ = -RT\ln K_c \tag{12}$$

$$K_c = \frac{C_s}{C_e} \tag{13}$$

$$\ln K_c = -\frac{\Delta H^0}{RT} + \frac{\Delta S^0}{R} \tag{14}$$

where C_s is the concentration of drug adsorbed (molL^{-1}); C_e is the equilibrium concentration of TMP in solution (mol L^{-1}) at a given temperature; T is the solution temperature (Kelvin); and R is the gas constant (8.314 JK^{-1} mol^{-1}). The enthalpies of the TMP-Al-PILC adsorption (ΔH^o) are obtained from van't Hoff plots as lnK_c versus 1/T. The thermodynamic parameters are shown in Table 3.13. It is observed that the values of ΔH^o are positive and 1.574-10.91 kJmol^{-1} for Al-K10 and Al-KSF, respectively. The van't Hoff plots of the interactions of the drug with the surface of the adsorbents require energy and this interaction is endothermic in nature. The low adsorption enthalpy values have been attributed to a number of physical interactions involving electrostatic attractions, nonpolar interactions, water bridging, hydrogen-type bonding, and ion-exchange reactions between the drug molecules and the adsorbent structure (Messina, & Schulz, 2006). In addition, there is the possibility of H-bond and water-bridge formation between the N or O groups in the TMP organic structure in chapter 1 (Fig. 1.12) and the -OH group that is present at the structure of Al-PILCs. The standard entropy (ΔS^o) was estimated from the intercept of the van't Hoof plot. The standard entropy values for the adsorption onto Al-KSF and Al-K10 were 34.71 and 3.700 Jmol^{-1}K^{-1}, respectively. The standard entropy change for TMP sorption process is positive. It indicates that degrees of freedom of adsorbed species are increasing. Most of ΔG^o values at various temperatures are positive. Only for Al-KSF at 318 K, the ΔG^o value is negative. Furthermore the ΔG^o of the process for Al-KSF decreased with increase in temperature, which indicated that the process may be spontaneous at high temperatures. The positive value of ΔG^o at various temperatures show the nature of adsorption is not spontaneous.

Table 3.13 Thermodynamic parameters for TMP adsorption on Al-K10 and Al-KSF

T (K)	K_c	ΔG^o (kJmol^{-1}K^{-1})	ΔS^o(Jmol^{-1}K^{-1})	ΔH^o(kJmol^{-1})
Al-K10				
303	0.344	2.69		
311	0.348	2.73	3.69	1.57
318	0.354	2.74		
Al-KSF				
303	0.860	0.38		
311	0.940	0.16	34.71	10.91
318	1.055	-0.14		

3.4 Characterization and swelling properties of poly (acrylic acid)/Zr-pillared Montmorillonite KSF superabsorbent composites

3.4.1 Swelling rate measurements of Zr-KSF based superabsorbents

Figure 3.64 displays the swelling rate of Zr-KSF based superabsorbents. It was found that the swelling ratio of superabsorbent hydrogel containing 0.05g of Zr-KSF was higher than superbsorbents containing 0.10 and 0.20g of Zr-KSF at swelling equilibrium, respectively. Additionally, the swelling rate of Zr-KSF (0.05g)-SA was the highest than the others and the time needing to reach swell equilibrium increases with increase of pillared clay amount. Zr-KSF based superabsorbents reached equilibrium within 80 min. The percentages of equilibrium swelling values were at about 10285 for Zr-KSF (0.05g)-SA, at about 9850 for Zr-KSF (0.10g)-SA and at about 9440 for Zr-KSF (0.20g)-SA. This may be attributed to crosslink density and elasticity of polymer network. Pillared clay act as crosslinking points because of carrying –OH groups in their

structure. The carboxylate groups of the polyacrylate chains may react with -OH groups of pillared clays. Increasing the amount of pillared clays in the polymeric network resulted in the generation of more crosslink points that increase the crosslink density of the composite, and then the elasticity of the polymer chains decrease. It was deduced that more crosslink points may occur between Zr-KSF (0.20g) pillared clay and SA. Shortly, the superabsorbent with lower pillared clay content had a higher initial swelling rate and higher water absorbency and required less time to reach swelling equilibrium.

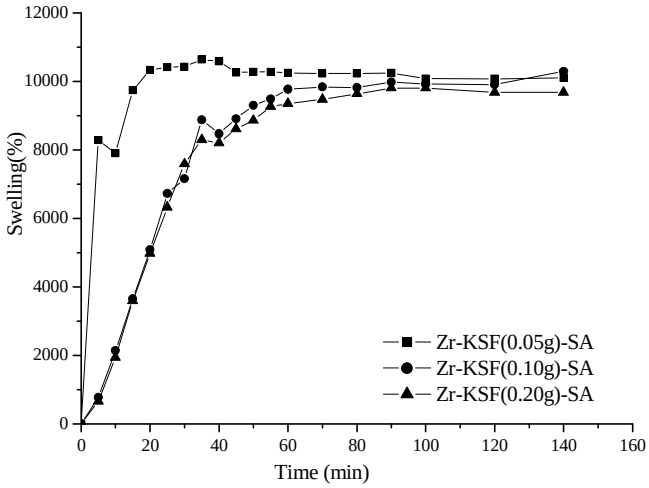

Figure 3.64 Swelling kinetics of superabsorbents composite in distilled water

3.4.2 pH-sensitivity of Zr-KSF based superabsorbents

To clarify pH sensitivity of pillared clay based superabsorbents, firstly the films were immersed in distilled water and then in different buffer solutions until swelling equilibrium. Figure 3.65 showed the effect of the pH on water absorbency of superabsorbents. The buffer solutions at pH 3.4, 4.0, 6.7 and 8.5 were prepared by using citric acid and $Na_2HPO_4.2H_2O$ solutions.

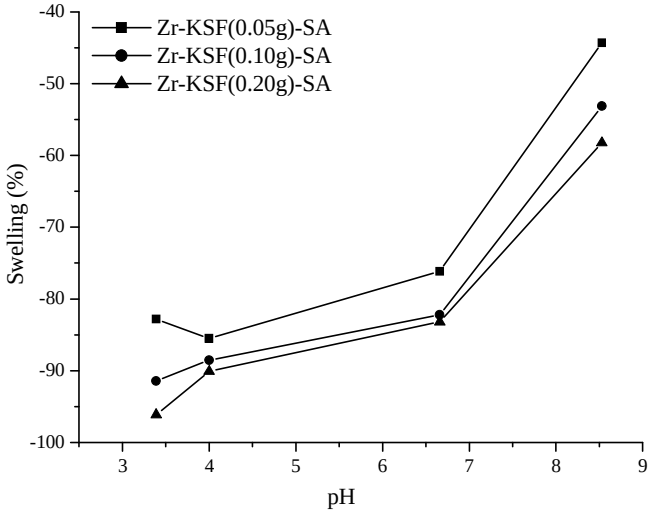

Figure 3.65 Effect of pH on the equilibrium swelling of superabsorbents

The absorbency of the superabsorbent composite increased sharply as the pH increased from 3.4 to 8.5. The superabsorbent composites were sensitive to the pH change. Shrinkage was occurred at acidic pH for all Zr-KSF based superabsorbents. The change in the swelling ratio by changing pH may be explained by Lee and Wum suggestion (Lee, & Wum, 1996); in an acidic environment, the $–COO^-$ groups on the polymeric chains turn into –COOH groups, while the –COOH groups on the polymeric chain turn into $–COO^-$ groups in basic solutions, and this behavior was interpreted as a buffer action of –COOH and $–COO^-$. In the acidic environment, the repulsion between polymeric chains decreases, which leads to the decrease of water absorbency. The –COOH groups present within the network remain almost nonionized, thus imparting almost non-polyelectrolyte type behavior to the hydrogel (El-Hamshary, 2007). Furthermore, there exist H-bonding interactions between carboxylic groups of acrylic acid and amide groups of acrylamide. These H-bonding interactions result in the formation of a compact or tight structure which does not permit much movement of polymeric chains within the hydrogel network, which lead to minimum swelling of hydrogel (El-Hamshary, 2007). The ionization of the carboxylic acid groups of the gel occurred. More hydrophilic polymer was occurred at higher pH value because of

ionization of the carboxylic acid group and contributed to the higher water absorption. As seen in Fig. 3.65, the swelling behavior of Zr-KSF based superabsorbent films seem to be pH dependent. The content of pillared clay in the network of the superabsorbent affected the swelling ratio. More shrinkage and lower swelling was obtained by increasing the content of Zr-KSF in the polymeric network. Additionally, croslinking might be increased in order of increasing the amount of pillared clay. The water content decreased due to increased level of crosslinking (Wu, Li, & Chen, 2004).

3.4.3 Swelling reversibility of superabsorbents

To reveal swelling reversibility, the Zr-KSF based superabsorbents were equilibrated at pH=1.2, and then alternated between solutions at pH=7.4 and pH=1.2 for about 120 minutes, respectively. A swelling was measured at about 900% for Zr-KSF (0.05g)-SA, 537% for Zr-KSF (0.10g)-SA and 540% for Zr-KSF (0.20g)-SA at pH= 7.4, respectively. Then the films put into pH=1.2 for 120 min. and approximately 3.50%, 0.60% and 23.0% deswellings for Zr-KSF(0.05g)-SA, Zr-KSF(0.10g)-SA and Zr-KSF(0.20g)-SA, respectively were determined. Besides, when the superabsorbent films altered from acidic to basic buffer and then to acidic buffer, pillared clay based superabsorbents showed a reversible swelling behavior with relatively fast response. Zr-KSF (0.05g)-SA had the fastest response to pH change. It can be added that reversible swell-shrink properties of pillared clay based superabsorbents would be beneficial characteristics for pH sensitive systems with controllable swelling ability. Also, this result indicates that the PAMA composite can be used as a recyclable water-managing material for the renewal of arid and desert environment (Zhang, Liu, Li, & Wang, 2006).

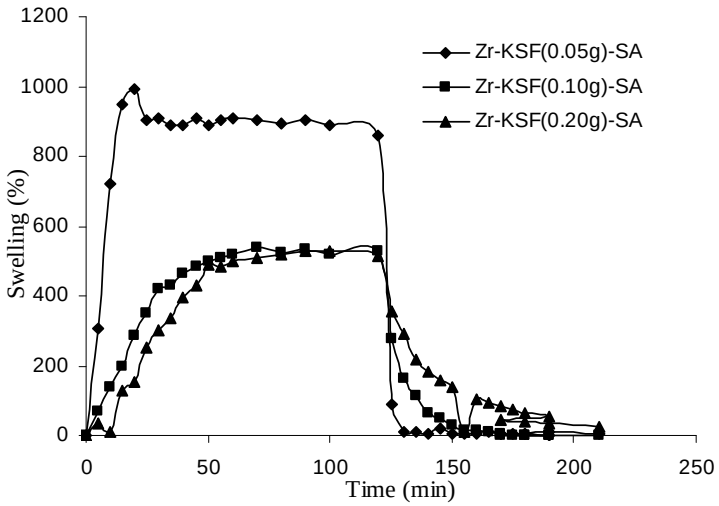

Figure 3.66 pH-dependent reversible swelling behavior of superabsorbents (Superabsorbents equilibrated at pH=1.2, then alternated between solutions at pH=7.4 and pH=1.2)

3.4.4 SEM images

The SEM micrographs of Zr-KSF, Zr-KSF (0.05g)-SA, Zr-KSF (0.10g)-SA and Zr-KSF (0.20 g)-SA were exhibited in Fig.3.67. A considerable difference was observed between pillared clay and superabsorbents. Polymeric network was predominant in superabsorbent hydrogel morphology. When the content of pillared clay was increased, the surface of polymeric network was affected, the signs of pillared clay were increased and surface of hydrogels were less smooth. Also SEM micrographs were supported the homogeneity of composed superabsorbents after graft polymerization had been occurred. Homogenous dispersion of pillared clay particles may be contributed to more crosslinking structure. Furthermore more crosslinking might be obtained by increasing pillared clay amount in the superabsorbents. SEM micrographs of superabsorbents clearly represented lower swelling capacities because of their highly rigid type structure.

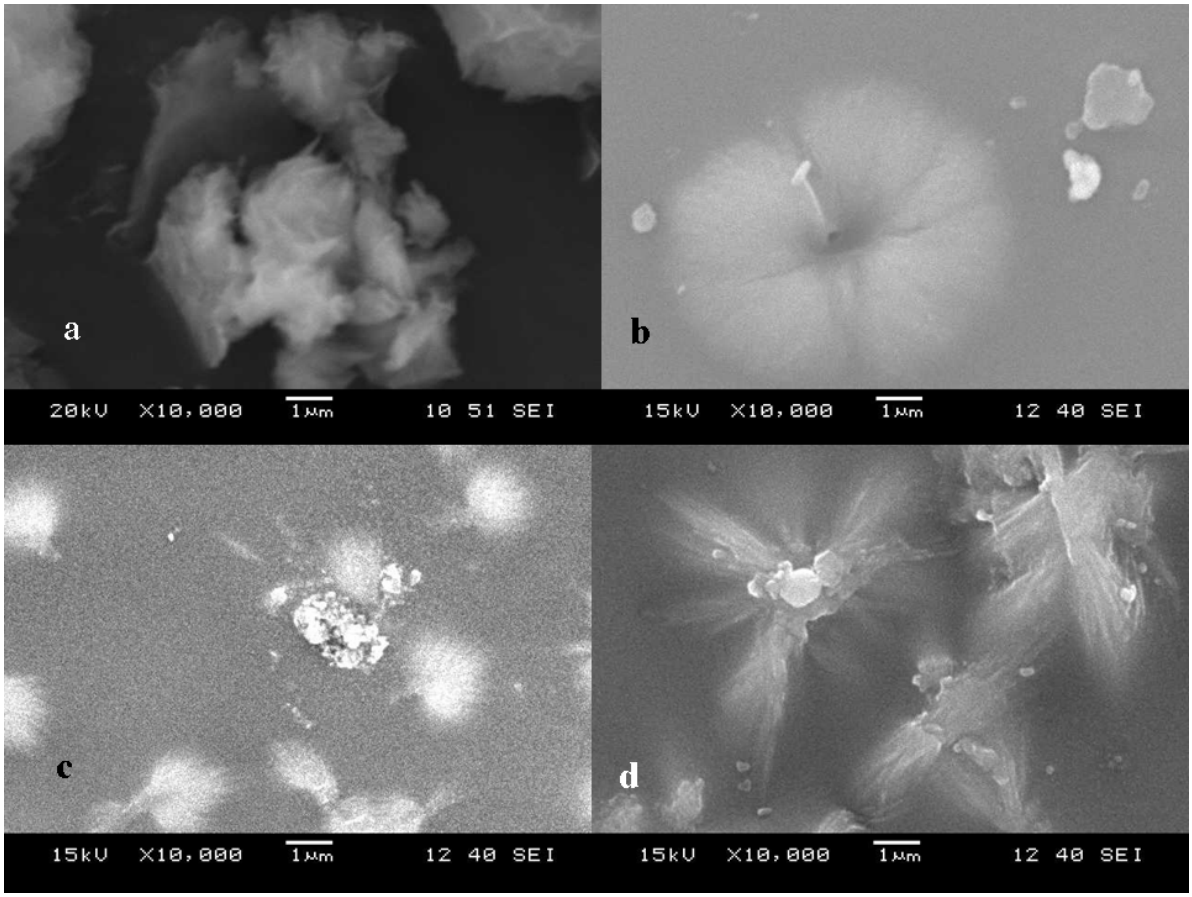

Figure 3.67 SEM micrographs of (a)Zr-KSF (b)Zr-KSF(0.05g)-SA (c)Zr-KSF(0.10g)-SA (d)Zr-KSF(0.20g)-SA (10000x magnification).

3.4.5 FTIR Analysis

FTIR spectra of Superabsorbent (SA) and Zr-PILC-SA were presented in Figure 3.68. As can be seen in the spectrum of Zr-KSF, the absorption bands at 3626 cm^{-1} and 3429 cm^{-1} was due to lattice OH and bound water stretching vibration, respectively. After grafting of SA, only one band at 3360 cm^{-1} appears. The disappearance of the OH lattice band (due to existence of the Si–O–H group) demonstrates esterification of carboxylic acid with silanol groups existing on Zr-KSF. This may be an evidence for the grafting reaction between Zr-KSF and the acrylic network of SA.

The band at 2950cm^{-1} is attributed to CH stretching of the acrylate unit for SA. After adding Zr-pillared clay this band decreased to 2937 cm^{-1}. The stretching vibration of C=O of the acrylate unit for SA was observed at 1702 cm^{-1}. This band of Zr-KSF-SA which was demonstrated at 1699 cm^{-1} was almost similar with that of SA. The bands at 1568 and 1407 cm^{-1} may be attributed to asymmetric and symmetric vibrations of R-COOK groups respectively. The band at 1568 cm^{-1} decreased to 1552 cm^{-1} with a sharp band after grafting of SA. The absorption band corresponding –COO- bending vibration of acrylate unit of SA can be assigned at 1037 cm^{-1}. It is intersting to note that this band was increased to 1120 cm^{-1} as a result of adding of Zr-KSF to the SA. Also there is a shoulder at 1048 cm^{-1} which may be due to stretching vibration of Si-OH group.

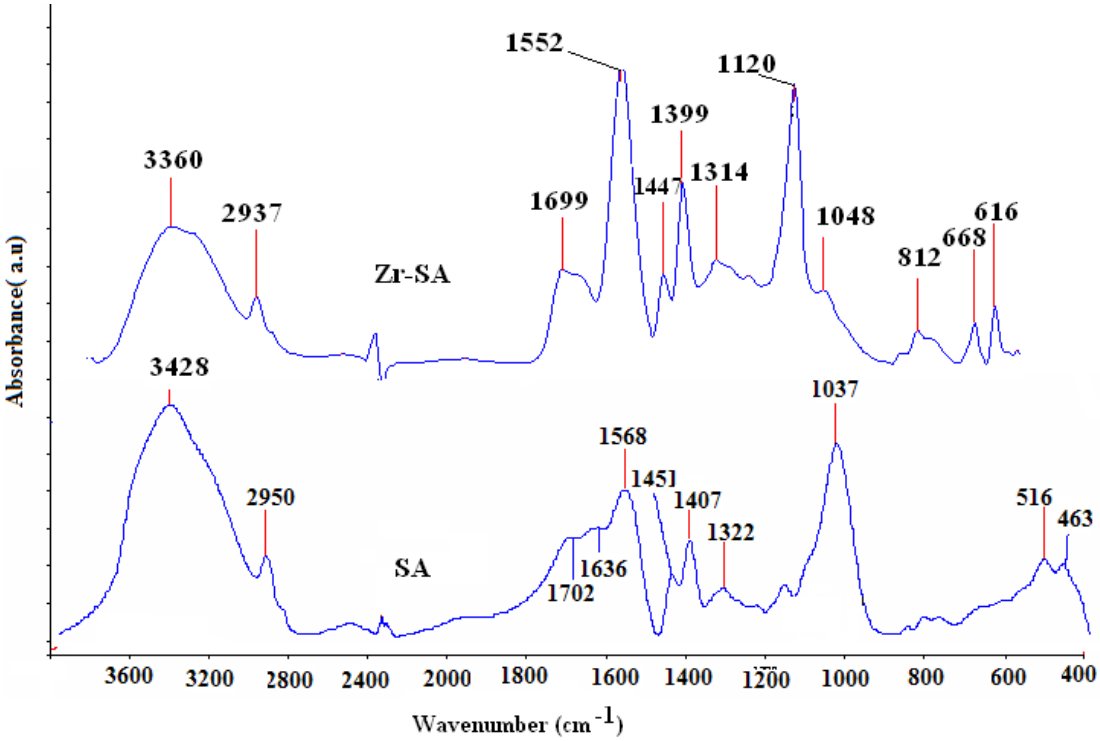

Figure 3.68 FTIR spectra of SA and Zr-KSF-SA

3.4.6 XRD analysis

The X-ray diffraction patterns of Zr-KSF (0.05g)-SA, Zr-KSF (0.10g)-SA and Zr-KSF (0.20g)-SA were shown in Fig. 3.69. The lattice spacings of montmorillonite KSF and Zr pillared KSF were 12.55Å at 2θ=6.99° and 19.13Å at 2θ=4.60°, respectively. 001 lattice spacing of KSF was increasing by pillaring with Zr polyoxications. After polymerization with pillared clays the diffraction peak corresponding to the montmorillonite (d_{001} basal spacing of montmorillonite layers) was not observed at about 2θ=5.0-6.0°. The absence of this peak indicates that the montmorillonite layers are exfoliated or highly expanded. The expansion mechanism probably originates from the growing polymer chains by adsorbed monomers on the clay layers pushing apart the layers even in high clay loadings (Kaşgöz, Durmuş, & Kaşgöz, 2008). Layers of montmorillonite were completely dispersed in a continuous polymer matrix as single layers. The XRD patterns Zr-KSF based composites showed two crystal peaks at 2θ of ~

20° and 30°, respectively. These data support the presence of layers of clays. The graphs of superabsorbents indicated that sharp crystal peaks were observed when the content of Zr-KSF was increased. Composites reflected more amorphous character.

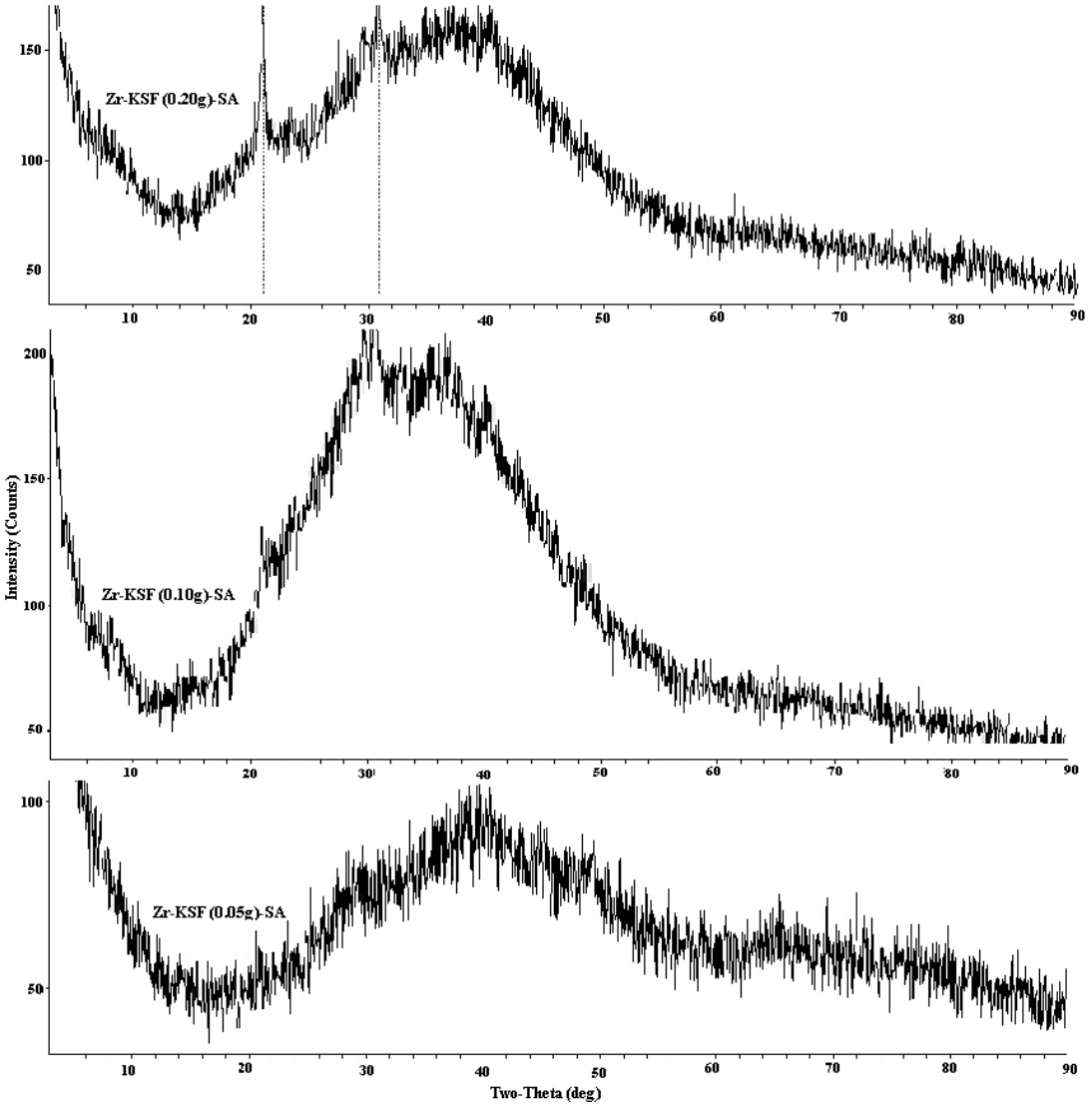

Figure 3.69 XRD patterns of Zr-KSF(0.05g)-SA; Zr-KSF(0.10g)-SA and Zr-KSF(0.20g)-SA.

CHAPTER FOUR

CONCLUSION

4.1 Conclusion

This thesis study was composed of four main parts. First part involved synthesis and characterization of Aluminum, Zirconium, and Iron pillared Montmorillonite KSF / Monmorillonite K10. Characterization and swelling behaviors of poly (acrylic acid)/Aluminium pillared Montmorillonite K10 and KSF were performed in the second part of the study. The third part of the study was related to sorption experiments of Aluminium pillared Montmorillonite K10 and Montmorillonite KSF. The final study involved the characterization and swelling properties of poly (acrylic acid)/Zr-pillared Montmorillonite KSF superabsorbent composites.

In the first part, synthesis of pillared clays was performed in suitable experimental conditions. XRD, FTIR, TGA, SEM and BET analysis were carried out to clarify whether pillaring was occurred or not. XRD results indicated that pillaring achieved an increase in the distance of layers of montmorillonite. Interlayer separations were between 4.42 and 10.0 Å. Zirconium pillared KSF series have higher interlayer separations than the other pillared KSF series. This was indicated as Zr-KSF > Al-KSF > Fe-KSF for interlayer separation. As seen pillared K10 series, Al-K10-OD*20x had the highest enlargement between interlayer. The interlayer separation of pillared K10 was increased in order of Zr–K10, Fe–K10, and Al–K10. Additionally, XRD data was reflected the main structure of precursors of pillared clays (KSF, K10).

When FTIR spectrums were examined, the main montmorillonite IR bands were observed. This was supported the pillaring was occurred by physical attractions. Only band shifted a little. The retention of all bands as in parent montmorillonite in the framework region clearly shows that the basic clay layer structure remains unaffected on

pillaring. These bands are slightly broader but their wavenumbers are almost the same as those of clays.

SEM micrographs of the pillared clays and clays gave information about the morphology of them. The montmorillonites appear as corn flake like crystals with fluffy appearance revealing its extremely fine platy structure. After pillaring, clay has become fluffier. Similar changes were observed on morphology of the precursor clay by pillaring when examined the micrographs of the pillared clay.

N_2 adsorption–desorption isotherms of pillared clays were beneficial for determined the surface areas of the pillared clays. The nitrogen adsorption–desorption isotherms of all pillared clays exhibit type IV of the BDDT classification, with a well defined H4 hysteresis loop. Fe-KSF-FD^+ had the highest BET surface area, total pore volume and average pore diameter between the pillared KSF samples. This might be affected the freeze drying and pillaring agent. Pillared clays freeze dried had the high surface areas than pillared clays oven dried. As a result of N_2 adsorption–desorption isotherms, it was concluded that pillared clays had much greater surface areas than K10 and KSF. It was beneficial for catalysis and adsorption studies.

TGA analyses of pillared clays were useful to found mass losses, dehydroxylation and collapse temperatures. This was beneficial information to determine the temperature of calcinations. Further more thermal stability of pillared clays was quite high. The thermogravimetric analysis of clays and pillared clays revealed a weight loss on heating in the range of 20 to 300°C which can be attributed to elimination of physical adsorbed water. On the other hand, the weight losses in the second stage have been assigned to the removal of chemisorbed water, water molecules coordinated to the pillars and dehydroxylation of the pillars.

All characterization methods were supported that pillaring was occurred, this event was performed physically. Surface areas and the interlayer separation of pillared clays

were increased. The pillared clays synthesized were used for catalysis and adsorption studies. Additionally, using pillared clays in preparation of superabsorbent as additives was the new approach. This was effective to increase the hardness of the composites.

This second study involved the preparation of pillared clay based superabsorbent composites. Al-K10 and Al-KSF used as pillared clays. After grafting occurred between pillared clays and the acrylic network, swelling character of composites were revealed out. pH affected swelling character of composites. The swelling behavior of Al-KSF and Al-K10 based superabsorbent films seemed to be pH dependent. It was very essential for new application fields for example drug delivery at human system. For both pillared clay based composite, shrinkage was occurred at low pH values. At basic pH condition, the composites showed swelling behavior. Additionally, reversible swell-shrink properties of Al-KSF and Al-K10 based superabsorbents revealed by using buffer solutions at different pH values. It was beneficial characteristics for pH sensitive systems with controllable swelling ability.

The percentages of equilibrium swelling values in distilled water were at about 7900 for Al-KSF SA and at about 5700 for Al-K10 SA. The products were characterized by SEM, FTIR and XRD. Characterization methods supported the swelling behavior of composites. SEM images indicated that the homogeny dispersion of pillared clay on Al-KSF based composite was lower than Al-K10 based composite and the pores were observed clearly from the morphology of Al-K10. From FTIR analysis, IR characteristic bands of clay were observed in pillared clays and the network of pillared clay based composites. It was understood that the clay layer structure remain unaffected by polymerization. The shifts seen of stretching vibrations of SiO_2 tetrahedra and OH bands supported ester formation between acrylic network and pillared clay.

The XRD results indicated that the peaks assigned to the 001 lattice spacing of montmorillonite were not observed and layers of montmorillonite are completely dispersed in a continuous polymer matrix as single layers thus pillared clay based

composites presented a low swelling value. It supported that the crosslinking was higher and swelling ratio of Al-K10 based composite is lower than Al-KSF based composite. It can be concluded that these properties of superabsorbents would be valuable for many application field in which hydrogels were used. Pillared clays could not protect the layered silicate structure upon fabricating composites with graft copolymerization of acrylic acid.

The third part represented the results of the characteristics of Al-PILCs and the performance of the pillared clay in the adsorption of trimethoprim. It was obtained that 6.22 and 9.18 Å increases in basal spacing of Al-KSF and Al-K10 are the maximum increase before the delamination occurs. The increase in surface area is effective on adsorption. The specific surface area of Al-K10 is lower than the surface area of K10. This result may be effected the adsorption efficiency. Pillaring KSF with aluminum hydroxides increased the surface area of KSF. Thus the adsorption performance of Al-KSF is higher than Al-K10 for the higher adsorbent dosage.

The analysis of experimental results by equilibrium sorption isotherms and kinetic models is important in developing accurate data that could be used for sorption design purposes. From the results, it could be concluded that the adsorption was highly dependent on initial concentration, adsorbent dosage, the solution pH and temperature. We have prepared aluminium pillared montmorillonite K10 and KSF for utilizing in batch adsorption of trimethoprim (TMP) from waste solutions. The synthesized adsorbent compared with the natural one, the adsorption capacities of Al-PILCs are low than the K10 and KSF. Besides Al-PILCs exhibit satisfactory characteristics to be included in treatment of hazardous wastes for TMP removal. From TGA analysis, it was clear that Al- PILCs have good thermal stability.

The removal percentage of TMP was highly depended on pH of solutions. TMP and the adsorbent surface, both carrying positive charges at acidic pH values may explain the poor adsorption of TMP on the surfaces of Al-PILCs. In contrast, the percentage of

adsorption is increased with an increase in pH for both Al-K10 and Al-KSF. The adsorption of trimethoprim increased with increasing contact time and become almost constant nearly after 120 min and 240 min for Al-K10 and Al-KSF, respectively. 120 min and 240 min of contact times are shorter than the precursor materials of Al-K10 and Al-KSF (K10 and KSF). The preliminary investigation on the effect of adsorbent dose on adsorption of Trimethoprim shows that Al-K10 exhibits higher removal capacity of TMP at lower adsorbent dosages in comparison with Al-KSF.

Kinetic studies indicated that the adsorption followed the pseudo second-order kinetic model with $R^2 > 0.978$ for all temperatures and for aluminium pillared clays. The fit of intraparticle diffusion was also studied. The linear portions of the intraparticle diffusion curves for Al-PILCs do not pass through the origin, it implies that the intraparticle diffusion is not the only rate controlling step and the complex adsorption mechanism was occurred.

The equilibrium adsorption data are satisfactorily fitted to three isotherm models are Langmuir, Freundlich, and Dubinin–Radushkevich. Freundlich isotherm best correlate the experimental data for Al-KSF. R^2 values obtained from Dubinin–Radushkevich isotherm is higher than the other isotherms for TMP adsorption onto Al-K10. Adsorption of TMP which release to environment and will affect the biotic process because of transferring resistance genes from harmless bacteria to pathogenic bacteria and on to humans interacting with aquatic environment is increased by increasing temperature onto Al-KSF and increased by decreasing temperature onto Al-K10. These results are supported by the isotherm and kinetic inputs. Sorption energy values obtained from DR equation were between 8 and16 $kJmol^{-1}$ for TMP sorption onto Al-KSF. This adsorption can be explained by ion-exchange mechanism at 303, 311 and 318 K and energy values are close to physical adsorption type. For adsorption TMP onto Al-K10 can be explained by physical adsorption type.

The thermodynamic parameters of standard enthalpy and entropy were found by applying van't Hoff equation and the Gibbs free energy values were estimated via the equilibrium constants. $\Delta H°$ indicates that adsorption is endothermic. The positive $\Delta S°$ values suggest that randomness increases during adsorption. For sorption TMP onto Al-KSF, $\Delta G°$ values are decreased by increasing temperature and at 303 and 311 K, $\Delta G°$ values are positive but at 318K Gibbs energy is negative and adsorption is spontaneous. For sorption TMP onto Al-K10, $\Delta G°$ values at 303, 311 and 318 K are positive and adsorption is not spontaneous.

The results showed that Al-PILCs are potential useful adsorbents for the removal of TMP from wastewater treatment plants. The usage and disposal of antibiotics to environment are impossible to stop so this study shows a way to overcome destructive impacts of antibiotics released into the environment and develop an appropriate system to remove pharmaceuticals present in wastewater treatment plants.

In the last study, swelling characters of poly (acrylic acid)/Zr-pillared Montmorillonite KSF superabsorbent composites were revealed out after grafting occurred between pillared clays and the acrylic network. It was found that swelling degree and fast response to pH change of the pillared clay based superabsorbent hydrogels was decreasing by increasing the content of the pillared clay in the network of the hydrogel. The swelling rate of Zr-KSF (0.05g)-SA was higher than Zr-KSF (0.10 g)-SA and Zr-KSF (0.20 g)-SA. Additionally, the time needed to reach swelling equilibrium decreased with decrease of pillared clay content. The swelling values of superabsorbents were significantly increased with the raise of pH in the range 3.4 -8.5.

FTIR analysis and SEM micrographs impressed that the zirconium pillared clay based superabsorbents were successfully obtained. Besides, XRD analysis of the samples showed that layers of montmorillonite were exfoliated in the hydrogel structure and were completely dispersed in a continuous polymer matrix as single layers.

Clays and pillared clays might be added to superabsorbent hydrogel to compose economic products. Modifying of poly (acrylic acid) composites with inorganic materials affected the swelling character and product cost. Decreasing of swelling ratio was observed by increasing the content of pillared clay. All Zr- KSF based poly (acrylic acid) composites were pH sensitive. The behavior of shrinkage at acidic and swelling at basic environment was useful for pH sensitive systems with controllable swelling ability such as controllable drug delivery. Also, the character of water absorbing and swelling reversibility was indicator of suitable applications in agriculture and horticulture.

REFERENCES

Adamczyk, Z. (2002). Adsorption of particles: Theory. *Encyclopedia of Surface And Colloid Science*. 499–516. Retrieved April 23, 2003, from http://dekker.com/servlet/product/DOI/101081EESCS12001 2922.

Aksu, Z., & Kabasakal, E. (2004). Batch adsorption of 2,4-dichlorophenoxy-acetic acid (2,4-D) from aqueous solution by granular activated carbon. *Separation and Purification Technology*, 35, 223-240.

Allen,S. J., Gan, Q., Matthews, R., & Johnson., P. A. (2003). Comporison of optimized isotherm models for basic dye adsorption by kudzu. *Bioresource Technology*, 88, 143-152. Retrieved June 22, 2004, from Elsevier database.

Ayyappan, R., Carmalin Sophia, A., Swaminathan, K., & Sandhya, S. (2005). Removal of Pb(II) from aqueous solution using carbon derived from agricultural wastes. *Process Biochemistry*, 40 1293-1299.

Baird. C. (1998). *Environmental Chemistry,* 2nd edn New York. W. H. Freeman and Company.

Barrault, J., Bouchoule, C., Echachoui, K., Frini-Srasra, N., Trabelsi, M. & Bergaya, F. (1998). *Applied Catalysis B-Environmental* 15 (3–4), 269–274.

Barrer, R. M. & MacLeod, D. M.(1995). Activation of montmorillonite by ion exchange and sorption complexes of tetra-alkyl ammonium montmorillonites. *Trans. Faraday Soc.* 51, 1290 – 1300.

Barrett, E. P., Joyner, L. G., Halenda, P. P. (1951). The determination of pore volume and area distributions in porous substances. I. Computations from nitrogen isotherms, *J. Am. Chem. Soc.*, 73, 373–380.

Bartley, GJ.J., Burch,R. (1985). Zr-containing pillared interlayer clays .3. Influence of method of preparation on the thermal and hydrothermal stability. *Applied Catalysis* 19 (1), 175–185.

Batt, A.L.& Aga, D.S. (2005). Simultaneous analysis of multiple classes of antibiotics by ion trap LC/MS/MS for assessing surface water and groundwater contamination. *Analytical Chemistry* 77 (9), 2940–2947.

Bjerrum, J., Schwarzcnbach, G., & Sillen, L.G. (1964). Stability Constants of Metal Ion Complexes, *Spec. Pulc. Chem. Soc.*, London17.

Binitha, N.N., Sugunan, S. (2006). Preparation, characterization and catalytic activity of titania pillared montmorillonite clays. *Microporous and Mesoporous Materials* 93, 82–89.

Blatt, H., Middleton, G., & Murray, R. (1980). *Origin of sedimentary rocks* (2d ed.): Englewood Cliffs, N.J., Prentice-Hall, 766 p.

Burch R., & Warburton C.I. (1986). Zr-containing pillared interlayer clays .1. Preparation and structural characterization. *Journal of Catalysis* 97 (2), 503-510.

Burch, R. & Warburton, C.I. (1987). Pillared clays as demetallization catalysts. *Applied Catalysis* 33 (2): 395-404.

Carrado, K. A., Kostapapas, A., Suib, S. L., Coughlin, R.W. (1986). Physical and chemical stabilities of pillared clays containing transition metal ions. *Solid State Ionics.* 22, 17.

Cavani, F., Trifiro, F., Vaccari, A. (1991). Hydrotalcite-type anionic clays: preparation, properties and applications. *Catalysis Today,* 11, 173-301.

Chevalier, S., Franck, R., Suquet, H., Lambert, J.F. & Barthomeuf, D. (1994). Al-Pillared Saponites .1. IR Studies. *Journal of The Chemical Society-Faraday Transactions* 90 (4), 667-674.

Clearfield, A. & Vaughan, P. A. (1956). The crystal structure of zirconyl chloride octahydrate and zirconyl bromide octahydrate. *Acta Crystallographica 9*, 555-558.

Colombo, P. (1993). Swelling-controlled release in hydrogel matrices for oral route. *Advanced Drug Delivery Reviews* 11 (1–2), 37–57.

Diaz-Cruz, M.S., de Alda, M.J.L. & Barcelo, D. (2003). Environmental behavior and analysis of veterinary and human drugs in soils, sediments and sludge. *Trac-Trends In Analytical Chemistry* 22 (6): 340-351.

Ding, Z., Kloprogge, J.T.,& Frost, R.L. (2001). Porous Clays and Pillared Clays-Based Catalysts. Part 2: A Review of the Catalytic and Molecular Sieve Applications. *Journal of Porous Materials 8*, 273–293.

Ding, Z., Zhu, H.Y., Greenfield, P.F., & Lu, G.Q. (2001). Characterization of pore structure and coordination of titanium in TiO_2 and SiO_2-TiO_2 sol-pillared clays. *Journal of Colloid and Interface Science* 238, 267–272.

Dollimore, D., Heal, G.R. (1964). An improvement for calculation of pore size distribution from adsorption data. *J. Appl. Chem.* 14, 109-114.

Dong, L.C., & Hoffman, A.S. (1991). A novel-approach for preparation of pH-sensitive hydrogels for enteric drug delivery. *Journal of Controlled Release* 15 (2), 141–152.

Dubinin, M.M., & Radushkevich, L.V. (1947). Equation of the characteristic curve of activatedcharcoal. *Proc. Acad. Sci*. USSR 55, 331–333.

El-Hamshary, H. (2007). Synthesis and water sorption studies of pH sensitive poly(acrylamide-co-itaconic acid) hydrogels. *European Polymer Journal* 43, 4830–4838.

Farmer, V.C., (1974). Infrared Spectra of Minerals, *Mineralogical Society*, London.

Figueras, F.(1988). Pillared Clays as Catalysts. *Catalysis Reviews* 30, 457 – 499.

Flegoa,C., Galassoa, L., Millinia, R., & Kirics, I. (1998). The influence of the composition on the thermal and acid characteristics of multi-component oxide pillared montmorillonite. *Applied Catalysis A: General* 168, 323-331.

Florey, K. (Ed.), (1978). *Analytical Profile of Drug Substances*, Vol. 7, New York, Academic, Press, p. 459.

Fodwen, L., Barrer, R.A., Tinker, P.B. (1984). *Clay Minerals: their Structure, Behaviour and Use*. London, UK: The Royal Society.

Freundlich, H., 1906. Adsorption in Solution. *Phys. Chemie*. 57, 384-410.

Geatti, A., Lenarda, M., Storaro, L., Ganzerla, R. & Perissinotto, M. (1997). Solid acid catalysts from clays: Cumene synthesis by benzene alkylation with propene catalyzed by cation exchanged aluminum pillared clays. *Journal of Molecular Catalysis A-Chemical* 121 (1), 111–118.

Gil, A., Gandia, L.M. (2000). Recent advances in the synthesis and catalytic applications of pillared clays. *Catal Rev Sci Eng* 42, 145–212.

Giles, C. H., McEwan, T. H., Nakhwa, S. N., & Smith, D. (1960). Studies in adsorption. Part II. A system of classification of solution adsorption isotherms, *J. Chem. Soc*. 4 3293-3973.

Gonzalez, F., Pesquera, C., Blanco, C., Benito, I., & Mendioroz, S. (1992). Synthesis and characterization of Al–Ga pillared clays with high thermal and hydrothermal stability, *Inorganic Chemistry* 31 (5), 7272–7731.

Grim, R.E. (1968). *Clay Mineralogy*. New York, USA: McGraw-Hill.

Han, Y.S., Matsumoto, H. & Yamanaka S. (1997). Preparation of new silica sol-based pillared clays with high surface area and high thermal stability. *Chemistry of Materials* 9 (9), 2013–2018.

Hillier, S. (1995*). Erosion, sedimentation and sedimentary origin of clays*, in Velde, B., ed., Origin and mineralogy of clays: New York, Springer-Verlag, p. 162-219.

Hitchings, G.H., Burchall, J.J. (1965). *Advances in Enzymology*, Vol. 27, New York, Wiley/Interscience, p. 417.

Horvath, G. & Kawazoe, K. (1983). Method for the calculation of effective pore-size distribution in molecular-sieve carbon. J*ournal of Chemical Engineering of Japan* 16 (6), 470-475.

Hutson, N.D., Hoekstra, M.J., & Yang, R.T. (1999). *Micropoous and Mesoporous Materials* 28, 267.

IUPAC Compendium of Chemical Terminology 2nd Edition, 1997.

Jones, J.R. & Purnell, JH. (1994). The catalytic dehydration of pentan-1-ol by alumina pillared texas montmorillonites of differing pillar density. *Catalysis Letters* 28, (2-4) 283-289.

Juma, N. G. (1998). The Pedospherre and its Dynamics: Minerology, 6.3 *Clay Crystals*. Retrieved May 19, 2005 from http://wwwsoils.rr.ualberta.ca/pedosphere/content/sectionof/page03.cfm.

Kabiri, K., & Zohuriaan-Mehr, M.J. (2004). Porous superabsorbent hydrogel composites: Synthesis, morphology and swelling rate. *Macromolecular Materials and Engineering* 289, 653–661.

Kaşgöz, H., Durmuş, A., & Kaşgöz, A. (2008). Enhanced swelling and adsorption properties of AAm-AMPSNa/clay hydrogel nanocomposites for heavy metal ion removal. *Polymers for Advanced Technologies* 19, 213–220.

Katdare, S.P., Ramaswamy, V., & Ramaswamy, A.V. (2000). Factors affecting the preparation of alumina-pillared montmorillonite employing ultrasonics. *Microporous Mesoporous Materials* 37, 329–336.

Kikuchi, E. & Matsuda, T. (1988). Shape selective acid catalysis by pillared clays. Catalysis *Today 2*, 297-307.

Kloprogge, J.T., Seykens, D., Geus, J.W., Jansen, J.B.H. (1992). Temperature influence on the Al13 complex in partially neutralized aluminum solutions - A Al- 27 nuclear-magnetic-resonance study. *Journal of Non-Crystalline Solids* 142 (1–2), 87–93.

Kloprogge, J.T. (1998). Synthesis of Smectites and Porous Pillared Clay Catalysts: A Review. *Journal of Porous Materials* 5, 5-41.

Kloprogge J.T., & Frost R.L. (1999). Infrared emission spectroscopy of Al-pillared beidellite. *Applied Clay Science* 15 (5–6), 431–445.

Knozinger, H. (1993). In: Joyner, R.W., van Santen, R.A. Eds. , *Elementary Reaction Steps in Heterogeneous Catalysis*, Kluwer, Dordrecht, NL, p. 267.

Kolpin, D.W., Furlong, E.T., Meyer, M.T., Thurman, E.M., Zaugg, S.D., Barber, L.B., Buxton, H.T. (2002). Response to Comment on,"Pharmaceuticals, hormones, and other organic wastewater contaminants in US streams, 1999-2000: A national reconnaissance". *Environmental Science and Technology* 36, 1202–1211.

Kurian, M., & Sugunan, S. (2006). Wet peroxide oxidation of phenol over mixed pillared montmorillonites. *Chemıcal Engineering Journal* 115 (3), 139–146.

Lagergren, S. (1898). Zur theorie der sogenannten adsorption gel¨oster stoffe. *Kunglinga Svenska Vetenskapsakademiens*, Handlingar, 24, 1–39.

Lambert, J. F., & Poncelet, G. (1997). Acidity in pillared clays: Origin and catalytic manifestations. *Topics Catal.* 4, 43–56.

Langmuir,I, (1918). Adsorption of gases on plane surfaces of glass, mica and platinum. *J. Am. Soc.* 40, 1361-1403.

Legrini, O., Oliveros, E., & Braun, A.M. (1993). Photochemical processes for water-treatment. *Chemical Reviews* 93 (2), 671–698.

Lee, W.F., & Wum, R.J. (1996). Superabsorbent polymeric materials. 1. Swelling behaviors of crosslinked poly(sodium acrylateco- hydroxyethyl methacrylate) in aqueous salt solution. *J. Appl. Polym. Sci.* 62, 1099–1114.

Lee, W.F., & Yang L.G. (2004). Superabsorbent polymeric materials. XII. Effect of montmorillonite on water absorbency for poly(sodium acrylate) and montmorillonite nanocomposite superabsorbents. *Journal of Applied Polymer Science* 92**,** 3422-3429**.**

Lei, L.C., Hu, X.J. & Yue, P.L. (1998). Improved wet oxidation for the treatment of dyeing wastewater concentrate from membrane separation process. *Water Research* 32 (9), 2753–2759.

Levy, S. B. (1997). In Antibiotic Resistance: Origins, Evolution, Selection and Spread; Chadwick, D. J., Goode, J. Eds.; *Ciba Foundation Symposium 207*; Wiley: West Sussex, England, pp 1–14.

Li, A., Wang, A.Q., & Chen, J.M. (2004). Studies on poly(acrylic acid)/attapulgite superabsorbent composite. I. Synthesis and characterization. *Journal of Applied Polymer Science* 92, 1596-1603.

Li, A., Zhang, J.P., & Wang A.Q. (2005). Synthesis, characterization and water absorbency properties of poly(acrylic acid)/sodium humate superabsorbent composite. *Polymers for Advanced Technologies* 16 (9), 675–680.

Lin, J.M., Wu, J.H., Yang, Z.F., & Pu, M.L. (2001). Synthesis and properties of poly(acrylic acid)/mica superabsorbent nanocomposite. *Macromolecular Rapid Communications* 22, 422–424.

Lin, S.H., & Juang, R.S. (2002). Heavy metal removal from water by sorption using surfactant-modified montmorillonite. *Journal of Hazardous Materials* 92, 315-326.

Lindberg, R., Jarnheimer, P.A., Olsen, B., Johansson, M., & Tysklind, M. (2004). Determination of antibiotic substances in hospital sewage water using solid phase extraction and liquid chromatography/mass spectrometry and group analogue internal standards. *Chemosphere* 57 (10), 1479–1488.

Liu, D.H.F., Liptak, B.G. & Bouis, P.A.(1997). *Environmental Engineers' Handbook, 2nd edn.* Lewis, Boca Raton, p. 1431.

Liu, W.Q., Zhao, L., Sun, G.D. & Min, E.Z. (1999). Saturation of aromatics and aromatization of C-3 and C-4 hydrocarbons over metal loaded pillared clay catalysts. *CatalysiseToday* 51 (1), 135–140.

Lothenbach, B., Furrer, G., & Schulin, R. (1997). Immobilisation of heavy metals by polynuclear aluminium and montmorillonite compounds. *Environmental Science Technology*, 31, 1452– 1462.

Louloudi, A. & Papayannakos, N. (1998). Hydrogenation of benzene on La-Ni and clay supported La-Ni catalysts. *Applied Catalysis A-General* 175 (1–2), 21–31.

Lourvanij, K. & Rorrer, G.L. (1997). Reaction rates for the partial dehydration of glucose to organic acids in solid-acid, molecular-sieving catalyst powders. *Journal of Chemical Technology and Biotechnology* 69 (1), 35–44.

Malik, U.R., Hasany, S.M., & Subhani, M.S. (2005). Sorptive potantial of sunflower sterm for Cr (III) ions from aqueous solution and its kinetic and thermodynamic profile. *Talanta 66*, 166-173.

Marczewski, A. W. (2002). A practical guide to isotherms of adsorption on heterogeneous surfaces. Retrieved February 1, 2004, from http://www.2002/ adsorption org/awm/ads/Ads.htm.

McKay, G., Bino, M. J., & Altemeni, A. (1986). External mass transfer during the adsorption of various pollutants onto activated carbon. *Water Research*, 20(1), 35-442.

Meier,W. (1986). M. Proc. 7th Intl. Zeolite Conf. , eds. Y. Murakami, A. Iijima and J. W. Ward, Kodansa/Elsevier 13.

Messina, P.V., & Schulz, P.C. (2006). Adsorption of reactive dyes on titania–silica mesoporous materials. *Journal of Colloid and Interface Science* 299, 305-320.

Miao, X.S., Bishay, F., Chen, M. & Metcalfe, C.D. (2004). Occurrence of antimicrobials in the final effluents of wastewater treatment plants in Canada. *Environmental Science & Technology* 38 (13) 3533–3541.

Miura, Y., Hirano, K., Nate, T., Kambayashi, T., Ohtsuka, M., & Nagai, T. (1991). *European Patent* 440, 256.

Manohar, D.M., Noeline, B.F., & Anirudhan, T.S. (2006). Adsorption performance of Al-pillared bentonite clay for the removalof cobalt(II) from aqueous phase. A*pplied Clay Science* 31, 194–206.

Mokaya, R., Jones, W., Davies, M.E. & Whittle, M.E. (1993). Chlorophyll adsorption by alumina-pillared acid-activated clays. *Journal of The American Oil Chemists Society* 70 (3), 241-244.

Moreno, S., Gutierrez, E., Alvarez, A., Papayannakos, N.G. & Poncelet, G. (1997). Al-pillared clays: from lab syntheses to pilot scale production – Characterisation and catalytic properties. *Applıed catalysis A-general* 165 (1–2), 103–114.

Moreno, S., Kou, R.S. & Poncelet, G. J. (1996). Hydroconversion of Heptane over Pt/Al-Pillared Montmorillonites and Saponites. A Comparative Study. *Journal of catalysis* 162 (2), 198-208.

Moreno, S., Kou, R.S. & Poncelet, G. J. (1997). Influence of preparation variables on the structural, textural, and catalytic properties of al-pillared smectites. *Journal of physical chemistry* B 101 (9), 1569-1578.

Moreno, S., Kou, R.S., Molina, R. & Poncelet, G. (1999). Al-, Al,Zr-, and Zr-pillared montmorillonites and saponites: Preparation, characterization, and catalytic activity in heptane hydroconversion. *Journal of catalysis* 182, 174–185.

Muha, G. M. & Vaughan, P.A. (1960). Structure of the complex ion in aqueous solutions of zirconyl and hafnyl oxalates. *Journal of Chemical Physics*. 33, 194-199.

Mrada, I., Ghorbela, A., Tichitb, D., & Lambertc, Jean-François. (1997). Optimisation of the preparation of an Al-pillared clay: thermal stability and surface acidity. *Applied Clay Science* 12, 349.

Nemecz, E. (1981). *Clay Minerals*, Budapest, Hungary: Akademiai Kiado.

Newman, A.C.D. (1987). *Chemistry of Clays and Clay Minerals, Monograph 6 of the Mineralogical Society*, London, UK: Longmans.

Occelli, M.L., & Finseth, D. H. (1986). Preparation and characterization of pillared hectorite catalysts. *Journal of Catalysis* 99 (2), 316-326.

Occelli, M.L. (1986). New routes to the preparation of pillared montmorillonite catalysts. *Journal of molecular catalysis* 35 (3): 377-389.

Ollis, D.F., Pelizzetti, E. & Serpone, N. (1991). Photocatalyzed Destruction of water Contaminants. *Environmental Science & Technology* 25 (9), 1522-1529.

Olphen, H.V., Fripiat, J.J. (1979). Data Handbook for Clay Minerals and other Non Metallic Materials, *Pergamon Press*, London, 1979.

Özcan, A. S., & Özcan, A. (2004). Adsorption of acid dyes from aqueos solutions onto acid-activated bentonite. *Journal of Colloid and Interface Science*, 276, 39-46.

Palinko, I., Lazar, K., Hannus, I. & Kirisci, I. (1996). Step toward nanoscale Fe moieties: intercalation of simple and Keggin-type iron-containing ions in-between the layers of Na-montmorillonite. *Journal of Physics and Chemistry of Solids*, 57, 1067-1072.

Reichle, W. T. (1986). Synthesis of anionic clay-minerals (mixed metal-hydroxides, hydrotalcite). *Solid State Ionics*, 22(1), 135-141.

Renew, J.E. & Huan, C.H. (2004). Simultaneous determination of fluoroquinolone, sulfonamide, and trimethoprim antibiotics in wastewater using tandem solid phase extraction and liquid chromatography-electrospray mass spectrometry. *Journal of Chromatography* A 1042 (1-2), 113-121.

Ross, J. R. H. (Ed.) (1988). *Catalysis Today*, *2*, Amsterdam. Elsevier Science Publishers. 235–238.

Rouquerol, F., Rouquerol, J., & Sing, K. (1999). Adsorption by Powders and Porous Solids, Principles, Methodology and Applications, *Academic Press,* London.

Salerno, P., Asenjo, M. B., & Mendioroz, S. (2001). Influence of preparation method on thermal stability and acidity of Al–PILCs. *Thermochimica Acta* 379, 101-109.

Sanchez, A., & Montes, M. (1998). Influence of the preparation parameters (particle size and aluminum concentration) on the textural properties of Al-pillared clays for a scale-up process. *Microporous Mesoporous Materials* 21, 117–125.

Schiavello, M. (1997). *Heterogeneous Photocatalysis*. Chichester. John Wiley & Sons.

Schoonheydt R.A.(1991). *Introduction to Zeolite Science and Practice*, edited by H. van Bekkum, E.M. Flanigen, and J.C. Jansen (Studies in Surface Science and Catalysis, Elsevier, Amsterdam, (1991), Vol. 58, p. 201.

Seki, Y., Torgürsül, A., & Yurdakoç, K. (2007). Preparation and characterization of poly(acrylic acid)-iron rich smectite superabsorbent composites. *Polymer Advance Technology* 18, 477–482.

Serpone, N. (1995). Brief introductory-remarks on heterogeneous photocatalysis. *Solar Energy Mateııals and Solar Cells* 38 (1-4), 369-379.

Sing, K.S.W., Everett, D.H., Haul, R.A.W., Moscou, L., Pierotti, R.A., Rouquerol, J., Siemieniewska, T. (1972). Apendix II: definitions terminology and symbols in colloid and surface chemistry. *Pure Appl. Chem.* 57, 603– 619.

Sing, K.S.W., Everett, D.H., Haul, R.A.W., Moscou, L., Pierotti, R.A., Rouquerol, J., & Siemieniewska, T. (1985) Reporting physisorption data for gas solid systems with special reference to the determination of surface-area and porosity (recommendations 1984) *Pure and Applied Chemistry,* 57, 603-619.

Singh, T.S. & Pant, K.K. (2004). Equilibrium, Kinetics and Thermodynamic Studies For Adsorption of As (III) on activated alumina. *Separation and Purification Technology*, 36, 139-147.

Smith J.V. & Dytrych W.J. (1984). Nets with channels of unlimited diameter. *Nature* 309 (5969): 607-608.

Soma Y., Soma M., & Harada I. (1986). The oxidative polymerization of aromatic molecules in the interlayer of montmorillonites studied by resonance Raman spectroscopy. *Journal of Contaminant Hydrology*, *1*, 95-106.

Storaroa, L., Lenardaa, M., Gazerlaa, R., & Rinaldi, A. (1998). Preparation of hydroxy Al and Al/Fe pillared bentonites from concentrated clay suspensions. *Microporous Materials* 6, 55-63.

Sylva, R.N. (1972). Rev. Pure *Apl. Chem*. 22, 115.

Tanaka, H., Kambayashi, T., Sugiyama, Y., Nagai, T., Nagata, K., Kubota, K., & Hirano, K. (1992). *European Patent* 501, 482.

Theng, B.K.G. (1974). *The Chemistry of Clay–Organic Reactions*, London, UK: Hilger.

Tsubakimoto, T., Shimomura, T., & Kobabyashi, H. (1987). *Japanese Patent* 62, 149, 335.

Toth, J. (2002). Adsorption Isotherms. *Encyclopedia of Surface and Colloid Science*, Dekker, New York 212-224.

Tzou, M. S. (1983). *Clay catalysts pillared by metal hydroxyl polymers.* Ph.D. Thesis, Michigan State University.

Vaccari, A. (1998). Clays and catalysis: a promising future. *Applied Clay Science, 14,* 161-198, Retrieved June 22, 2001, from Elsevier database.

Vaccari A. (1999). Clays and catalysis: a promising future. *Applied Clay Science*, 14 161–198.

Van Olphen, H., Fripiat, J.J. (1979). *Data Handbook for Clay Minerals and Other Non-metallic Materials*, Pergamon, UK: Oxford.

Vaishya, R.C., & Gupta, S.K. (2002). Modelling arsenic (III) adsorption from water by sulfate-modified iron oxide-coated sand (SMIOCS), *J. Chem. Technol. Biotechnol.* 78 (2002) 73–80.

Vaughan, D.E.W, Lussier, R.J., & Magee, J. S. (1979). U.S. Patent 4, 176,090.

Vaughan, D.E.W. 1987. US Patent 4,666,877 to W.R. Grace & Co.

Vaugan, D.E.W. (1988). Pillared clays: a historical perspective. *Catalysis Today* 2, 187-198.

Velde, B. (1995). Composition and mineralogy of clay minerals, in Velde, B., ed., *Origin and mineralogy of clays*: New York, Springer-Verlag, p. 8-42.

Walker, C.O. (1987). US Patent 4, 664, 816.

Wang, S.B., Zhu, H.Y. & Lu, G.Q. (1998). Preparation, characterization, and catalytic properties of clay-based nickel catalysts for methane reforming. *Journal of Colloid and Interface Science* 204 (1), 128–134.

Wang, Y.J. & Li, W.Z. (2000). Kinetics of acetic acid esterification with 2-methoxyethanol over a pillared clay catalyst. *Reaction Kinetics and Catalysis Letters* 69 (1), 169-176.

Warburton, C. I. (1988). Preparation and catalytic properties of Iron oxide and Iron sulphide pillared clays. *Catalysis Today* 2, 271- 280.

Weber, W.J., Morris, J.C, & Sanit, J. (1963). Kinetics of adsorption on carbon from solution, *Eng. Div. ASCE* 89, 31–59.

Weber, T. W., & Chakkravorti, R.K. (1974). Pore and solid diffusion models for fixed bedadsorbers. *American Institude of Chemical Engineers Journal*, 20,228.

Wilson, M.J. (Ed.). (1987*). A. Handbook of Determinative Methods in Clay Minerology.* New York.USA: Chapman and Hall.

Wu, S., Li, H., & Chen, P. J. (2004). Modeling Investigation of Volume Variation Kinetics of Fast Response Hydrogels. *Journal of Macromolecular Science, Part C: Polymer Reviews* 44, 113-130.

Wu, J.H., Lin, J.M., Zhou, M., & Wei, C.R. (2000). Synthesis and properties of starch-graft-polyacrylamide/clay superabsorbent composite. *Macromolecular Rapid Communications* 21, 1032-1034.

Wu, J.H., Wei, Y.L., Lin, H.M., & Lin, S.B. (2003). Study on starch-graft-acrylamide/mineral powder superabsorbent composite. *Polymer* 44,6513–6520.

Xie, Z.X., Zhao, Z.L., & Zhang, Y.B. (1980). X-ray Spectroscopy Analysis, *Science press*. China, p. 69.

Yamanaka, S., Doi, T., Sako, S., & Hattori, M. (1984). High surface-area solids obtained by intercalatıon of iron-oxide pillars in montmorillonite. *Materials Research Bulletin*. 19, 161-168.

Yang, R.T., Chen, J.P., Kikkinides, E.S., Cheng, L.S. & Cichanowicz,J.E. (1992). Pillared clays as superior catalysts for selective catalytic reduction of no with NH_3. *Industrial & Engineering Chemistry Research* 31 (6), 1440–1445.

Yao, K.J., & Zhou, W.J. (1994). Synthesis and water absorbency of the copolymer of acrylamide with anionic monomers. *Journal of Applied Polymer Science* 53 (11), 1533-1538.

Zhang, J. P., Li, A., & Wang, A. Q. (2005). Study on superabsorbent composite. V. Synthesis, swelling behaviors and application of poly (acrylic acid-co-acrylamide)/sodium humate/attapulgite superabsorbent composite. *Polymers for Advanced Technologies* 16, 813–820.

Zhang, J.,& Wang, A. (2007). Study on superabsorbent composites. IX: Synthesis, characterization and swelling behaviors of polyacrylamide/clay composites based on various clays. *Reactive and Functional Polymers* 67(8), 737-745.

Zhang, J., Liu, R., Li, A., & Wang, A. (2006). Preparation, swelling behaviors and application of polyacrylamide/attapulgite superabsorbent composites. *Polymers for Advanced Technologies* 17, 12–19.

Zhou, W.J., Yao, K.J., & Kurth, M.J. (1996). Synthesis and swelling properties of the copolymer of acrylamide with anionic monomers. *Journal of Applied Polymer Science* 62 (6), 911–915.